**BrightnESS²**

**Bringing Together a Neutron Ecosystem for Sustainable Science with ESS**

**H2020-INFRADEV-3-2018-1**

**Grant Agreement Number: 823867**

# Deliverable Report
# D.2.1 Preliminary report on engineering: Calibration protocol for all strain scanning instruments and definition of criteria for the Neutron Quality Label

BrightnESS² is funded by the European Union Framework Programme for Research and Innovation Horizon 2020, under grant agreement 823867

## 1. Project Deliverable Information Sheet

| | | |
|---|---|---|
| BrightnESS² Project | Project Ref. No. 823867 | |
| | Project Title: BrightnESS² – Bringing Together a Neutron Ecosystem for Sustainable Science with ESS | |
| | Project Website: brightness.esss.se | |
| | Deliverable No.: D.2.1 | |
| | Deliverable Type: | |
| | Dissemination Level: | Contractual Delivery Date: 31.03.2020 Delayed with P.O. Approval - 30.06.2020 |
| | | Actual Delivery Date: 26.06.2020 |
| | EC Project Officer: René Martins | |

## 2. Document Control Sheet

| | | |
|---|---|---|
| Document | Title: Pilot Project for a Neutron Quality Label for Residual Stress Analysis: Development of a Common Calibration Protocol | |
| | Version: | |
| | Available at: | |
| | Files: | |
| Authorship | Written by | Ranggi S. RAMADHAN (ILL)<br>Sandra CABEZA (ILL) |
| | Contributors | Thilo PIRLING (ILL)<br>Saurabh KABRA (STFC-UKRI)<br>Michael HOFMANN (MLZ)<br>Joana R. KORNMEIER (MLZ)<br>Andrew VENTER (NECSA)<br>Deon MARAIS (NECSA) |
| | Reviewed by | Arno Hiess (ESS)<br>Ute Gunsenheimer (ESS) |
| | Approved | BrightnESS² Steering Board |

BrightnESS² is funded by the European Union Framework Programme for Research and Innovation Horizon 2020, under grant agreement 823867

## 3. List of Abbreviations and Acronyms

| | |
|---|---|
| CMM | Coordinate Measuring Machine |
| Col. | Collimator |
| GV | Gauge Volume |
| IGV | Instrumental Gauge Volume |
| Mono. | Monochromator |
| N.B. | North Bank |
| NGV | Nominal Gauge Volume |
| Pos. | Position |
| Prim. | Primary (incident) beam |
| PSD | Position Sensitive Detector |
| S.B. | South Bank |
| Sec. | Secondary (diffracted) beam |
| SGV | Sampled Gauge Volume |
| Std. | Standard |
| TOF | Time-of-flight |

## 4. List of Figures



BrightnESS² is funded by the European Union Framework Programme for Research and Innovation Horizon 2020, under grant agreement 823867

## Table of Content



BrightnESS² is funded by the European Union Framework Programme for Research and Innovation Horizon 2020, under grant agreement 823867

BrightnESS² is funded by the European Union Framework Programme for Research and Innovation Horizon 2020, under grant agreement 823867

BrightnESS² is funded by the European Union Framework Programme for Research and Innovation Horizon 2020, under grant agreement 823867

## 5. Executive Summary

This report provides the quantification and benchmarking of the calibration and positioning accuracy at the four participating neutron strain scanners towards residual stress analysis by neutron diffraction. This report also proposes a common calibration protocol and reporting standard, as a part of the Neutron Quality Label (NQL) for residual stress. Methods included the definition of common calibration samples, calibration measurements, comparison of data analysis using different software tools, interpretation of the findings and identification of further developments. All details about measurement results can be found in the annex. Results from the calibration measurements (directly on the instrument setup) show that all the participating instruments can attain positioning uncertainties better than 100 µm. This confirms the positioning uncertainty analysis from the Round Robin exercise of VAMAS TWA20, where most of the participating instruments also demonstrated indirectly a positioning uncertainty around 100 µm. The lessons learned from the calibration measurements are used to establish the common calibration protocol and reporting template to achieve standardised and rigorous experimental methods. From this, NQL was proposed as a quality standard for residual stress analysis using neutron diffraction, following a certain calibration guideline and reporting requirements.

The report concludes that the participating instruments work harmoniously in achieving the critical standard for residual stress analysis for engineering application. This has been further reinforced by the definition of the common calibration protocol and reporting standard. NQL will be first implemented in the participating neutron sources. Other facilities are invited to contact any of the participating sources and perform a similar calibration exercise as here presented in order to be approved by the partners and attain the NQL.

BrightnESS² is funded by the European Union Framework Programme for Research and Innovation Horizon 2020, under grant agreement 823867

# 6. General Remarks, Terms and Symbols

## 6.1. Introduction

The neutron diffraction-based method for internal strain analysis of polycrystalline materials has specific advantages, which allows for the non-destructive depth-resolved determination of the complete stress tensor within real-sized engineering components. Apart from it being used extensively by academia, it has not matured into becoming a technique routinely used by industry, notwithstanding having proven to be beneficial in the research and development of products in vital sectors such as aerospace, transport, energy, and manufacturing [1–9]. Industrial demand for this technique is however steadily growing, driven by the continuous strategic competition for better performance and weight reduction of components that inherently leads to increased complexity and demand on materials performance and fabrication techniques. Accordingly, the complexity of residual stress analysis requirements for engineering applications has been fostered through the invaluable information provided by neutron strain analysis in selective projects. In this landscape, neutron strain scanning is a powerful and versatile method for characterising metal and ceramic products to aid in the optimisation of materials and processes for increased safety and durability of structures and components. Neutron sources have also devoted efforts in the recent years to attract industry with projects such as SINE2020 addressing feasibility studies [10].

At the same time, the landscape of neutron scattering in Europe is going through a period of dramatic change. The number of operational neutron sources will be significantly reduced in the coming years due to older sources reaching the end of their licensed operational lifetimes [11]. Substantial efforts are being made to ensure the future availability of neutrons for the scientific and industrial communities. The European Spallation Source (ESS) that will start its user program in 2023 represents a major investment (€1.84 billion over 12 years) to increase the capability of neutron research in Europe. This is complemented by upgrade programs at other major national and multi-national facilities. Projects such as BrightnESS (2015-2018) and BrightnESS$^2$ (2019-2021) [12] have been launched in support of the long-term sustainability of the neutron community and the network of neutron sources in Europe.

The demonstration of better integration and capability inter-comparison amongst neutron strain scanners are necessary in order to promote neutron diffraction residual stress mapping into becoming an analysis tool routinely utilised by industry. This will consequently expand the user base of the technique. Through Work Package 2 (WP2), the BrightnESS$^2$ project aims to "define the best way to provide neutron instrumentation, associated characterisation methods and analysis tools in a strategic and coordinated fashion to the European user community and beyond". This document reports the work performed in WP2.3(A), which focuses on the quantitative analysis and benchmarking of four participating neutron strain scanners. This involves the development of common calibration protocols and reporting standard, as a part of the Neutron Quality Label for residual stress. Three European neutron strain scanning instrument are joined by one instrument from South Africa for this exercise, representing the international outreach of the BrightnESS$^2$ project. The benchmarking and standardisation amongst four different instruments aim at instilling awareness and confidence within the industrial community on the precision, reliability, reproducibility, quality and accuracy of results, and ultimately its interchangeability.

BrightnESS$^2$ is funded by the European Union Framework Programme for Research and Innovation Horizon 2020, under grant agreement 823867

### 6.2. List of contributors

| | | |
|---|---|---|
| Ranggi S. RAMADHAN<br>Sandra CABEZA<br>Thilo PIRLING | Author<br>Task Manager<br>Participant | *Institut Laue Langevin (ILL), 71 Avenue des Martyrs, CS 20156, 38042 Grenoble Cedex 9, France* |
| Saurabh KABRA | Participant | *ISIS Neutron and Muon Facility, STFC-UKRI, Rutherford Appleton Laboratory, Harwell Campus, OX11 0QX, United Kingdom* |
| Michael HOFMANN<br>Joana R. KORNMEIER | Participant<br>Participant | *Heinz Maier-Leibnitz Zentrum (MLZ), TU Munchen, Lichtenbergstr, 1, D-85747 Garching, Germany* |
| Andrew VENTER<br>Deon MARAIS | Participant<br>Participant | *Necsa SOC Limited, Church Street Extension West, Pelindaba Campus, Brits District, North West Province, South Africa* |

### 6.3. Definition of terms

Note: Most of the definitions are taken from the ISO 21432:2019(en) "Non-destructive testing — Standard test method for determining residual stresses by neutron diffraction" [13].

**Accuracy** (from "International vocabulary of metrology - Basic and general concepts and associated terms (VIM)" JCGM 200:2012)
Closeness of agreement between a measured quantity value and a true quantity value of a measurand.

**Attenuation coefficient**
Adjustment of position and orientation of the sample and all instrument components, such that reliable strain measurements by neutron diffraction can be performed at the desired location in the sample.

**Beam defining optics**
Arrangement of devices used to determine the properties of the neutron beam such as the wavelength and intensity distribution, divergence, and shape of the gauge volume. These include apertures, slits, collimators, monochromators, mirrors, etc.

**Bragg peak**
Sharp increase in intensity distribution where the scattering angle satisfies the Bragg condition for a specific *hkl* lattice plane.

**Centre of $\omega$-rotation**
A fixed axis on the instrument around which the sample stage/ $\omega$-table rotates.

**Diffraction**
Elastic scattering based on wave interference phenomena.

BrightnESS² is funded by the European Union Framework Programme for Research and Innovation Horizon 2020, under grant agreement 823867

**Gauge Volume**
Volume from which the diffraction data is obtained. The gauge volume is determined by the intersection of the incident/primary and diffracted/secondary neutron beam.

> **Nominal gauge volume (NGV)** is the volume of space defined by the intersection of parallel beams of neutrons (incident and diffracted beams), which are transmitted through the two defining apertures (e.g., slits, collimators), Figure 6-1(A).
>
> **Instrumental gauge volume (IGV)** is the volume of space defined by the intersection of the actual beam paths through the two defining apertures, taking into account beam divergence and the intensity profile. A common method of determining the IGV (position, dimension) involves scanning a calibration sample with dimensions smaller than the aperture openings through the NGV (see Section 8.2 for details), Figure 6-1(B).
>
> **Sampled gauge volume (SGV)** is the intersection of the IGV with the sample under investigation, Figure 6-1(C).

**Lattice spacing**
Spacing between adjacent parallel crystallographic lattice planes. Also referred to as *d*-spacing.

**Monochromatic instrument**
Neutron instrument employing a single (or very narrow band of) neutron energies (wavelengths).

**Monochromatic beam**
Neutron beam with a single (or very narrow band of) neutron energies (wavelengths).

**Polychromatic beam**
Neutron beam containing a wide (continuous) band of neutron energies (wavelengths).

**Precision** (from "International vocabulary of metrology - Basic and general concepts and associated terms (VIM)" JCGM 200:2012)
Closeness of agreement between indications or measured quantity values obtained by replicate measurements on the same or similar objects under specified conditions. Measurement precision is usually expressed numerically by measures of imprecision, such as standard deviation, variance, or coefficient of variation under the specified conditions of measurement.

**Primary beam**
Incident neutron beam directed at the instrument centre of rotation.

**Pseudo-strain**
Incorrectly determined strain value due to errors in the detection of peak position at near surface positions where the instrumental gauge volume is only partially submerged in the sample with the centre of gravity of the sampled gauge volume subsequently not coinciding with the reference point. This results in the diffracted intensity being shifted in angular extent and projected as an incorrect geometrical peak shift (pseudo peak shift) on the position sensitive neutron detector.

**Reference point**
Centroid of the instrumental gauge volume. The reference point coincides with a point on the centre of the $\omega$-rotation axis after instrument (beam apertures) alignment.

**Reflection geometry**
Measurement orientation where the incident and diffracted beams enter and exit from the same surface, i.e., scattering vector normal to the sample surface.

BrightnESS² is funded by the European Union Framework Programme for Research and Innovation Horizon 2020, under grant agreement 823867

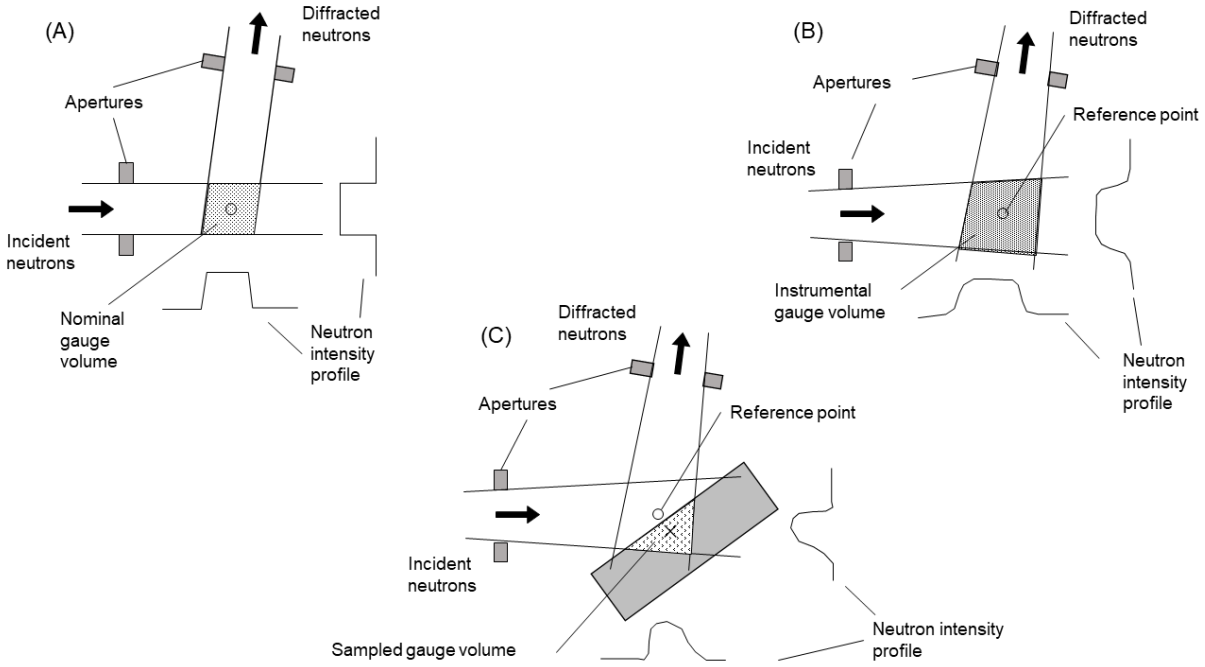


*Figure 6-1 Illustration of the (A) nominal, (B) instrumental, and (C) sampled gauge volume, adapted from* [14]

**Residual stress**
Self-balancing stresses that exist in a material at a constant temperature condition with no external force applied. Generally classified into three types: i) Type-I residual stresses which are homogeneous over a very large number of crystal grains of the material, also called macrostresses; ii) Type-II residual stresses which are homogeneous within a small number of adjacent crystal grains of the material (a single grain or phase); iii) Type-III residual stress which are homogeneous over a few interatomic distances. Type-II and Type-III are collectively called microstresses.

**Scan**
A series of sequential discrete point measurements along a certain path.

**Secondary beam**
Also referred to as diffracted beam. Neutrons scattering from the sample gauge volume towards the detector.

**Surface scan**
Procedure to determine the position of a specimen surface or interface with respect to the reference point. Performed by scanning the instrument gauge volume across the sample surface into the bulk material, and fitting an appropriate mathematical model to the resulting position dependant neutron intensity curve. Also termed entry scan or intensity scan.

**Time-of-flight**
Time taken by a neutron of a given speed (i.e. energy or wavelength) to cover the distance from a defined starting point to the detector. The neutron wavelength can be determined by the neutron time-of-flight for a known flight path, i.e., distance from starting point (e.g., moderator) to the detector.

**Transmission geometry**
Measurement orientation where the incident and diffracted beams enter and exit from different surfaces.

BrightnESS² is funded by the European Union Framework Programme for Research and Innovation Horizon 2020, under grant agreement 823867

**Uncertainty** (from "International vocabulary of metrology - Basic and general concepts and associated terms (VIM)" JCGM 200:2012)
Non-negative parameter characterizing the dispersion of the quantity values being attributed to a measurand, based on the information used.

**Wall scan**
A scan comprising of surface scans through both surfaces of a wall, covering the full thickness.

### 6.4. Symbols

| Symbol | Definition | Units |
|---|---|---|
| $d$ | Lattice spacing | Å |
| $d_{0,hkl}$ | Stress-free lattice spacing of particular *hkl* reflection | Å |
| $d_{hkl}$ | Lattice spacing of particular *hkl* reflection | Å |
| E | Diffraction elastic constant | $kg.m^{-1}.s^{-2}$ |
| $h$ | Vertical height of GV | mm |
| $hkl$ | Indices of a crystallographic lattice plane | |
| $Q$ | Scattering vector | |
| $v$ | Poisson's Ratio | |
| $w$ | Horizontal width of GV | mm |
| $X,Y$ | Axes of instrument coordinate system | |
| $x,y,z$ | Axes of the sample/ sample stage coordinate system | |
| $\chi$ | Sample tilt | degrees |
| $\varepsilon$ | Strain | με |
| $\varepsilon_{i,j,k}$ | Component of normal strain tensor in general *i, j, k* coordinate axes | με |
| $\gamma_{ij,jk,kl}$ | Component of shear strain tensor in general *i, j, k* coordinate axes | με |
| $\lambda$ | Neutron wavelength | Å |
| $\omega$ | Angular rotation of the sample stage | degrees |
| $\sigma_{i,j,k}$ | Component of normal stress tensor in general *i, j, k* coordinate axes | MPa |
| $\sigma_{x,y,z}$ | Principal stress in sample *x, y, z* coordinate axes | MPa |
| $\tau_{ij,jk,kl}$ | Component of shear stress tensor in general *i, j, k* coordinate axes | MPa |
| $2\vartheta$ | Diffraction angle | degrees |
| $2\vartheta_{det}$ | Detector angular position | degrees |

BrightnESS² is funded by the European Union Framework Programme for Research and Innovation Horizon 2020, under grant agreement 823867

# 7. Background and Objectives

## 7.1. Motivation

Technical development and standardisation of neutron diffraction for residual stress analysis have been performed through previous projects including the Versailles Project on Advanced Materials and Standards: Technical Working Area 20 (VAMAS TWA20) [15] and the Residual Stress Standard using Neutron Diffraction (RESTAND) program. These documents, in conjunction with the ISO 21432:2019(en) standard [13] serve as the guideline for residual stress analysis with neutron diffraction. In recent years, the European Network on Neutron Techniques Standardisation for Structural Integrity (NeT) focused on the material science and simulation, and aimed to develop the experimental and numerical techniques and standards for the reliable characterisation of residual stresses in structural welds [16].

ENGIN-X (ISIS, UK), SALSA (ILL, France) and STRESS-SPEC (FRMII, Germany) are leading neutron strain scanners in Europe, which in the last two decades have been contributing to the development and application of neutron diffraction for residual stress analysis for both academia and industry. Other instruments, including MPISI (Necsa, South Africa), also play a major role in promoting and utilising the technique worldwide. In recent years, the expertise of the community in the method has been consolidated with facilities acknowledging each other as partners in offering similar, and sometimes complementary, capabilities to the user community. Industrial users have however voiced a perceived disparity of 'measurement quality' and lack of standardised procedures between different neutron strain scanners. This plays a significant role in preventing neutron diffraction residual stress mapping to be an established tool for industry. The four aforementioned instruments decided to initiate a coordinated effort to address the problem.

The perception of disparity amongst the instruments may originate from different factors such as, for example, the lack of reporting of positional error (i.e., uncertainties between the intended and effective measurement position) and the lack of benchmarking this parameter between the instruments. Measurement quality is currently mostly indicated by the standard error in stress values, which is derived from the fitting uncertainties of the Bragg peak position with analytical functions. While the VAMAS TWA20 reported the positioning uncertainty from Round Robin exercises, it was performed only by indirect methods, i.e., by comparing the strain profiles from the neutron measurements against the theoretical strains. The ISO 21432:2019(en) already mentioned the importance of positioning uncertainty especially in regions of high strain gradient, and stated that a series of measurements may be required for assessment. However, the standard only describes the procedures for positioning and aligning the sample in a neutron beam in general terms. Therefore, it is necessary to have a practical guideline to characterise the positioning uncertainty directly from the instrumentation, and also to benchmark the performance of different instruments and setups using a common protocol.

## 7.2. Objectives and methods

To advance the previous standardisation initiatives and to contribute towards the integration of neutron diffraction strain scanning as routine characterisation tool within industry, the suggested next step is to perform quantitative analyses of the instruments with investigations of specific sample geometries at the four participating neutron strain scanners. These are ENGIN-X, SALSA, STRESS-SPEC which are the premier European instruments, and MPISI of Nesca, which is the BrightnESS² partner from outside Europe. The main objectives of this work are:

BrightnESS² is funded by the European Union Framework Programme for Research and Innovation Horizon 2020, under grant agreement 823867

1. To design specific test cases to quantify the accuracy and the precision of an instrument setup, as an additional indicator of measurement quality.
2. To design and manufacture a set of common calibration samples to be distributed among the participating instruments.
3. To benchmark the accuracy and the reliability of results from the participating neutron strain scanners through calibration measurements and analysis methods, including the benchmarking of the positional accuracy and data analysis software.
4. To define a common calibration protocol and standard of reporting of instrumental setup and parameters among the participating instruments.
5. To identify and propose further implementations in the common calibration of instruments.

To achieve these objectives, multiple group discussions have been organised between March 2019 to May 2020, attended by the scientists of the four participating instruments. The discussion covered the review of previous Round Robin exercises, the statement of current benchmarking problems among neutron strain scanners, the design of the common calibration samples and test cases, the interpretation of the data, and finally the preparation of the Neutron Quality Label (NQL).

A beamtime campaign of calibration measurements on the four participating instruments using the specifically designed samples has been carried out as the core activity of this project: the lessons learned from the measurements were used to benchmark the instruments, to develop the common calibration protocol, and as an input to define the standard instrument setup report.

### 7.3. Neutron Quality Label (NQL)

Neutron Quality Label (NQL) is proposed as a quality standard for residual stress analysis using neutron diffraction, following a certain calibration guideline and reporting requirements. The aim of this standard is to promote the confidence of the industry on the neutron diffraction technique for residual stress analysis and the interchangeability between the neutron strain scanners. The work presented in this deliverable (D2.1) includes of the first two steps in the preparation of the NQL, which are the internal certification/ benchmarking of the participating neutron strain scanners, and the formulation of the common calibration protocol and reporting standards. The next step, which is the final validation of the NQL, is its application in the industrial measurements. This will be presented in deliverable D2.6.

The NQL will be first implemented in the participating neutron sources. In order to attain it, other facilities are invited to contact any of the participating sources and arrange a similar calibration report as in the exercise presented in order to be approved by the partners.

BrightnESS² is funded by the European Union Framework Programme for Research and Innovation Horizon 2020, under grant agreement 823867

# 8. Technical Overview

## 8.1. Neutron diffraction for residual stress analysis

### 8.1.1. Theory

When a neutron beam with a wavelength range ($\lambda$) impinges onto a polycrystalline sample, its lattice spacing ($d_{hkl}$) can be determined from the measured position of a Bragg peak ($\theta_{hkl}$) using Bragg's law, Eq. (8.1):

$$\lambda = 2d_{hkl} \sin \theta_{hkl} \tag{8.1}$$

A sample is considered stress relieved when its lattice spacing corresponds to the stress-free value of the material, $d_{0,hkl}$. In a stressed sample, the lattice spacing is stretched or compressed, which is observed as shift in the Bragg peak position, allowing the elastic strain ($\varepsilon_{hkl}$) to be calculated from:

$$\varepsilon_{hkl} = \frac{d_{0,hkl} - d_{hkl}}{d_{0,hkl}} = \frac{\Delta d_{hkl}}{d_{0,hkl}} \tag{8.2}$$

The measured strain direction is the bisector $Q$ of the scattering angle $2\vartheta$. If the elastic constant $E$ and Poisson's ratio $v$ of the sample material is known, the mean elastic stress within the gauge volume can be calculated from Hooke's tensorial law, Eq. (8.3). Full determination of the strain tensor requires measurements of strain in at least six independent directions. If the principal strain directions within the body are known, measurements along these three orthogonal directions are sufficient [17], Eq. (8.4-8.6).

$$\begin{Bmatrix} \sigma_i \\ \sigma_j \\ \sigma_k \\ \tau_{ij} \\ \tau_{jk} \\ \tau_{kl} \end{Bmatrix} = \frac{\mathrm{E}}{(1+v)(1-2v)} \begin{bmatrix} 1-v & v & v & 0 & 0 & 0 \\ v & 1-v & v & 0 & 0 & 0 \\ v & v & 1-v & 0 & 0 & 0 \\ 0 & 0 & 0 & 1-2v & 0 & 0 \\ 0 & 0 & 0 & 0 & 1-2v & 0 \\ 0 & 0 & 0 & 0 & 0 & 1-2v \end{bmatrix} \begin{Bmatrix} \varepsilon_i \\ \varepsilon_j \\ \varepsilon_k \\ \gamma_{ij} \\ \gamma_{jk} \\ \gamma_{kl} \end{Bmatrix} \tag{8.3}$$

$$\sigma_x = \frac{\mathrm{E}}{(1+v)(1-2v)} [(1-v)\varepsilon_x + v(\varepsilon_y + \varepsilon_z)] \tag{8.4}$$

$$\sigma_y = \frac{\mathrm{E}}{(1+v)(1-2v)} [(1-v)\varepsilon_y + v(\varepsilon_x + \varepsilon_z)] \tag{8.5}$$

$$\sigma_z = \frac{\mathrm{E}}{(1+v)(1-2v)} [(1-v)\varepsilon_z + v(\varepsilon_x + \varepsilon_y)] \tag{8.6}$$

BrightnESS² is funded by the European Union Framework Programme for Research and Innovation Horizon 2020, under grant agreement 823867

### 8.1.2. Neutron strain scanner

Neutron strain scanner is a neutron diffraction instrument optimised for three-dimensional spatially-resolved determination of residual stress through the measurement of average lattice spacing in polycrystalline materials. One of the major differentiating factors for classifying neutron strain scanners is whether it belongs to a continuous or pulsed neutron source. A continuous source generally offers higher flux, therefore allowing faster counting time and/or higher spatial resolution and/or penetration depth, but requires monochromatisation to select an optimum wavelength for single peak analysis of different sample materials. In contrast, a pulsed source allows simultaneous measurement of multiple diffraction peaks through the time-of-flight (TOF) method. Notwithstanding their different modes of operation, TOF and monochromatic strain scanners share the same main components in their configuration:

- **Sample stage.** A platform which usually comprises high-precision translation and rotation stages to position the sample. The stage enables accurate sample manipulation to enable measurement of strains at different locations within the sample (strain mapping) and different directions (multiple strain components). Additional equipment such as an Eulerian cradle and/or extra rotation stages is in some cases available to provide additional degrees of movement.
- **Beam apertures.** Collimators and/or slits containing high thermal neutron absorbing materials that enable tailoring of the beam dimensions. These optics shape the beam incident on the sample and limit the field-of-view of the detector as it acquires the beam diffracted from the gauge volume. The beam optics therefore directly influences the geometry of the instrumental gauge volume (IGV).
- **Sample alignment system.** A system which is typically based on mechanical (e.g., CMM touch probe) or optical (e.g., laser, camera or theodolite) probes that aid with the initial positioning and alignment of the sample with respect to the reference point (centroid of instrumental gauge volume).
- **Neutron detector system.** A system that records the diffracted neutron intensities as a function of angle (2-dimensional PSD in monochromatic instrument) or time-of-flight (in TOF instrument). The detector angular position ($2\vartheta_{det}$) with respect to the incident beam also defines the geometry of the instrumental gauge volume and the scattering vector, i.e., strain component.

### 8.1.3. Neutron diffraction for residual stress mapping

Stress and strain in most engineering components usually have directional and positional dependence, which requires measuring strain at a number of locations, i.e., strain mapping. This is achieved by translating and rotating the sample stage to desired positions. Most neutron diffraction investigations involve a general three-dimensional stress state that requires measurements along the principal (maximum) strain directions in three mutually orthogonal directions. After positioning the sample for a specific measurement, the diffracted intensity is recorded for a specified measurement time or number of counts. The general procedure for residual stress analysis at a single measurement point is:

1. **Mount and align the sample for measurement of strain along the first direction.** Secure the sample on the sample stage (directly or via Eulerian cradle or other sample environment system). Using the sample positioner system (*xyz*-translation stage or hexapod) align the sample so that the measurement point, indicated by the green circle in Figure 8-1(A), is accurately positioned at the reference point, Figure 8-1(B), coinciding with the centre of $\omega$-rotation shown by the red cross in Figure 8-1(B). The sample alignment is carried out with the help of the sample alignment system, whether mechanical or optical. Finally, the $\omega$-angle and

BrightnESS² is funded by the European Union Framework Programme for Research and Innovation Horizon 2020, under grant agreement 823867

detector angular positions are adjusted according to the strain direction for the desired reflection. Measure the diffracted signal against the specified measurement time.

2. **Measurement of strain along the second direction.** For instruments with a single PSD, the measurement in the second horizontal strain direction is performed by rotating the $\omega$-angle, Figure 8-1(C) by 90° when in principal direction. Since the reference point coincides with the centre of $\omega$-rotation, no additional sample alignment is needed. On instruments with two detector banks at $2\vartheta_{det} = \pm 90°$, two orthogonal strain components are acquired simultaneously in one measurement, Figure 8-1(B).
3. **Measurement of strain along the third direction.** For most instrument configurations, measurement in the third strain direction is achieved by removing and manually rotating the sample to have the desired direction along the scattering vector. This requires that the sample is re-mounted and re-aligned to enable measurement at the position of the previous measurements, Figure 8-1(D). Note that by using an Eulerian cradle or a robotic arm, this step can be performed without sample remounting.
4. **Measurement of another reflection and/or strain component.** In cases such as for composite materials and/or complex stress states, measurement of strains for more than 3 directions and/or from more than one *hkl* reflection is required and therefore other $2\vartheta_{det}$ and/or other angular orientation is necessary Figure 8-1(E).

Considering the procedures above, it is of the utmost importance to ensure adequate precision of the alignment of the reference point with the centre of $\omega$-rotation. In addition, it is worth noting the fact that neutron diffraction residual stress analysis is often used for measurement of engineering components (large and/or complex geometry, heavy load, etc). This situation, together with a possible lost in allowed positioning, hinders the use of Eulerian cradle or robotic arms and emphasizes the importance of precise sample alignment systems. Therefore, the positional accuracy between reference point vs. the centre of $\omega$-rotation and the precision of the sample alignment system are of the main subject of this report.

### 8.1.4. Entry scan for sample surface determination

Another procedure that is necessary to be described from the neutron diffraction residual stress mapping routine is the sample surface position determination by means of entry scans. It is a procedure where the gauge volume is immersed incrementally from outside into the bulk sample, Figure 8-2(A). The resulting intensity curves, both for reflection, Figure 8-2(B), and transmission geometry, Figure 8-2(C), are fitted with a model (that takes into account the coincidence gauge volume growth, measurement geometry and beam attenuation) to determine the position of the sample surface. The entry scan is useful in cases where very accurate positioning of/from the sample surface is needed, for example for near-surface residual stress analysis. In some cases, it also complements sample and/or instrument alignment methods. More detailed information about the entry scan methods are available elsewhere [17,18]. Additionally, the entry scan method is used for pseudo-strain correction (see Section 8.3.2).

## 8.2. Instrument calibration and alignment procedures

### 8.2.1. Instrument calibration

Calibration measurements are performed to ensure the accuracy of the absolute position of the Bragg peaks in the wavelength or time-of-flight spectrum. Elemental powders, typically silicon, ceria or alumina are used since they diffract neutrons well, have known d-spacing and non-overlapping diffraction peaks, exhibit a fine grain size, and are free from macrostresses. The angular (on a monochromatic instrument) or the temporal (on a TOF instrument) positions of the Bragg peaks are then compared against the tabulated data, and the instrument is calibrated accordingly.

BrightnESS² is funded by the European Union Framework Programme for Research and Innovation Horizon 2020, under grant agreement 823867

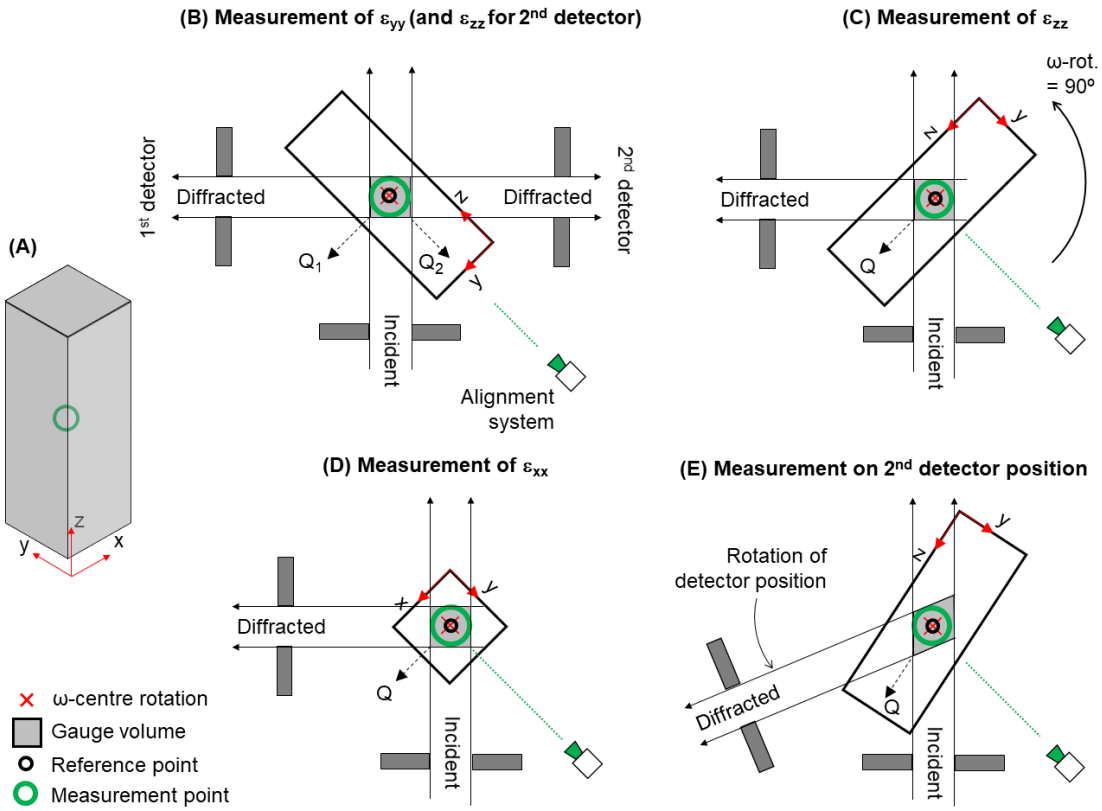


*Figure 8-1 Illustration of stress measurement steps at a neutron strain scanner: (A) The sample and its axes, with a desired measurement point indicated by the green circle; (B) Alignment of the measurement point to the instrument reference position and the measurement of the $\varepsilon_{yy}$ with the first detector and the $\varepsilon_{zz}$ with the second detector; (C) Measurement of the $\varepsilon_{zz}$ by rotating the ω by 90°; (D) Measurement of the $\varepsilon_{xx}$ by manually rotating the sample about the y-axis of the sample by 90° followed by re-mounting and re-alignment; (E) Measurement of another hkl reflection by changing the detector position.*

### 8.2.2. Instrument alignment

Instrument alignment involves adjusting the beam optics components (apertures) to ensure that the reference point, i.e., the centroid of the IGV, coincides with the centre of *ω*-rotation to allow changing of the measurement direction by rotating the sample without any need of re-alignment. Generally, instrument alignment is performed every time there is a configuration change in the optical path, e.g., changing from slit to radial collimator setup, and prior to sample characterisation. While there are slight variations of the procedures among instruments, the underlying principles are the same. The procedures of the instrument alignment techniques are described below, with some examples corresponding to the participating neutron instruments provided.

1. **Find the centre of *ω*-rotation.** The determination of the centre of *ω*-rotation can be done mechanically or optically:
    - Mechanical determination of the centre of *ω*-rotation, as performed on STRESS-SPEC, MPISI, and ENGIN-X, is carried out using accurately machined calibration pins, example shown in Figure 8-3(A) and (B), and a dial gauge. The methods vary slightly from instrument to instrument but essentially they comprise of rotating the pin by changing the *ω*-angle and, from the dial gauge offset reading, calculate the centre of rotation correction. A detailed example of this exercise on MPISI is available in [20].
    - Optical determination of the centre of *ω*-rotation, as performed on SALSA, is carried out using a telecentric camera with image recognition software, in conjunction with a pin with fiducial sphere, Figure 8-3(C). Firstly, the sample is placed in the camera field of view. Then the position of the sample at different *ω*-angles (range of ±360°) is tracked by the image

BrightnESS² is funded by the European Union Framework Programme for Research and Innovation Horizon 2020, under grant agreement 823867

recognition software. Since the $\omega$-rotation axis is parallel with the optical axis of the camera, the trace of the sample at different $\omega$-angles forms a circle, which can be fitted to determine the centre of $\omega$-rotation.

2. **Adjust the sample alignment system.** The sample alignment system is adjusted with respect to the centre of $\omega$-rotation. For a mechanical alignment system, e.g., CMM probes, the position of the centre of $\omega$-rotation is recorded. For system such as theodolites and telecentric cameras, the optical axes are aligned to the centre of $\omega$-rotation.
3. **Align the beam apertures optical axes.** The optical axes of incident/primary and diffracted/secondary beam apertures are aligned using a calibration pin, preferably with diameter smaller than the GV width. The pin is securely mounted at the centre of $\omega$-rotation. There are two options for alignment procedures:
   i. Scan the apertures with the pin stationary at the centre of $\omega$-rotation, Figure 8-4(A), or;
   ii. Scan the pin across the beams. The pin scan for secondary beam aperture is preferably carried out along the centre line of the primary beam, and vice-versa, Figure 8-4(B). This is to prevent the influence of the beam intensity profiles producing false measurement.

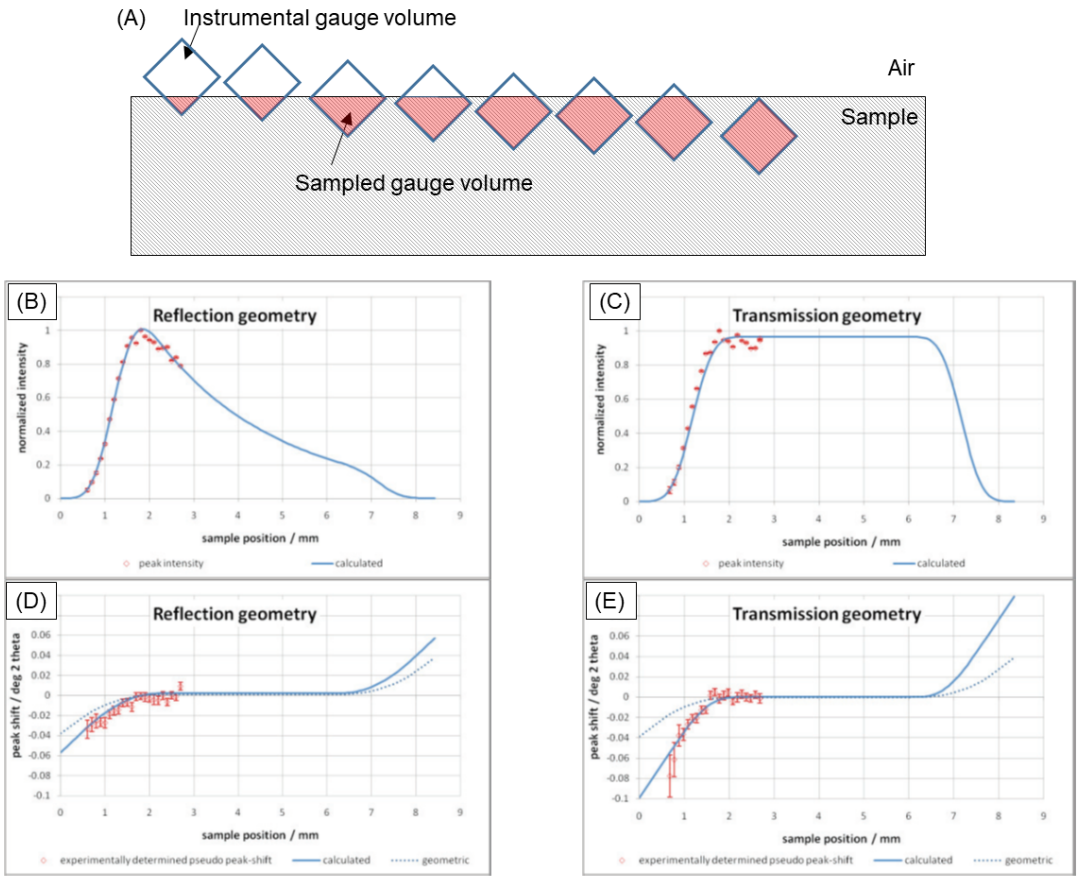


*Figure 8-2 (A) Illustration of the entry scan procedure; Entry curve and the analytical model for (B) reflection and (C) transmission geometries; experimentally determined pseudo peak shift and analytical model, showing geometric shift (dotted line) and taking into account the wavelength distribution (solid line) for (D) reflection and (E) transmission geometry [19].*

BrightnESS² is funded by the European Union Framework Programme for Research and Innovation Horizon 2020, under grant agreement 823867

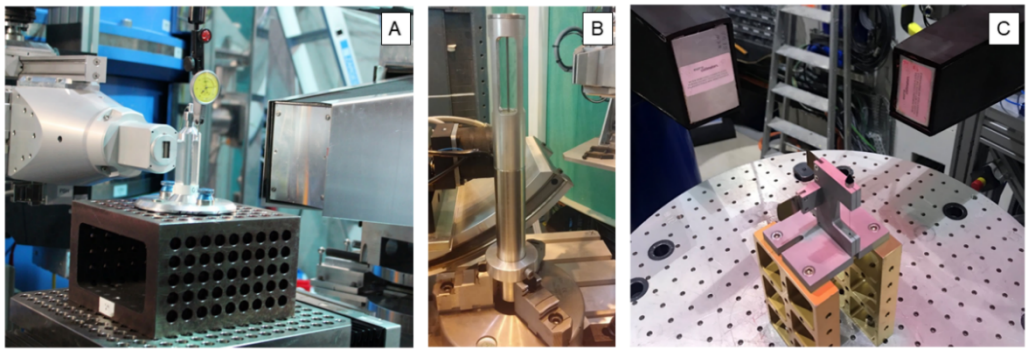


*Figure 8-3 Example of samples used for instrument alignment purposes on (A) STRESS-SPEC, (B) MPISI, and (C) SALSA.*

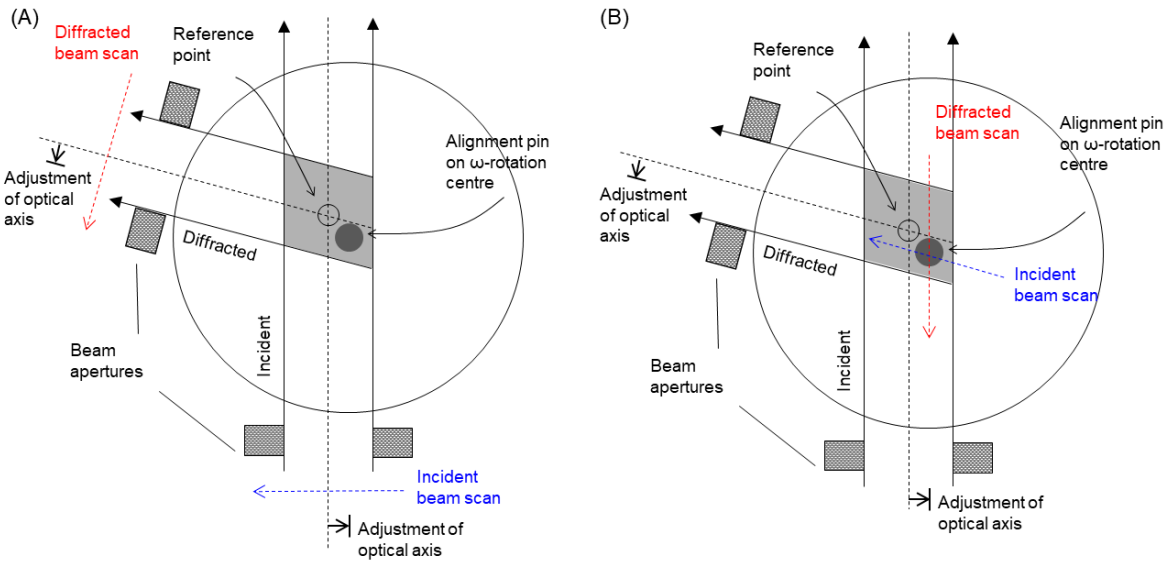


*Figure 8-4 Alignment of the beam apertures using (A) aperture scans, and; (B) pin scans.*

From the intensity curve, the position of the pin centre relative to the beam aperture optical axis can be determined and an adjustment of the later is made accordingly. Using the option (ii), projection of the offset needs to be considered when making the adjustment, if the $2\vartheta_{det}$ is not exactly at 90°. The acceptable accuracy of this alignment is 10% of the GV width, i,e., 100 µm for 1 mm GV width.

## 8.3. Uncertainties of neutron diffraction residual stress mapping

In a three-dimensional spatially-resolved residual stress analysis on a neutron strain scanner, the uncertainty can generally be categorised into two contributions: i) error in the positioning of the sample with respect to the reference point and; ii) error in the lattice spacing determination. With this report the emphasis is on the characterisation of the former, while the details on the combined standard uncertainty calculation for strain measurement is given in the ISO 21432:2019(en) [13].

### 8.3.1. Position inaccuracy

Positioning inaccuracy of the sample with respect to the reference point will introduce a systematic error in the location of measured strain. Reviewing the instrumentation and the procedures of neutron diffraction residual stress analysis in previous sections, the possible source of positional inaccuracy are:

BrightnESS² is funded by the European Union Framework Programme for Research and Innovation Horizon 2020, under grant agreement 823867

1. **Error due to the mechanical components of the instrument** (e.g., accuracy of the translation and rotation of the sample stage). The accuracy is different for each instrument, and the corresponding value for the participating neutron strain scanners are listed in Table 9-1.
2. **Misalignment between reference point and centre of *ω*-rotation**. Due to this misalignment, a rotation of the sample (for example to measure different strain component) will result in displacement of the gauge volume relative to the sample. The misalignment can be caused by the inaccuracy in the instrument alignment procedures.
3. **Misalignment between two detector banks.** At instruments with two detector banks (e.g., TOF configurations), misalignment between the optical axes will cause the measurements of two strain components effectively taken from volumes at two different locations.
4. **Precision of sample alignment system.** Since the stress measurement procedures require re-mounting and re-alignment, the ability of the alignment system to re-position the sample to the same measurement location influence the positional accuracy.
5. **Positional change of GV for different detector position.** Dependent on the beam optics employed, changing the detector angular position may lead to shifts in the GV position, among other factors, might be caused by the non-concentricity between the centre of *ω*- and detector rotation.
6. **Accuracy of the entry curve analysis software.** A neutron entry scan can be used to determine the sample surface position (Section 8.1.4), which might be a reference for the position of measurement points. Therefore, the accuracy of the entry curve analysis software affects the positional accuracy.

### 8.3.2. Error in lattice spacing determination

The underlying principle of residual stress analysis by neutron diffraction is an accurate determination of relative lattice spacing. There are a number of factors influencing the accuracy of lattice spacing determination:

1. The detector angular or temporal response to the diffracted beam, for monochromatic and TOF instruments, respectively, determines the accuracy of the absolute Bragg peak position. The detector response is usually calibrated using a powder sample with a known lattice parameters and well-defined peaks (see 8.2.1). The repeated measurement of a calibration sample is one of the methods to determine the stability of the instrument setup, and can be compared to the fitting uncertainties.
2. Fitting uncertainties introduces errors to the lattice spacing determination. Due to the shape of the Bragg peak (instrumental and sample material effect), a mathematical model is normally used to fit the signal and to determine the absolute Bragg peak position. These fitting uncertainties are widely used to determine the strain, and eventually the stress, error (see [14] for details).
3. Pseudo peak shift, example shown in Figure 8-2(D) and (E), due to geometric displacement of the centre of gravity of the intensity distribution in the sampled gauge volume, and in addition the beam divergence and the wavelength distribution within the gauge volume, may introduce a false contribution to the absolute Bragg peak position. This is especially sensitive in the case when a position-sensitive detector (PSD) is used in a monochromatic instrument. This effect can be well characterised and corrected, which detailed description of the method available elsewhere [19,21].

The contribution of these errors in lattice spacing determination is well reported, and therefore will not be further investigated in this work. Microstructural contributions such as grain size, crystallographic texture, choice of $d_0$ reference, elastic constant, etc. are also beyond the scope of the present project task.

BrightnESS² is funded by the European Union Framework Programme for Research and Innovation Horizon 2020, under grant agreement 823867

## 9. Beamtime Campaign for Instrument Benchmarking

The beamtime calibration campaign was carried out to evaluate the positional accuracy of the setup and alignment of the participating neutron strain scanners. Note that the evaluations were performed after the routine instrument alignment procedures on each instrument. More specifically, the key objectives of the measurements are:

1. To quantify the misalignment between the reference point and the centre of $\omega$-rotation.
2. To quantify the GV shift due to the change of detector position, for instruments with a single detector.
3. To quantify the misalignment between GVs from different detectors, for instruments with multiple detectors.
4. To quantify the precision of the instrument's sample alignment system (i.e., cameras & theodolites).
5. To quantify the accuracy and the robustness of the entry curve analysis software used on the instruments.

The measurement campaigns were performed on the four participating instruments between July 2019 and February 2020. Three sets of samples, designed in accordance with the above-mentioned objectives, were prepared and delivered to the four participating instruments. A standard of measurement procedures was followed. This was a dynamic exercise where, from each measuring campaign, results were shared and discussed among participants to adapt slight variations in the priority of measurements and to accommodate different specifications between the instruments.

### 9.1. Participating neutron strain scanners

The technical specifications of the four participating strain scanners are listed in Table 9-1, with short descriptions of the main components and setups of each are given in the following subsections.

#### 9.1.1. SALSA

SALSA is a monochromatic neutron strain scanner optimised for residual stress analysis of engineering components [22]. SALSA is one of the suite of forty instruments at the continuous reactor source of the Institut Laue-Langevin (ILL) in Grenoble, France. It is installed on a super-mirror neutron guide with relative critical angle of reflection $m$ = 2. The super-mirror guide delivers high neutron flux, while the instrument's location on a guide-tube ensures low background. A schematic of the main components of the instrument is provided in Figure 9-1.

The SALSA monochromator is double-focusing type with a column of bent Si perfect crystals. This provides the advantage of increased neutron flux at the sample position due to a lateral condensation of the beam and higher angular resolution due to focusing in momentum space. In combination with radial focusing collimators, the configuration aims at maximising the flux at the sample position and while achieving optimum lateral and angular resolution. The neutron flux at the sample position is in the range of $10^7$ n/cm$^2$/s. The Si monochromator provides a wavelength range of 1.3-3 Å, ideal for most engineering metal applications (Fe-, Al-, Ni-, Ti- alloys, etc.). Wavelength selection and flux optimisation is done by changing the beam take-off angle from the monochromator and displacing the delta table accordingly [22]. Neutron detection is carried out by a 2-D microstrip PSD with an active area of 80 × 80 mm$^2$, covering 5° in $2\vartheta$. The resolution is 128 × 128 pixel, with extrapolation between the filaments producing effective resolution of 256 × 256 pixel.

Radial collimators and/or slits can be used for gauge volume definition, both on the primary (incident) beam and the secondary (diffracted) beam sides. The suite of radial collimators on SALSA provide options to respectively define a beam with full-width-at-half-maximum of either 0.6 mm, 2 mm or

BrightnESS² is funded by the European Union Framework Programme for Research and Innovation Horizon 2020, under grant agreement 823867

4mm (horizontal and vertical, arranged in series) for both the primary and secondary beam. For more flexible gauge volume dimensions, automated slit systems may be used instead.

One of the unique features of SALSA is its use of hexapod as sample manipulator. This is basically a robot with six degrees of freedom achieved by using six independent hydraulically controlled (parallel kinematic) pistons. The construction is compact, light, yet very stiff and therefore ideal for accurate manipulation of heavy samples. It enables sample support of over 850 kg, with a range of motion of ±300 mm translation in *x* and *y*, 150 mm in *z*, and tilt range of ±30°. A ¼ Eulerian cradle and a compact rotation stage are also available to mount on top of the hexapod to provide an extra angular motion for sample orientation vs. scattering vector *Q* (i.e., strain component). The hexapod slides on air-pads on a 2.5 $m^2$ delta table, adding 700 mm horizontal translation and 360° omega-rotation to the work-space of the hexapod. The delta table is the base for all primary and secondary optics supports, also containing the omega rotation bearing below the hexapod, hence providing the link between the incoming and diffracted beam axes, coupled with omega. The concept enables maintaining the measuring geometry after wavelength changes and/or adjustments (change of the take-off angle). A telecentric camera system with on-screen measurement features is used for sample alignment. The movement direction of the sample along the axes follows the nomination provided in the schematics of Figure 9-1, with a more detailed description of SALSA can be found elsewhere [22].

Data reduction is performed by the Large Array Manipulation Program (LAMP) software developed at ILL. Strain/stress calculations as well as pseudo-strain correction from entry scans are performed using in-house developed MathCad-based codes (Pirling, personal communication, 2019), and a Phyton-based routine (Cabrera and Cabeza, personal communication, 2019).

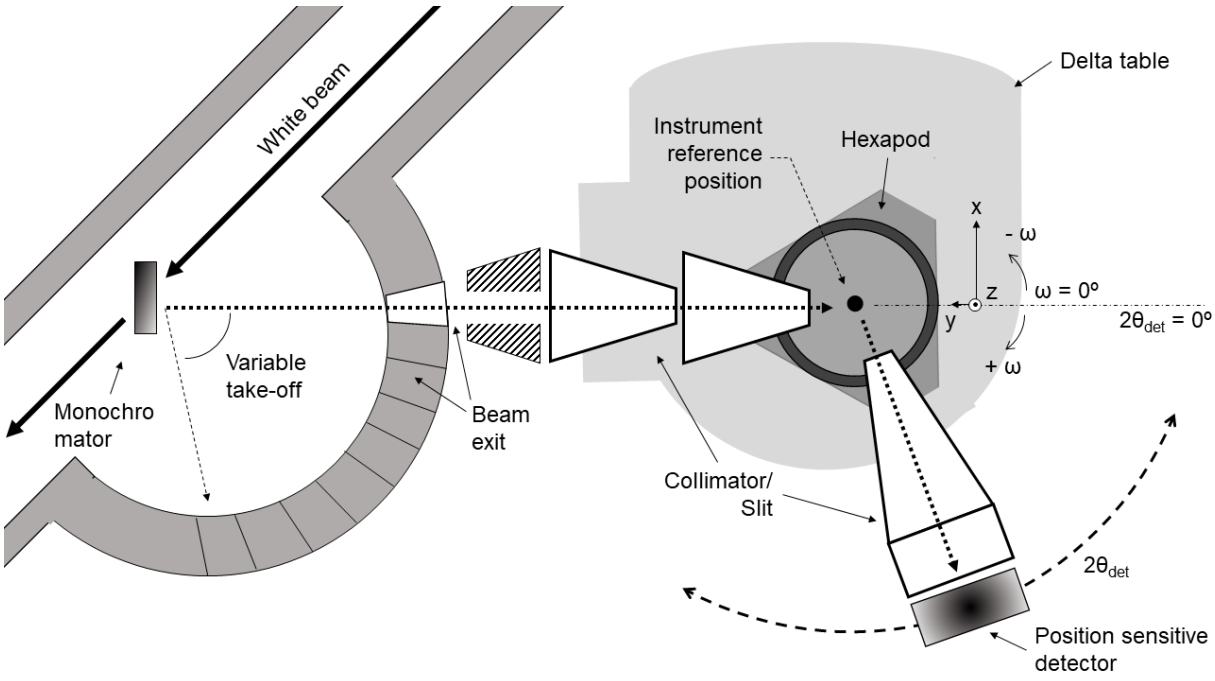


*Figure 9-1 Schematics of the main components of SALSA*

BrightnESS² is funded by the European Union Framework Programme for Research and Innovation Horizon 2020, under grant agreement 823867

*Table 9-1 Technical specification of the four participating strain scanners*

| Instrument Name | SALSA | STRESS-SPEC | MPISI | ENGIN-X |
|---|---|---|---|---|
| Location | ILL, Grenoble France | FRMII, Munich, Germany | SAFARI-1, Pretoria, South Africa | ISIS, Didcot, United Kingdom |
| Mode of operation | Constant wavelength | Constant wavelength | Constant wavelength | TOF |
| Monochromator/ Moderator & Take-off angle [°] | Bent Si(400), (422), (511), (311), 55 -123 | Ge(511), Bent Si(400), Pyrolytic Graphite(002), 35 - 110 | Bent Si(110), (551), (331), (553), 83.5 | Methane moderator |
| Wavelength [Å] | 1.3 – 3 (Monochromatic) | 1 – 2.4 (Monochromatic) | 2.53, 1.01, 1.65, 0.93 (Monochromatic) | 0.5 – 6 (Polychromatic) |
| Beam optics [mm] | Primary slit 0.3 – 5 horiz., 0.4 – 50 vert.; Secondary slit 0.3, 5 horiz., 25, 50 vert. Radial col. 0.6 & 2 | Primary slit up to 7 × 17; Secondary slit up to 15; Radial col. 0.5, 1, 2, & 5 | Slit 0.3-5 horiz., up to 20 vert; Radial col. 1, 2, 5, & 10 | Primary slits 0.2-20 vert. 0.2-10 horiz. Secondary radial col. 0.5, 1, 2, 3, & 4 |
| Sample positioning system (SPS) | Hexapod, max. load 1000 kg, *xy*-range ±300 mm, *z*-range 150 mm, tilt & rotation, ¼ cradle | *xyz*-stage max. load 300 kg, *xy*-range ±125 mm, *z*-range 300 mm, Eulerian cradles | *xyz*-stage, max.load 250 kg, 250 mm range to all axis, ¼ cradle | *xyz*-stage, *xy*-range ±250 mm, *z*-range 700 mm, 370° in *ω*, max. load 1000 kg |
| SPS accuracy | ±20 µm for > 500 kg sample | ±10 µm for 250 kg sample | ±10 µm for 250 kg sample | 10 µm/100 mm for 500 kg sample |
| Detector | PSD 80 × 80 mm², 256 × 256 pixel | $^3$He-PSD, 256 × 256 mm², 256 × 256 pixel, resolution $\Delta x,y < 1.3$ mm | DENEX $^3$He-PSD 300 × 300 mm² resolution 2 mm horiz. × 3 mm vert. | +/- 90° diffraction banks, ZnS scintillator, 3 m horizontal resolution |
| Sample alignment | Telecentric camera + CMM touch & laser probe | Theodolite | Theodolite | Theodolite |

### 9.1.2. ENGIN-X

ENGIN-X is a renowned time-of-flight (TOF) neutron strain scanner located at the ISIS neutron and muon source, Didcot, UK, and the only TOF instrument participating in the current project. ENGIN-X is located in the extension building of Target Station 1 (TS-1), with the primary flight-path, i.e., the distance from the instrument reference point to the methane moderator, of ~50 m. Figure 9-2 illustrates the main components of ENGIN-X, with the instrument axes placed at the instrument reference position. Two sets of disk choppers located at 6 m and 9 m from the moderator are available to shape the incident spectrum, with the full range of the polychromatic beam available from 0.5 - 6 Å. The neutron flux at the sample position is in the range of $10^6$ n/cm²/s. The instrumental gauge volume across the incident beam is defined by a set of motorised slits, with a vertical dimension of 0.3-30 mm and horizontal dimension of 0.3-10 mm. The slit assembly is retractable along the rail in the beam direction and can be adjusted in the *y*-axis direction to align the beam with the instrument reference point.

BrightnESS² is funded by the European Union Framework Programme for Research and Innovation Horizon 2020, under grant agreement 823867

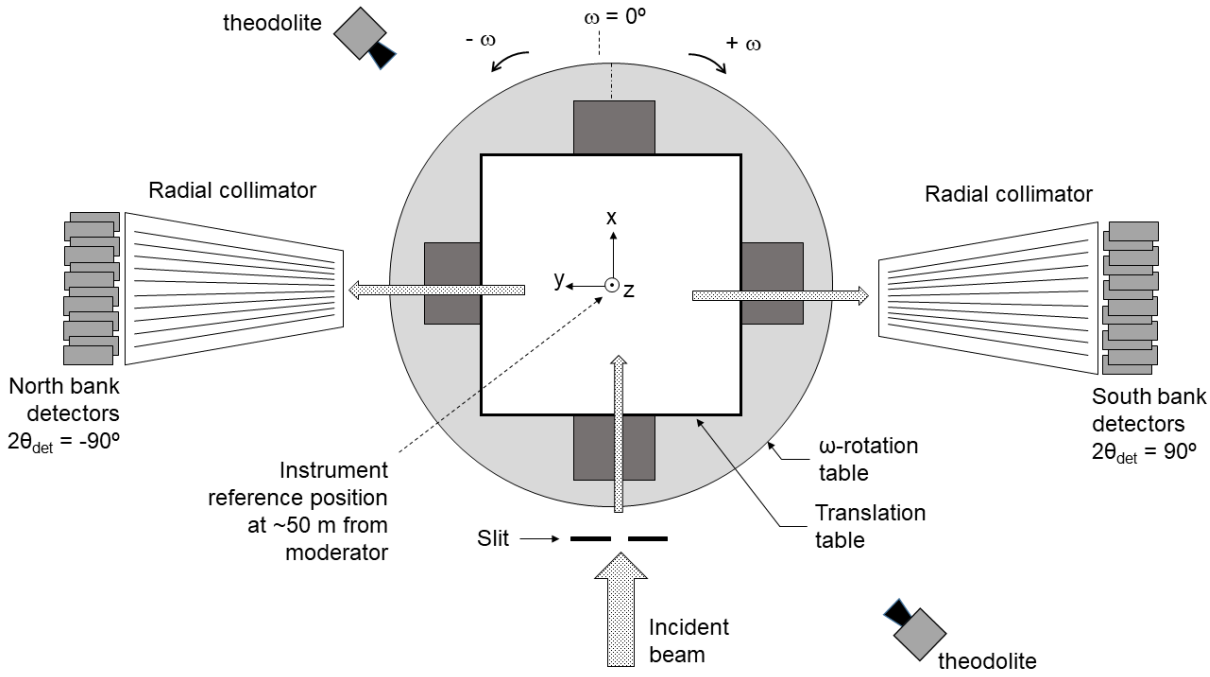


*Figure 9-2 Schematics of the ENGIN-X main components*

ENGIN-X has two detector banks (North (NB) and South (SB)) of ZnS scintillators, fixed at 2θ = ±90° to the incident beam and ~1.53 m from the instrument reference point, covering ±16° in the horizontal plane and ±21° in the vertical plane. The instrumental gauge volume along the incident beam is defined using radial collimators, which are interchangeable with 0.5, 1, 2, 3, and 4 mm gauge-width (FWHM) options. The ENGIN-X sample stage consists of a translation table positioned on top of an *ω*-rotation table, offering sample movement in the *x, y, z*, and *ω* axes, with a range of motion of ±250 mm in *x* and *y*, 700 mm in *z*, and 370° in *ω*. It can handle a sample weighing up to 1 tonne, with movement accuracy of 10 µm/100 mm for a 0.5 tonne sample. A pair of theodolites is installed for precise alignment of samples, which positions are illustrated in Figure 9-2. Open-Genie-based software is available for data reduction, while Align software (Luzin, personal communication, 2019) is available for the determination of the sample surface position from entry scans. The movement direction of the sample along the axes follows the nomination provided in the schematics of Figure 9-2. A more detailed description of ENGIN-X can be found elsewhere [23].

### 9.1.3. STRESS-SPEC

STRESS-SPEC is a monochromatic neutron diffractometer which offers strain scanning as well as texture analysis capabilities. It is located at the SR-3 thermal beam port of the 20 MWth FRM II reactor in Munich, Germany. The instrument offers a flexible monochromator setup using three different monochromators: Ge(511), bent Si(400) and pyrolitic graphite PG(002). These, together with variable take-off angles ranging from 35° to 110°, allow optimisation between resolution and intensity for each measurement case. The wavelength range of the incident beam is 1 - 2.4 Å, and the neutron flux at the sample position is in the order of $10^7$ n/cm$^2$/s.

The schematic drawing of the STRESS-SPEC instrument is presented in Figure 9-3. The instrumental gauge volume across the incident beam is defined by a set of slits, which is continuously variable up to 7 mm horizontal and 17 mm vertical opening. Across the secondary beam, the slits are continuously variable up to 15 mm. In addition, radial collimators with FWHM of 0.5 mm, 1 mm, 2 mm, and 5 mm are also available. To manipulate and scan the position of the sample, an *xyz*-sample positioning stage with 300 kg capacity is available. The travel of the *xy*-translation is ±125 mm and the *z*-translation is 300 mm, with a precision of ~10 µm. A full circle Eulerian cradle with a maximum load of 5 kg and ¼

BrightnESS² is funded by the European Union Framework Programme for Research and Innovation Horizon 2020, under grant agreement 823867

circle Eulerian cradle for heavy samples are also available. Additionally, a positioning system consisting of a Stäubli-6-axes robotic arm (payload up to 30 kg) can be mounted instead of the standard sample stage, which offers more flexibility and allows automatic sample changes.

STRESS-SPEC uses an in-house built $^3$He position sensitive detector [24], with an active area of 256 × 256 mm$^2$ with 256 × 256 pixel. The position of the sample is mainly aligned using a theodolite located in the instrument as shown in Figure 9-3. STeCa software is used for data reduction [25], while determination of sample surface position from entry scans is performed using Align software (Luzin, personal communication, 2019). The movement direction of the sample along the axes follows the nomination provided in the schematics of Figure 9-3. A more detailed description of STRESS-SPEC can be found elsewhere [26].

### 9.1.4. MPISI

MPISI is a monochromatic strain scanner located on radial beamline 5 of the 20 MWth SAFARI-I research reactor, near Pretoria, South Africa. The instrument uses a double-focusing Si multiwafer monochromator, with the (110), (551), (331) and (553) reflections accessible by horizontal rotation of the monochromator. The horizontal focus is variable to enable increased neutron flux at the sample position due to lateral condensation of the beam and higher angular resolution due to focusing in momentum space. The primary beam is extracted through the 83.5° take-off angle, giving respective wavelengths 2.53 Å, 1.01 Å, 1.65 Å and 0.93 Å. The Si(331) reflection is normally used for strain analysis since it provides the reflection of interest in most engineering materials close to diffraction angle 2$\vartheta$ of 90°, hence optimum gauge volume definition. The neutron flux at the sample position is in the order of $10^6$ n/cm$^2$/s.

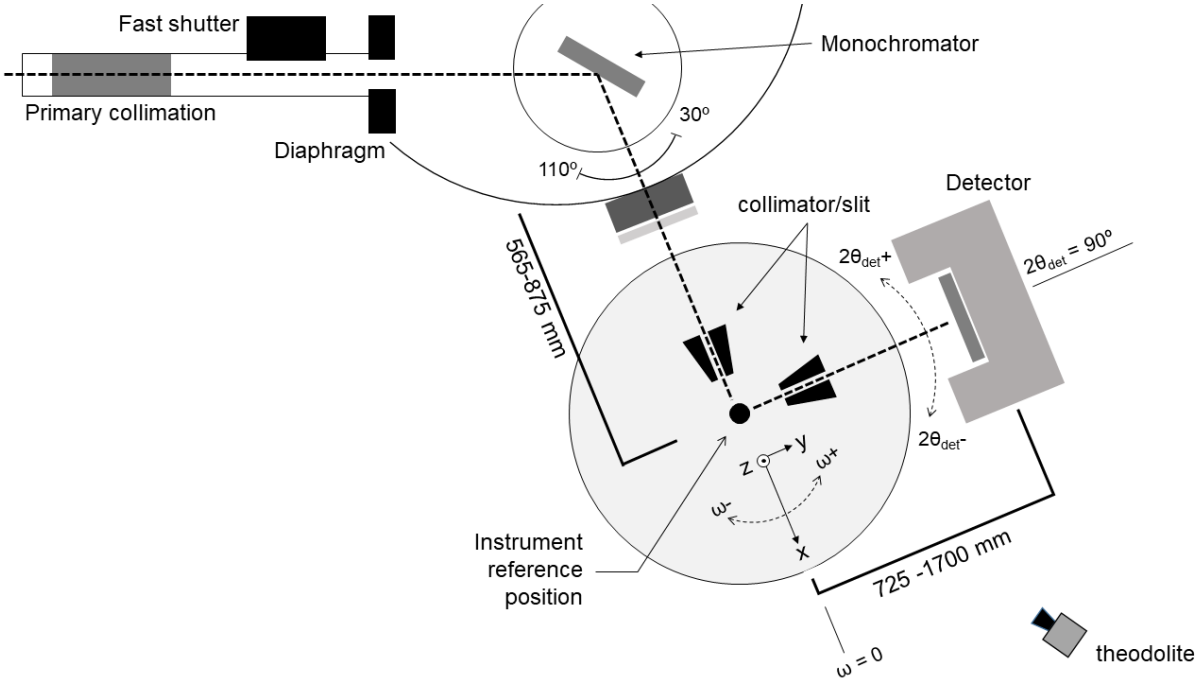


*Figure 9-3 Schematics of the STRESS-SPEC main components*

BrightnESS² is funded by the European Union Framework Programme for Research and Innovation Horizon 2020, under grant agreement 823867

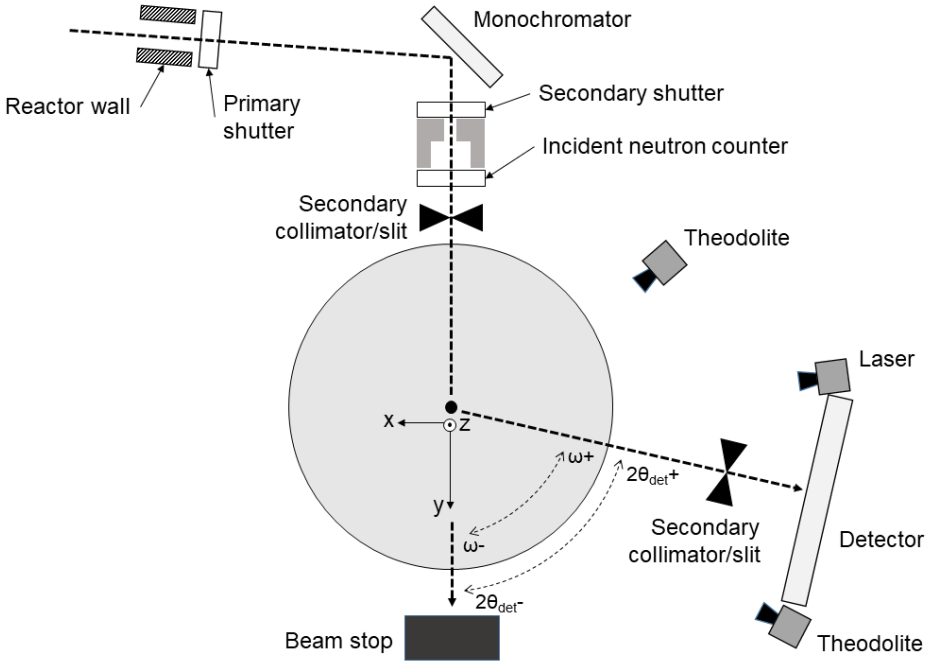


*Figure 9-4 Schematics of the MPISI main components*

The gauge volume is defined by primary and secondary slits with variable dimension 0.3 – 5 mm in the horizontal and up to 20 mm in the vertical. The secondary slit is interchangeable with radial collimators with FWHM of 1 mm, 2 mm, 5 mm and 10 mm. The sample stage used in the instrument is a Huber integrated *xyz*-stage with maximum load of 250 kg and 250 mm travel on all linear stages. A ¼ Eulerian cradle is also available. The MPISI's detector is a $^3$He-filled Denex 300TN multiwire area neutron detector with 300 × 300 mm$^2$ active area, providing $2\vartheta$ coverage of ~14° at 1150 mm from the sample. The sample alignment system at the instrument consists of a pair of theodolites located at the positions indicated in the schematics in Figure 9-4. ScanManipulator [27], an in-house developed software platform, is used to perform comprehensive data treatment, including determination of the sample surface position from entry scans and Bragg peak fitting. Align software (Luzin, personal communication, 2019) is also used interchangeably for entry curve analysis. The movement direction of the sample along the axes follows the nomination provided in the schematics of Figure 9-4. A more detailed description of MPISI can be found elsewhere [28].

### 9.2. Test samples

For the purpose of evaluating the setup and alignment of the instruments, test samples with specific geometries were manufactured. Three identical sets of calibration samples were prepared and the sample sets shown in Table 9-2 supplied to the instruments. Each set comprises three different samples: 1) Calibration Foils & pin sample; 2) 5-wall sample, and; 3) Tube sample. While the prototype of the Foils & pin sample (Set 0) was measured, the results are not reported in this text, and SALSA results related to Foils & pin sample presented in this report are from the measurement of Set 1. As a benchmark reference for the wall thickness from neutron measurements, the geometry of the samples was characterised using a coordinate measurement machine (CMM) at ILL. The specifications of each calibration sample are detailed in the following sections.

BrightnESS² is funded by the European Union Framework Programme for Research and Innovation Horizon 2020, under grant agreement 823867

*Table 9-2 Distribution of the sample sets for measurement campaigns. Set 0 is the prototype of the Foils & pin sample. SALSA results related to Foils & pin sample presented in this report are from the measurement of Set 1.*

| | SALSA | ENGIN-X | STRESS-SPEC | MPISI |
|---|---|---|---|---|
| Foils & pin Sample | Set 0, 1 | Set 0 | Set 2 | Set 3 |
| 5-wall sample | Set 1 | Set 2 | Set 1 | Set 3 |
| Tube sample | Set 1 | Set 2 | Set 1 | Set 3 |

### 9.2.1. Calibration Foils & pin sample

The Foils & pin sample consists of two thin foils, individually mounted perpendicular to each other (namely top and bottom foil) and a vertical pin, all three made of ferritic steel and mounted on an aluminium frame, as shown in Figure 9-5(A) and (B). The thickness of the foils is 0.3 mm, and they are inserted into a window-like structure on the frame to avoid bending of the foils and to ensure perpendicularity between them. The foil length exposed by the window is 12.5 mm. Interchangeable pins are available (with diameters of 0.3 mm, 1 mm, and 2 mm) and can be mounted in the assembly. A fiducial sphere with 1 mm diameter sits on top of the pin, as a reference to help with aligning the vertical pin to the reference point, Figure 9-5 (A).

The sample was used to determine the instrumental gauge volume (i.e. dimensions and centroid position for a given set up). The perpendicular foil configuration allows for the measurements in transmission ($Q$ vector perpendicular with the scan direction) and reflection ($Q$ vector parallel to the scan direction) geometry without the need of rotating the sample about the $\omega$-axis.

### 9.2.2. 5-wall sample

The 5-wall sample consists of five identical walls with thickness of 8 mm, evenly spaced with a distance of 22 mm, and width of 20 mm. The sketch with sample dimensions is shown in Figure 9-6(A). The 5-wall sample was machined from a block of austenitic steel, Figure 9-6(B), and has general tolerances as specified by ISO 2768-f. The naming convention of the wall surfaces are according to Figure 9-6(C), where the five walls are numbered from 1 to 5, and each wall has two surfaces A and B, therefore Wall1A, Wall1B, Wall2A, ..., Wall5B. The 5-wall sample allows repeated scans of identical and a relatively simple-to-align geometry, and therefore can be efficiently used to study the reproducibility and precision of the alignment system using a single sample. Measuring the thickness of the walls with a CMM and comparing it against the neutron measurements, allow for the quantification of the accuracy of the entry scan software.

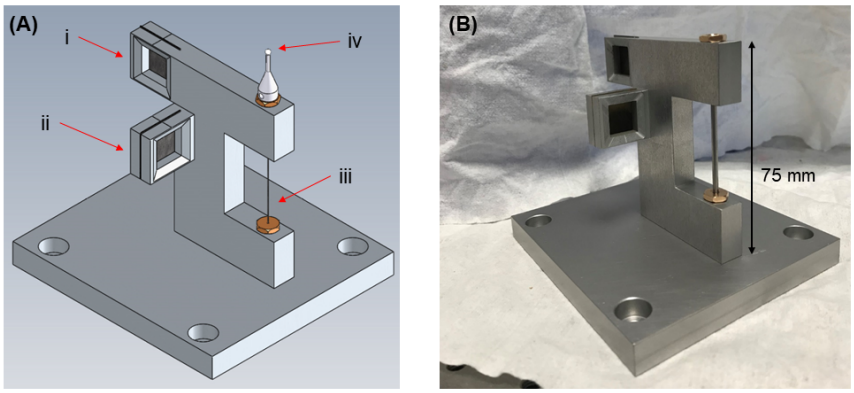


(i) → Top foil (0.3 mm)
(ii) → Bottom foil (0.3 mm)
(iii) → Pin (variable: 0.3 mm, 1 mm, 2 mm)
(iv) → Fiducial sphere

*Figure 9-5 (A) Drawing of the Foils & pin sample, indicating the main parts; (B) photograph of the Foils & pin sample. The foils are mounted in aluminium frame to prevent bending.*

BrightnESS² is funded by the European Union Framework Programme for Research and Innovation Horizon 2020, under grant agreement 823867

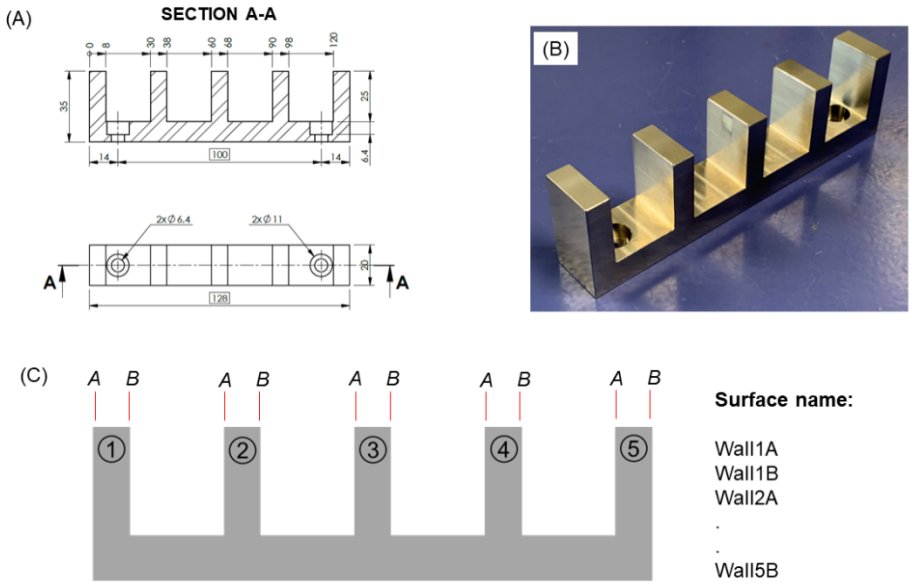


*Figure 9-6 (A) Drawing and; (B) photograph of the 5-wall sample; (C) The naming convention of the wall surfaces for the neutron measurements.*

### 9.2.3. Tube sample

The Tube sample has an outer diameter of 100 mm and wall thickness of 5 mm, Figure 9-7(A). It is machined from an austenitic steel block with general tolerances specified by ISO 2768-f. The Tube sample was used to study the robustness of the different entry curve analysis software tools to locate curved surfaces, encompassing a more complex immersion of the GV into surface and bulk material. Important features of the Tube sample are radial line and offset line. The 'radial line' is a line perpendicular to the sample surface which intersects the tube axis, while the 'offset line' is a line which is parallel with the radial line, with a given offset on the same horizontal plane.

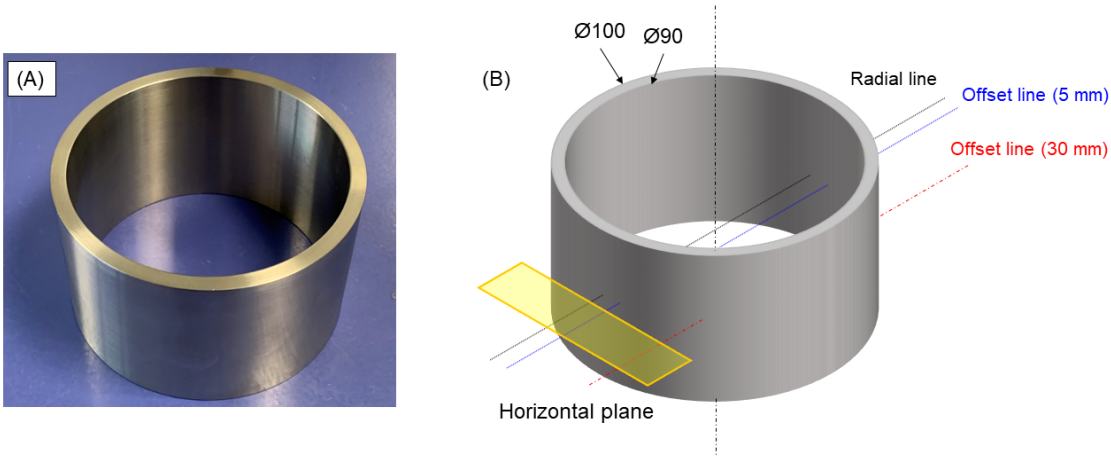


*Figure 9-7(A) Photograph and; (B) drawing of the Tube sample. Examples are given for the offset line at 5 mm and 30 mm.*

BrightnESS² is funded by the European Union Framework Programme for Research and Innovation Horizon 2020, under grant agreement 823867

# 10. Quantification of Reference Point Position

## 10.1. Methods

In order to investigate the relationship between detector angular position ($2\vartheta_{det}$) and the GV position as applicable to monochromatic instruments, pin scans were performed. The pin of the Foils & pin sample was scanned towards the primary beam, and the $\omega$-angle was kept fixed during the measurement at different detector positions to eliminate additional uncertainty due to $\omega$-rotation. The illustration of an example of the pin scan exercise carried out in this work is given in Figure 10-1, while the summary of the pin scan exercises on the participating instruments is given in Table 10-1. The incident wavelength on all of the instruments was around 1.67 Å. Note that for some of the setups, re-alignment was performed for each detector position and/or two different beam aperture setups (secondary collimator and slit). The position-dependent intensity values were fitted with a Gaussian function to determine the centre position of the GV for each detector position.

*Table 10-1 Pin scan exercises on the participating strain scanners to determine GV position at different detector position.*

| Instrument | Measured reflection *hkl* | Detector position ($2\vartheta_{det}$) | GV size: $w \times h$ (prim. beam) × $w$ (sec. beam), mm³ | Beam apertures (Primary Secondary) | Re-alignment at each detector position |
|---|---|---|---|---|---|
| SALSA | Fe(211) | 93.5° | 0.6 × 2 × 0.6 | Col. – Col. | No |
| | Fe(110) | 49.8° | | | |
| STRESS-SPEC | Fe(211) | 92° | 1 × 10 × 1 | Slit – Col. | No |
| | Fe(200) | 72° | | Slit – Slit | Yes |
| | Fe(110) | 49° | | | |
| MPISI | Fe(211) | 90° | 1 × 10 × 1 | Slit – Slit | Yes |
| | Fe(110) | 50° | | | |
| | Fe(220) | 105° | | | |

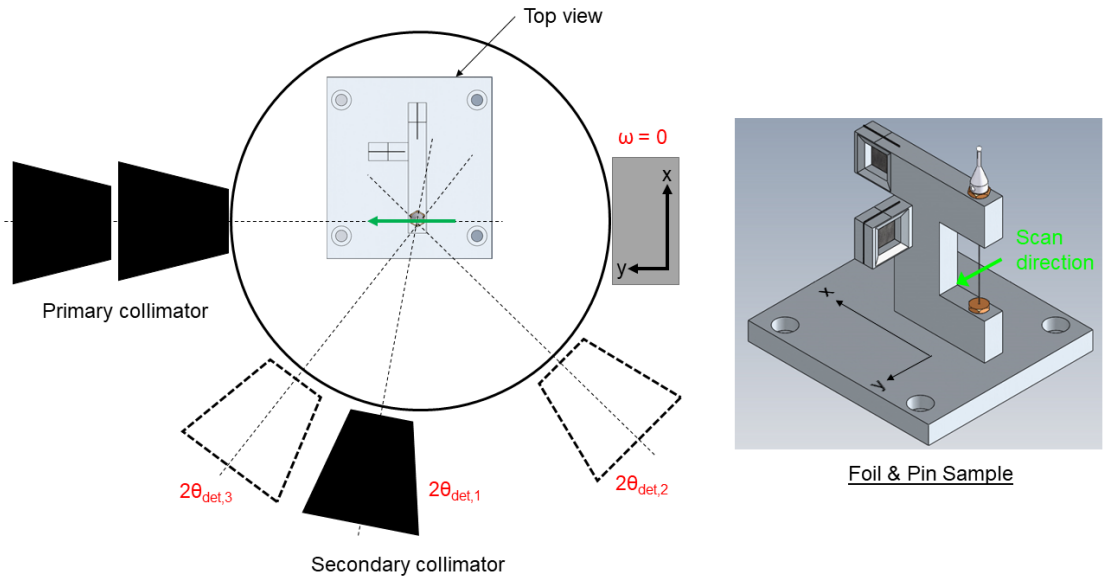


*Figure 10-1 Illustration of pin scan to study the effect of detector position to GV position. Pin scans were performed using different detector positions while keeping the ω-angle constant.*

BrightnESS² is funded by the European Union Framework Programme for Research and Innovation Horizon 2020, under grant agreement 823867

In order to determine the position of the reference point (IGV centroid) with respect to the centre of $\omega$-rotation, scans were performed on the top and bottom foil. The scans were executed with the foils aligned parallel to the bisectors between the primary beam and the secondary beam. At one particular detector position, the measurements were carried out for three orthogonal $\omega$-angles, with the examples given in Figure 10-2. The summary of the foil scan exercises on the participating instruments is given in Table 10-2.

During the measurement on ENGIN-X, which was the first instrument to be characterised in the project task, only the prototype of the Foils & pin sample was available and the foil scan exercises have not yet been proposed. Therefore, the data from the wall scans of the 5-wall sample was used instead to determine the position of the reference point with respect to the centre of $\omega$-rotation. The wall scans were mainly intended to determine the precision of the sample alignment system and to evaluate the accuracy of the entry curve analysis software. However, on ENGIN-X, the wall scans were carried out using four orthogonal $\omega$-angles, i.e., −135°, −45°, 45°, and 135°, therefore the position of the reference point can be estimated. The wavelength range used was 0.7-3.1 Å, and the intensity curve from multiple Fe reflections, including Fe(111), Fe(200), Fe(220), Fe(222) and (311) was integrated. The gauge volume dimension was 2 mm × 2 mm × 10 mm, and both the north and the south detector banks were installed. The measurement position is illustrated in Figure 11-1.

*Table 10-2 Foil scan exercises to determine the position of reference point with respect to the centre of ω-rotation.*

| Instrument | Measured reflection *hkl*/ Detector position ($2\vartheta_{det}$) | $\omega$-angle | GV size: $w \times h$ (prim. beam) × w (sec. beam), mm³ | Beam apertures (Primary Secondary) | Re-alignment at each detector position |
|---|---|---|---|---|---|
| SALSA | Fe(211)/ 93.5° | 46.75°<br>−43.25°<br>−133.29° | 0.6 × 2 × 0.6 | Col. – Col. | No |
| STRESS-SPEC | Fe(211)/ 92° | 136°<br>46°<br>-44° | 1 × 10 × 1 | Slit – Col. | No |
| | Fe(200)/ 72° | −54°<br>36°<br>126° | | Slit – Slit | Yes |
| MPISI | Fe(211)/ 90° | 135°<br>45°<br>−45°<br>−135° | 1 × 10 × 1 | Slit – Slit | Yes |
| | Fe(110)/ 50° | 25°<br>115°<br>−155° | | | |

## 10.2. Data analysis

Neutron counts at a narrow wavelength range around the Bragg peak position were integrated and used to plot the intensity curve of each scan. For the foil scans, the intensity curve was fitted with a Gaussian function to accurately determine the measured foil position. An example is given in Figure 10-3 from the STRESS-SPEC measurements for Fe(211) at an $\omega$-angle of 136°. By comparing the alignment position and the measured position of the foil, the offset was determined. From the example, the measured positions were y = -0.09 and x = 2.47 (in mm) and the alignment positions for the were y = 0.00 and x = 2.40 (in mm) for the top and bottom foils, respectively. Therefore, offsets for the top and bottom foils were -0.09 and 0.07 (in mm), respectively.

BrightnESS² is funded by the European Union Framework Programme for Research and Innovation Horizon 2020, under grant agreement 823867

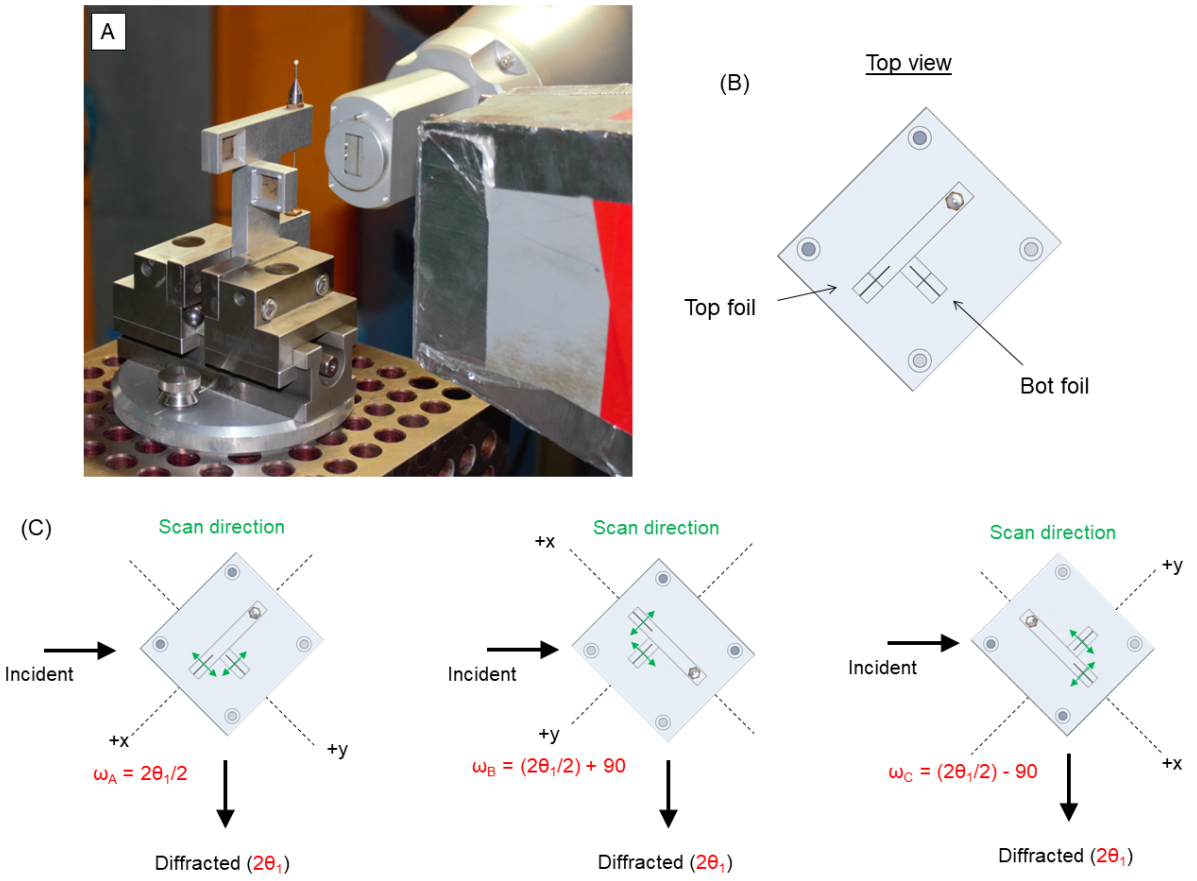


*Figure 10-2 Illustration of foil scans to determine the position of reference point relative to the centre of ω-rotation. (A) Measurement on STRESS-SPEC; (B) Top view drawings of the Foils & pin sample; (C) measurements were made on the top and bottom foil at the bisector angles. At one detector position, measurements were made on three orthogonal ω-angles.*

The cross-section of the offsets from the two foil measurements at a particular *ω*-angle represents the sample position relative to the reference point (cross symbols in Figure 10-4). The coordinates of the sample positions *x* and *y* were then transformed by angle *ω* to the instrument reference position *XY*. From measurement at a minimum of three *ω*-angles, the centre of *ω*-rotation position relative to the reference point can be determined from the centroid of a circle passing through the sample positions, Figure 10-4. For measurements using more than three *ω*-angles, a least square best fit is used and yield a circle which provides the centroid based on the measured positions. The radius of the fitted circle represents the positional alignment uncertainty of the foils. This analysis can either be carried out mathematically or using the aid of graphical analysis tool, for example GeoGebra software [29], which was used in this report. It is important to note that, in this analysis, the centre of *ω*-rotation is represented as relative position to the reference point, i.e., the position is actually fixed in the sample stage coordinate system (the black and grey dots in Figure 10-6 to Figure 10-8 are actually a single point), while the reference point position varies for different detector angular positions.

## 10.3. Results

### 10.3.1. The effect of detector angular position on the GV position

Table 10-3 presents the measured GV positions at different detector positions, determined from the pin scan exercises on the participating monochromatic instruments. The findings are:

BrightnESS² is funded by the European Union Framework Programme for Research and Innovation Horizon 2020, under grant agreement 823867

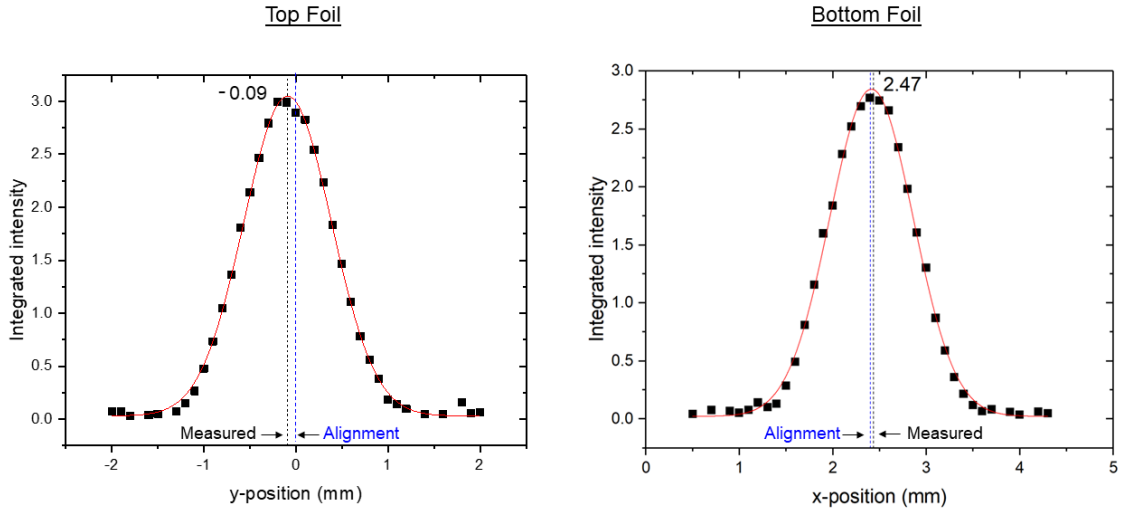


*Figure 10-3 Example of the intensity curves from the foil scan, taken from the STRESS-SPEC measurements for Fe(211) at an ω-angle of 136°. The curves were fitted using a Gaussian function to determine the real position of the foils.*

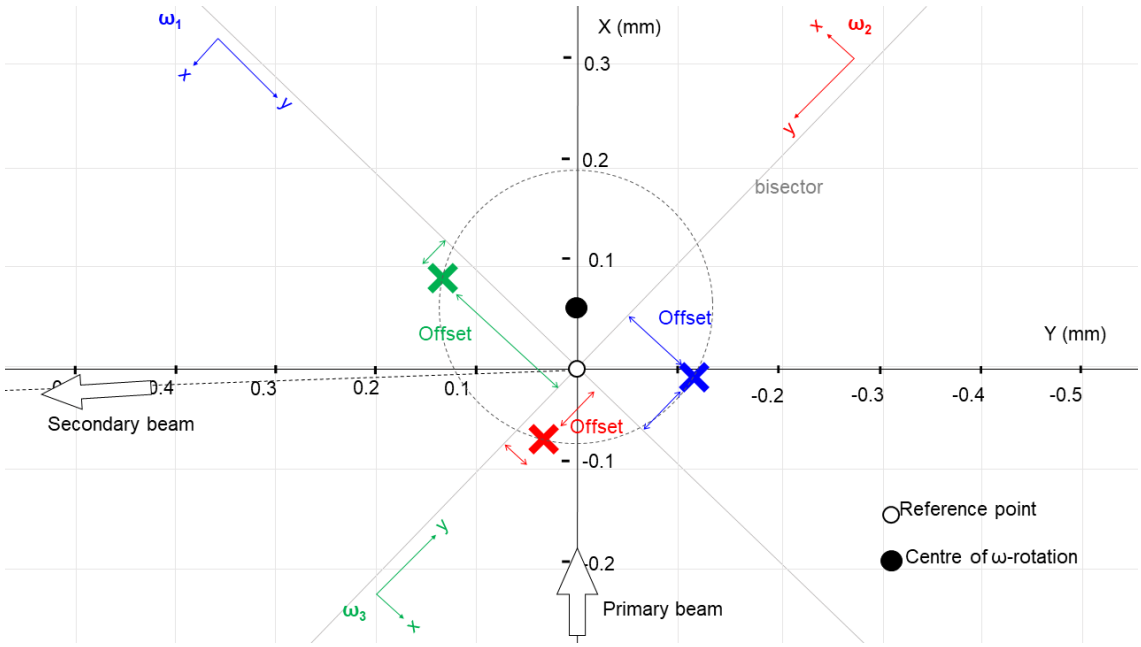


*Figure 10-4 Determination of centre of ω-rotation relative to reference point position. The crossed symbols are the sample positions, obtained from the cross section of the offset of the foil scans at corresponding ω-angles. The centroid of circle passing through these sample positions is the centre of ω-rotation.*

1. Without re-alignment of the secondary beam aperture at each detector position, the GV position clearly shifted with changes in the detector position. On SALSA, the change of detector angular position of 44° (From $2\vartheta_{det}$ of 93.5° to 49.5°) moved the GV position ~100 µm, Table 10-3(i). On STRESS-SPEC, changing the detector angular position from $2\vartheta_{det}$ = 92° to 72° moved the GV position ~150 µm, and changing it further to 49° moved the GV position ~200 µm, Table 10-3(ii). Possible causes of this effect may include the misalignment between the centre of $2\vartheta_{det}$-rotation and the centre of $\omega$-rotation, issues related to mechanical components which drive and guide the movement of the secondary optics as well as the 'pivot' effect which results from the projection of the position of the diffraction peak through a secondary aperture as described in [30].

BrightnESS² is funded by the European Union Framework Programme for Research and Innovation Horizon 2020, under grant agreement 823867

2. With re-alignment of the secondary beam aperture at each detector position, the GV position is reproducible for different detector angular positions. On STRESS-SPEC, at detector angular positions of $2\vartheta_{det}$ = 92°, 72°, and 49°, the GV positions are reproducible within ~50 µm, Table 10-3(iii). Meanwhile on MPISI, at detector angular position of $2\vartheta_{det}$ = of 90°, 50°, and 105°, the GV positions are reproducible with differences less than 90 µm, Table 10-3(iv).

*Table 10-3 Measured GV positions for different detector positions $2\vartheta_{det}$, from pin scan exercises.*

(i) SALSA; $\omega$ = 0°; Fe(211) and (110); without re-alignment

| $2\vartheta_{det}$ | GV position in *y*-axis (unit in mm) | | |
|---|---|---|---|
| | Theoretical | Measured | Standard error |
| 93.5° | 0.00 | 0.02 | 0.01 |
| 49.5° | 0.00 | 0.10 | 0.01 |

(ii) STRESS-SPEC; $\omega$ = −90°; Fe(211), Fe(200) and (110); secondary radial collimator, without re-alignment

| $2\vartheta_{det}$ | GV position in *y*-axis (unit in mm) | | |
|---|---|---|---|
| | Theoretical | Measured | Standard error |
| 92° | 0.00 | 0.03 | 0.00 |
| 72° | 0.00 | -0.18 | 0.01 |
| 49° | 0.00 | -0.24 | 0.01 |

(iii) STRESS-SPEC; $\omega$ = 0°; Fe(211), Fe(200) and (110); secondary slit, with re-alignment

| $2\vartheta_{det}$ | GV position in *y*-axis (unit in mm) | | |
|---|---|---|---|
| | Theoretical | Measured | Standard error |
| 92° | 0.00 | -0.29 | 0.00 |
| 72° | 0.00 | -0.25 | 0.01 |
| 49° | 0.00 | -0.26 | 0.01 |

(iv) MPISI; $\omega$ = 0°; Fe(211), Fe(110) and (220); secondary slit, with re-alignment

| $2\vartheta_{det}$ | GV position in *y*-axis (unit in mm) | | |
|---|---|---|---|
| | Theoretical | Measured | Standard error |
| 90° | 0.00 | 0.03 | 0.01 |
| 50° | 0.00 | 0.09 | 0.01 |
| 105° | 0.00 | 0.05 | 0.02 |

### 10.3.2. Position of reference point vs. centre of $\omega$-rotation

Using the graphical analysis described in Section 10.2, the position of the reference point with respect to the centre of $\omega$-rotation can be determined. Figure 10-5 shows the result of the graphical analysis for SALSA. From Figure 10-5, it can be observed that the reference point was misaligned from the centre of $\omega$-rotation of ~310 µm. After the measurement, it was found later that this relatively large misalignment was due to a defect of the Foils & pin calibration sample of SALSA, i.e., misalignment between the fiducal sphere centre vs. the pin axis. The offset between the alignment position and the measured position of the foils can be found in Annex A.1.2.

Applying the same analysis method as used above, the position of the STRESS-SPEC reference point relative to the centre of $\omega$-rotation can be determined. The details of the offset between the alignment position and the measured position of the foils can be found in Annex A.2.2. Figure 10-6 shows the graphical analysis for the measurement using the primary slit and secondary collimator, which was performed without re-alignment at different detector positions. It can be observed that, for detector angular position of $2\vartheta_{det}$ = 92°, the misalignment of the reference point of the instrument and the centre of $\omega$-rotation was ~60 µm. For the detector position of 72°, the misalignment was ~250 µm. Figure 10-7 shows the analysis for the measurement using primary and secondary slits, which was performed with re-alignment at different detector positions. It can be observed from Figure 10-7 that,

BrightnESS² is funded by the European Union Framework Programme for Research and Innovation Horizon 2020, under grant agreement 823867

for $2\vartheta_{det}$ = 92°, the misalignment of the reference point from the centre of $\omega$-rotation is ~70 µm, and changing the detector position to 72° only shifts the misalignment by ~20 µm.

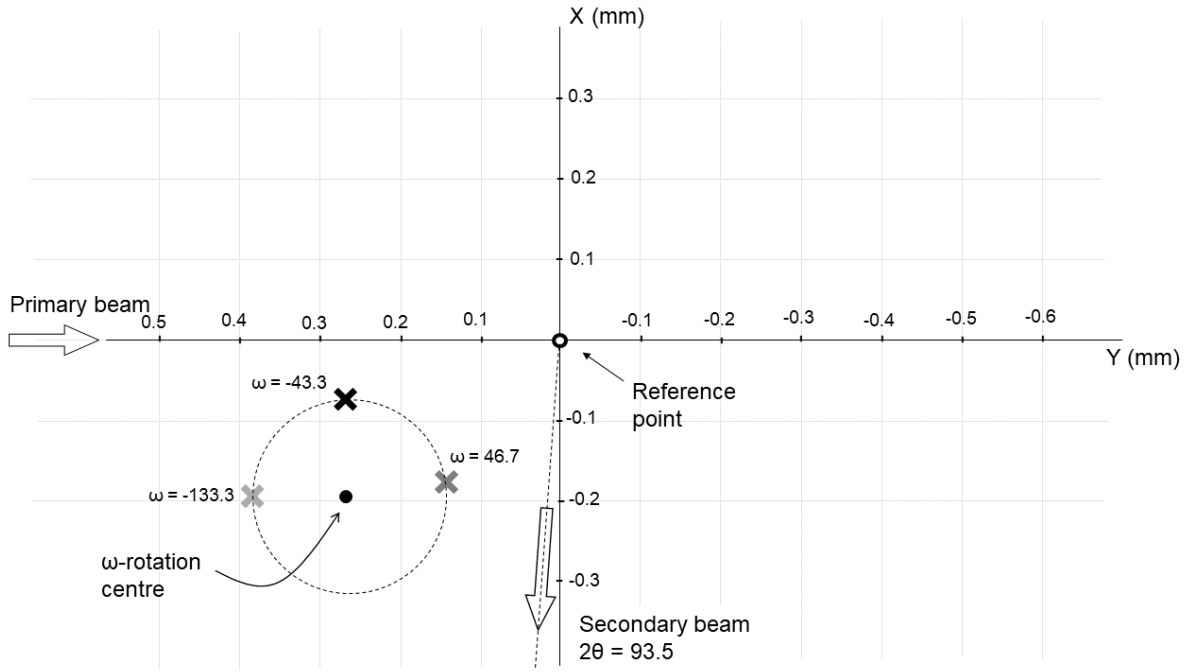


*Figure 10-5 Reference point relative to the centre of ω-rotation at SALSA.*

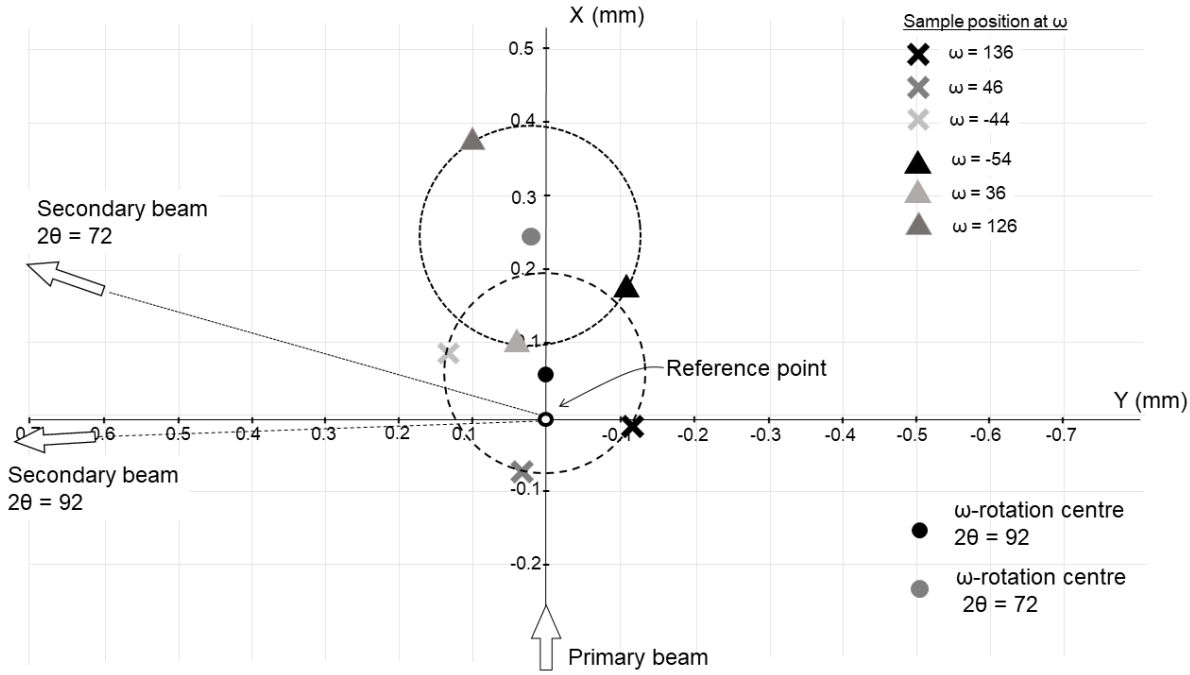


*Figure 10-6 Reference point relative to the centre of ω-rotation at STRESS-SPEC using a radial collimator in the secondary beam. The measurements were performed without re-alignment at different $2\vartheta_{det}$.*

Figure 10-8 shows the graphical analysis for the measurement on MPISI. The details of the offset between the alignment position and the measured position of the foils can be found in Annex A.3.2. It can be observed that for $2\vartheta_{det}$ = 90°, the misalignment of reference point from the centre of $\omega$-

BrightnESS² is funded by the European Union Framework Programme for Research and Innovation Horizon 2020, under grant agreement 823867

rotation is ~90 µm, and changing the detector position to 50° only resulted in a shift of the misalignment by ~20 µm.

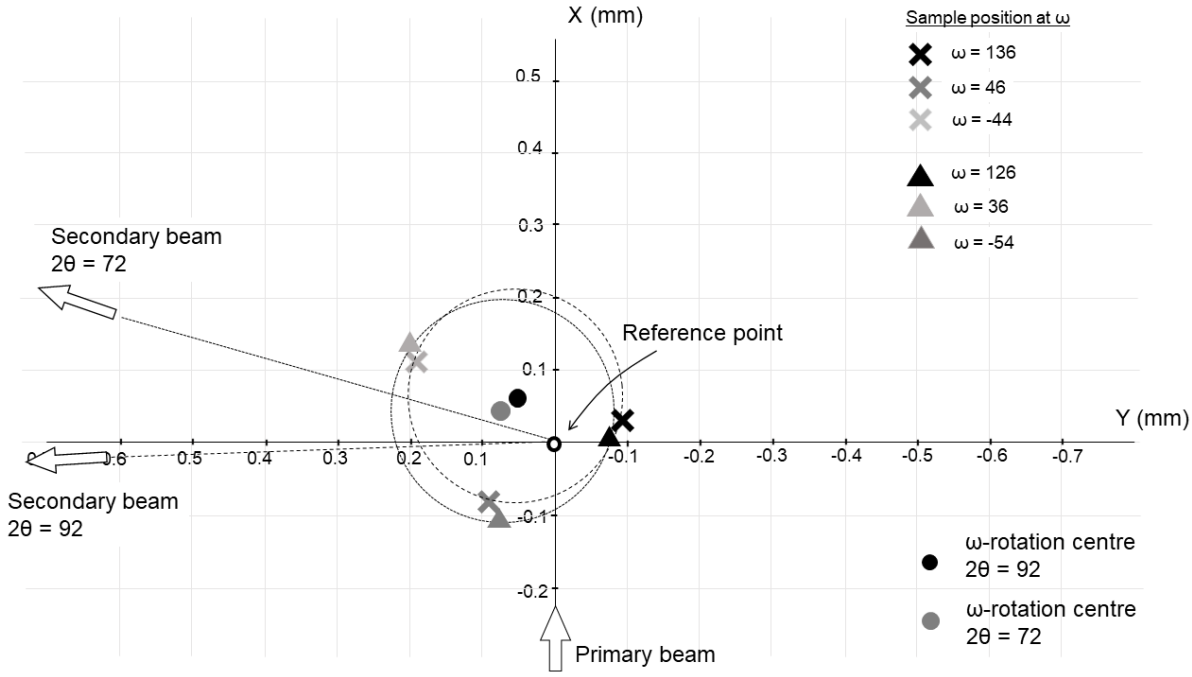


*Figure 10-7 Reference point relative to the centre of ω-rotation at STRESS-SPEC using the secondary slit setup. The measurements were performed with re-alignment at different $2\vartheta_{det}$.*

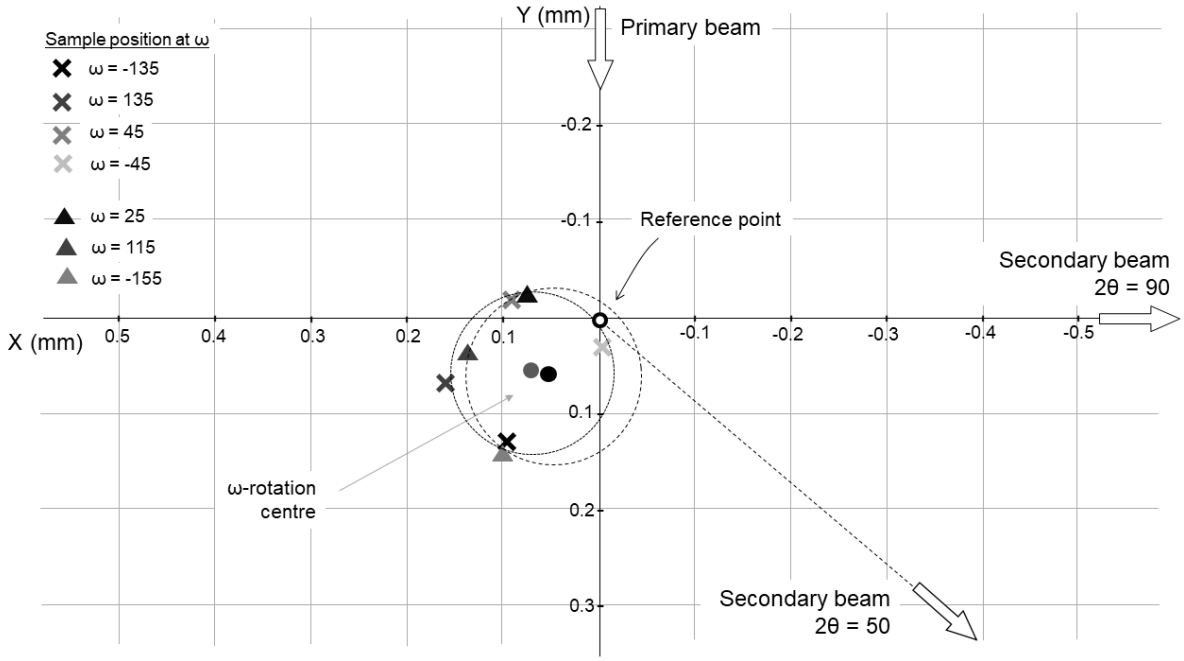


*Figure 10-8 Reference point relative to the centre of ω-rotation at MPISI using a primary and secondary slit setup. The measurements were performed with re-alignment at different $2\vartheta_{det}$.*

The average offset between the measured position and alignment position (which is aligned with the centre of *ω*-rotation) of the 5-wall sample surfaces measured on ENGIN-X can be found in Annex A.4.1. These average offsets, which data are available for four orthogonal *ω*-angles, were used to approximate the reference points from the two detector banks. The results are shown in Figure 10-9. The four dark grey squares indicate the intersection of the four offsets from the north bank

BrightnESS² is funded by the European Union Framework Programme for Research and Innovation Horizon 2020, under grant agreement 823867

measurement, while the four light grey dots indicate those from the south bank measurement. From the results, it can be inferred that the north bank detector has a misalignment from the centre of *ω*-rotation of ~60 µm towards the primary beam, while the south bank detector has a misalignment of ~90 µm in the same direction. It is also indicated that the primary beam has a misalignment of ~90 µm from the centre of *ω*-rotation.

### 10.4. Discussion

For the three monochromatic instruments with single PSDs, it can be confirmed that the GV position moved with the change of detector position (pin scan result in Table 10-3(i) and (ii), also foil scan results in Figure 10-6). This alteration was observed to be up to 200 µm for a 40° rotation when using a GV with 1 mm width, representing a shift of 20% in the GV. If this is not accounted (corrected) for especially in sample investigations that require measurements at multiple detector positions (such as composite samples), the measured stress will be averaged from different volumes within the sample, increasing the positioning uncertainty. Therefore, a few take-away points from these exercises are:

1. The instrument alignment should be performed within the specific detector positions where the sample characterisation needs to be carried out.
2. For characterisation which requires measurement at multiple detector position, re-alignments at each detector position should be carried out if possible. Results from the pin scan shown in Table 10-3(iii) and the foil scan results in Figure 10-7 and Figure 10-8 indicates that the reproducibility of the alignment procedures of the secondary beam optics, with the GV positions at different $2\vartheta_{det}$ (range = 49° - 92°) were within 50 µm precision. For this approach, note that the $d_0$ reference measurements must be performed at each detector position. This is because the re-alignment of the beam aperture translates to a shift in the $2\vartheta$ position of the Bragg peak.
3. If the re-alignment is not performed, the GV position alteration as a function of detector angular positions must be well characterised and reported in the positioning uncertainty analysis.
4. For TOF instruments with multiple detectors fixed at different positions, the uncertainties originated from the misalignment between different detector banks. The result showed that the alignment between the North and South detector banks on ENGIN-X was better than 40 µm.

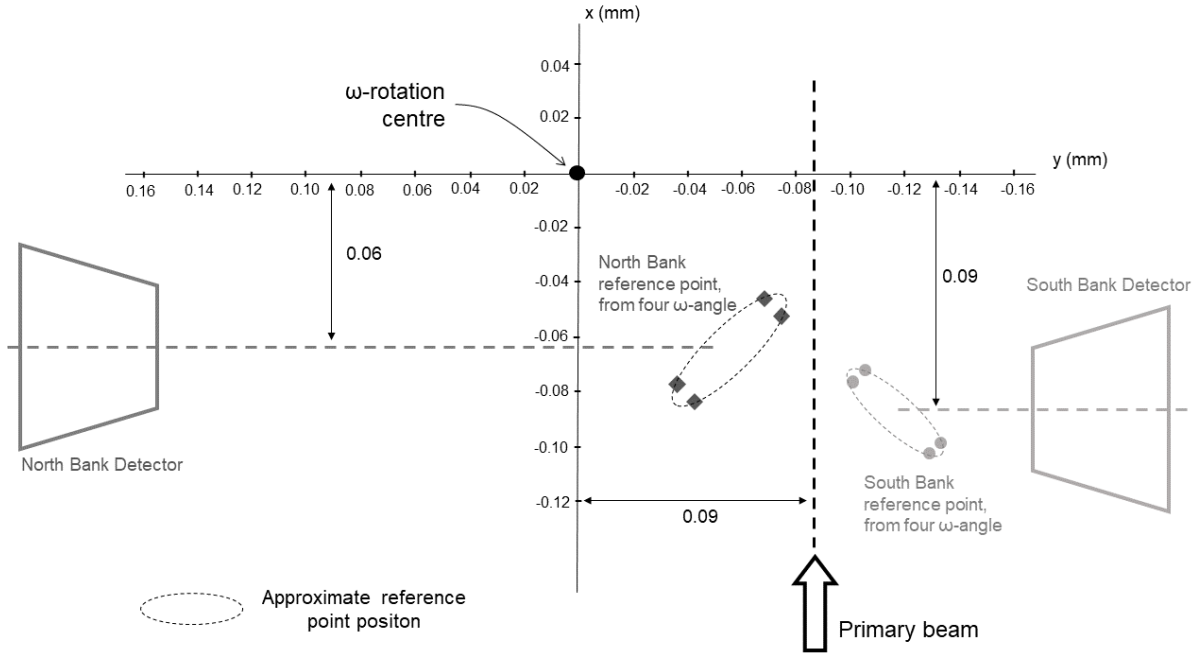


*Figure 10-9 Approximate reference point positions relative to the centre of ω-rotation on ENGIN-X.*

BrightnESS² is funded by the European Union Framework Programme for Research and Innovation Horizon 2020, under grant agreement 823867

The misalignment between the reference point and the centre of $\omega$-rotation reflects the quality of the instrument alignment. Results shown in Figure 10-6 to Figure 10-8 indicate that the participating instruments were aligned to better than 100 µm (<70 µm for STRESS-SPEC, ~90 µm for ENGIN-X and MPISI). One exception on the result was the SALSA measurement, where the reference point was misaligned from the centre of $\omega$-rotation for ~310 µm. This, however, confirmed to be related to inaccuracy of the manufacturing tolerance and assembly process of the calibration sample, i.e., misalignment between the fiducial sphere and the main pin in the SALSA calibration sample, Figure 9-5(A). The determination of SALSA's reference point was carried out by tracking the fiducial sphere using a telecentric camera and image-recognition software. The beam apertures were aligned to the vertical pin, which is supposed to be precisely on the same position below the sphere. However, it was later observed that there was a ~200 µm misalignment between the sphere and the pin due to assembling inaccuracies of the inserts of the pin. This misalignment is within the order of the reference point to the centre of $\omega$-rotation displacement as measured on SALSA. In any case, this shift could be detected and quantified during the alignment and corrected for following strain measurements.

BrightnESS² is funded by the European Union Framework Programme for Research and Innovation Horizon 2020, under grant agreement 823867

# 11. Precision of Sample Alignment System

## 11.1. Methods

To quantify the precision and reproducibility of the sample alignment system, surface scans were performed on the walls of the 5-wall sample, with the measurement location indicated in Figure 11-1. Alignments using the sample alignment system, i.e., theodolites on STRESS-SPEC, MPISI, and ENGIN-X, and cameras for SALSA, were performed for each surface of the walls. The neutron beam scans for different reflections were performed in both transmission and reflection geometries. The precision is determined from the standard deviation of the offsets between the surface positions found by neutrons and the positions determined by the sample alignment system. The standard deviations were calculated for each setup, i.e., detector angular position and $\omega$-angles, to eliminate the possible side effects of other uncertainties. The measurement details for each of the participating neutron strain scanners are presented in Table 11-1.

*Table 11-1 Details of the wall scan exercises to evaluate the precision of the sample alignment system on the participating instruments.*

| Instrument | Measured reflection $hkl$/ $2\vartheta_{det}$ | GV size: $w \times h$ (prim. beam) $\times w$ (sec. beam), mm³ | Beam apertures (Primary Secondary) | Additional info |
|---|---|---|---|---|
| SALSA | Fe(220)/ 83.6° | 0.6 × 2 × 0.6 | Col. - Col. | 800 counts<br>400 counts |
| STRESS-SPEC | Fe(220)/ 83° [a]<br>Fe(311)/ 102° [a]<br>Fe(311)/ 77.5° [b] | 1 × 8 × 1 | Slit - Col. | [a] Si Mono.<br>[b] Ge Mono. |
| MPISI | Fe(220)/ 80°<br>Fe(200)/ 55° | 1 × 10 × 1<br>2 × 10 × 2 | Slit - Slit<br>Slit - Col. | |
| ENGIN-X | Spectrum:<br>Fe(111)-(311)/ +/-90° | 2 × 10 × 2<br>1 × 15 × 1 [c] | Slit - Col. | [c] Detector only at $2\vartheta_{det}$= −90° |

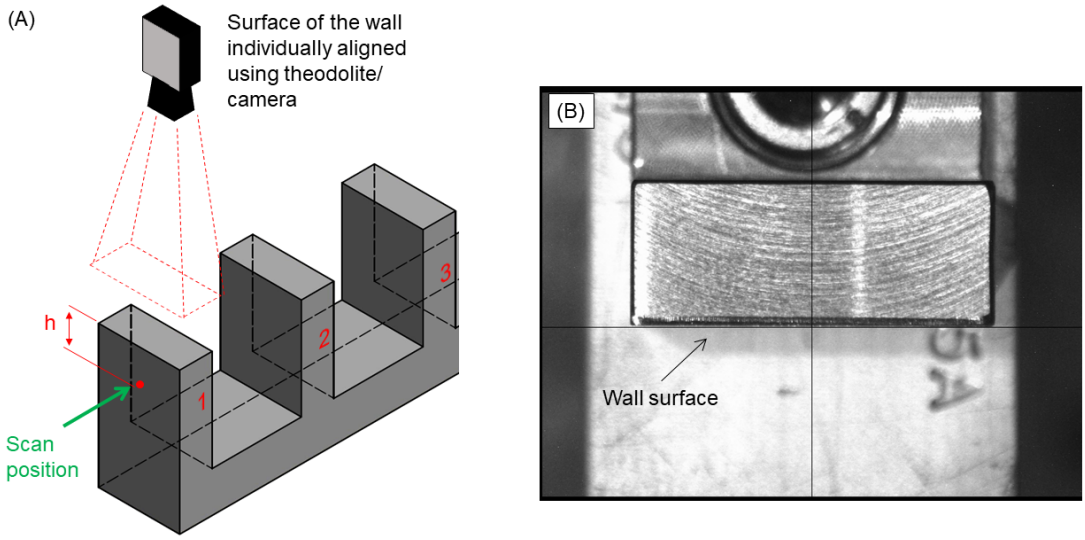


*Figure 11-1 Illustration of wall scans to determine the precision of the sample alignment system: (A) The position of the wall surface was determined using the instrument specific sample alignment system, i.e., theodolite or camera; neutron scans were performed on the walls at the position indicated by the green arrow. (B) Example of the field-of-view of the telecentric-camera on SALSA while determining the surface of the wall.*

BrightnESS² is funded by the European Union Framework Programme for Research and Innovation Horizon 2020, under grant agreement 823867

## 11.2. Results

The standard deviation of the offsets represents the ability of the sample alignment system in repeatedly arriving at the same position, in this case simulated by the surfaces of the walls, i.e., the precision of the alignment system. The summary of this exercise is presented in Table 11-2, while the full report of the results can be found in Annex A.1.3, A.2.3, A.3.3, and A.4.1.

On SALSA, it can be observed that the measurements with better counting statistics (longer counting times) has the lowest standard deviation, thus yielding the highest precision at 50 µm. The measurements with shorter counting times yields lower precision at 110 µm for transmission geometry and 140 µm for reflection geometry. The lower precision, however, are due to the lower statistical quality of the data and thus larger fitting uncertainties. Therefore, the results from higher counting times measurement reflects the precision of the sample alignment system better. On STRESS-SPEC, it can be observed that, for multiple monochromator configurations, $2\vartheta_{det}$ angle setups, and measurement geometries, the standard deviation of the offsets were consistently ~100 µm or lower, which reflects the precision of the sample alignment system on STRESS-SPEC. On ENGIN-X, the standard deviations of the offsets from different $\omega$-angles, detector banks, and collimator sizes (1 mm and 2 mm) indicated that the sample alignment system on ENGIN-X has a precision better than 100 µm. For MPISI, it is observed that the offsets for multiple $2\vartheta_{det}$ setups and measurement geometries have standard deviations ~100 µm, which indicates the precision of the sample alignment system. It is worth noting that specifically for the analysis of datasets from the MPISI measurement, the results analysed using Align and ScanManipulator software show excellent agreement.

*Table 11-2 Standard deviation of the offsets from the measurement of the 5-wall sample, indicating the precision of the sample alignment system of the instruments.*

| Instrument | Measured reflection *hkl*/ $2\vartheta_{det}$ | Measurement geometry | Details | Std. deviation of offset (mm) |
|---|---|---|---|---|
| SALSA | Fe(220)/ 83.6° | Transmission | 800 counts | 0.05 |
| | | Transmission | 400 counts | 0.11 |
| | | Reflection | 400 counts | 0.14 |
| STRESS-SPEC | Fe(220)/ 83° | Transmission | Align | 0.10 |
| | | Reflection | | 0.12 |
| | Fe(311)/ 102° | Transmission | | 0.05 |
| | | Reflection | | 0.08 |
| | Fe(311)/ 77.5° | Transmission | | 0.03 |
| MPISI | Fe(220)/ 80° | Transmission | Align | 0.10 |
| | | | ScanManipulator | 0.11 |
| | | Reflection | Align | 0.09 |
| | | | ScanManipulator | 0.09 |
| | Fe(200)/ 55° | Transmission | Align | 0.09 |
| | | | ScanManipulator | 0.09 |
| | | Reflection | Align | 0.08 |
| | | | ScanManipulator | 0.11 |
| ENGIN-X | Spectrum/ +/- 90° | Transmission | S.B. ($\omega$ = −135°)* | 0.04 |
| | | | N.B. ($\omega$ = −45°)* | 0.09 |
| | | | S.B. ($\omega$ = 45°)* | 0.03 |
| | | | N.B. ($\omega$ = 135°)* | 0.07 |
| | | | N.B. ($\omega$ = −135°)** | 0.03 |
| | | | N.B. ($\omega$ = 45°)** | 0.06 |
| | | Reflection | N.B. ($\omega$ = −135°)* | 0.05 |
| | | | S.B. ($\omega$ = −45°)* | 0.04 |
| | | | N.B. ($\omega$ = 45°)* | 0.05 |
| | | | S.B. ($\omega$ = 135°)* | 0.04 |
| | | | N.B. ($\omega$ = −45°)** | 0.09 |

*)2 mm Collimator; **)1 mm Collimator ; N.B = North Bank; S.B = South Bank

BrightnESS² is funded by the European Union Framework Programme for Research and Innovation Horizon 2020, under grant agreement 823867

### 11.3. Discussion

Since the sample was mounted and aligned once at the beginning of experiments, the precision of the sample alignment system should be independent of the measurement setup such as monochromator configuration, detector angular position, measurement geometries, even beam aperture setup and sample remounting (ENGIN-X with 1 mm and 2 mm collimators), which has been proven by the results. As indicated by the SALSA results, the one apparent dependency was the statistical quality of the data, i.e., the measurements with lower counting times produced Bragg peaks with lows signal-to-noise ratio and thus the entry curve from the surface scan has larger scatter. In summary, it can be inferred that the instruments sample alignment systems provided a precision better than 100 µm throughout, i.e., in the same order of magnitude as the accuracy of the reference point position studied in section 5 and within the error considered for neutron diffraction stress measurements [15].

Also, it can be observed that for higher counts a precision of 50 µm can be achieved at SALSA, i.e., better than 10% of the 0.6 mm GV width. This is expected since the alignment on SALSA used a digital telecentriccamera system with resolution of ~40 µm, integrated with on screen measurement features. Using theodolite alignment systems, other instruments also proved a good level of precision of better than 100 µm, i.e., 10% of the GV width or better.

BrightnESS² is funded by the European Union Framework Programme for Research and Innovation Horizon 2020, under grant agreement 823867

# 12. Accuracy of Entry Curve Analysis Software

## 12.1. Methods

In order to quantify the accuracy of the entry curve analysis software, the exercise is to determine the dimension of a known geometry using neutrons by performing wall scans, and comparing the results with those obtained from another measurement methods, in this case a coordinate measurement machine (CMM). The different investigations were as follows:

1. Scans were made on the wall surfaces of the 5-wall sample, Figure 12-1(B) to quantify the accuracy of the software in determining the position of flat surfaces which are perpendicular to the beam propagation plane. A digital inclinometer with 0.1° accuracy was used to align the sample to the absolute horizontal plane.

2. Scans were performed on the wall surfaces of the 5-wall sample with tilts introduced, to study the robustness of the software in detecting surfaces not parallel with the beam plane, as for some cases in engineering component characterisation. Using the digital inclinometer, the introduced tilt was $\chi$ = 2° and 10°, Figure 12-1(C) and (D).

3. Scans were performed on the Tube sample to study the robustness of the software in determining the position of curved surfaces, again representative of some real component characterisation. Scans were performed along the radial line and on a slight offset to the radial line, with the axis of the tube vertical, Figure 12-2(B). Scans were also performed with the axis of the tube horizontal, Figure 12-2(C). Details on the scan positions for the measurement on each instrument can be found in the Annex Figure A-1, A-2, A-3, and A-4.

Not all of the above exercises were repeated on all instruments, i.e., examples of each of those proposed exercises where gathered between the different instruments. The details of the measurements performed on the participating instrument are provided in Table 12-1.

*Table 12-1 Gauge volume size (primary width × primary height × secondary with, in mm³) used during the scans for quantification of the accuracy of entry curve analysis software*

| | Flat surface, perpendicular | Flat surface, non-perpendicular | Curved surface, radial line, axis vertical | Curved surface, offset line, axis vertical | Curved surface, radial line, axis horizontal |
|---|---|---|---|---|---|
| SALSA | 0.6 × 2 × 0.6 | - | 0.6 × 2 × 0.6 | - | - |
| STRESS-SPEC | 1 × 8 × 1 | 1 × 2 × 1 | 1 × 2 × 1 | 1 × 2 × 1<br>offset 5, 30 mm | 1 × 2 × 1 |
| MPISI | 1 × 10 × 1<br>2 × 10 × 2 | 1 × 10 × 1 | 1 × 10 × 1 | 1 × 10 × 1<br>offset 5 mm | 1 × 10 × 1 |
| ENGIN-X | 2 × 10 × 2<br>1 × 15 × 1 | - | 2 × 10 × 2 | 2 × 10 × 2<br>offset 30 mm | - |

The CMM measurements on the sample features were performed at the Material Science Support Laboratory of the ILL. The measurements utilised a Mitutoyo Euro-C776 APEX machine coupled with an SP600 scanning probe system (resolution of 0.1 µm) in conjunction with MCOSMOS V4 software. The full details of the CMM results are presented in the Annex (Table. A-29). It is important to note that CMM measurement has not been carried out for the sample Set 3, which was measured on MPISI, at the time of reporting. Instead, the average values of CMM measurements from the other two sets, which have a standard deviation of < 10 µm, were used. Also note that the thickness of the wall at tilt

BrightnESS² is funded by the European Union Framework Programme for Research and Innovation Horizon 2020, under grant agreement 823867

$\chi$ = 2° and 10°, i.e., the width of the walls sectioned by horizontal plane, was calculated by applying simple trigonometry to the measured wall thickness at $\chi$ = 0° (at 7.6 mm from the top of the wall, which was the location of the CMM and neutron scans). The thickness of the tube wall at the offset line (at 5 mm and 10 mm) was calculated from the measured thickness of the wall at the radial line.

### 12.1.1. Entry curve data analysis

The analysis software used to fit the entry scan intensity curves are primarily based on the model presented by Brand and Prask [18]. The model requires input of gauge volume size (defined by primary and secondary beam width and scattering angle) and the linear attenuation coefficient. The MathCad-based analysis tool, developed in-house for SALSA, is the only tool available that incorporates curvature radius as additional input for intensity curve modelling, at the time of reporting.

Figure 12-3 shows an example of an intensity curve of Wall 1 of the 5-wall sample in transmission and reflection geometries. The intensity curves fitted using Align and ScanManipulator, Figure 12-3(A) and (B), respectively, were from the same measurements on MPISI, while those fitted using the MathCad-based code were from measurements on SALSA, Figure 12-3(C). For all analysis tools, the linear attenuation coefficient input was fixed between 0.1−0.12 $mm^{-1}$. Using the Align software, the single slit size parameter was refined. ScanManipulator allows the primary and secondary slit width parameters to be specified independently and were fixed in accordance to measured values obtained during the instrument alignment process.

## 12.2. Results

In this work, the accuracy of the entry curve analysis software was determined from the average difference of the features dimensions between wall scan and CMM results, which is presented in Table 12-2. For the MathCad-based code used on SALSA, it can be observed that the wall scan and the CMM results for flat surfaces perpendicular to the beam propagation plane have an average difference of ~40 µm. For the curved surface at the radial line, the differences was ~60 µm. The full details of the measurement results are presented in Annex A.1.4.

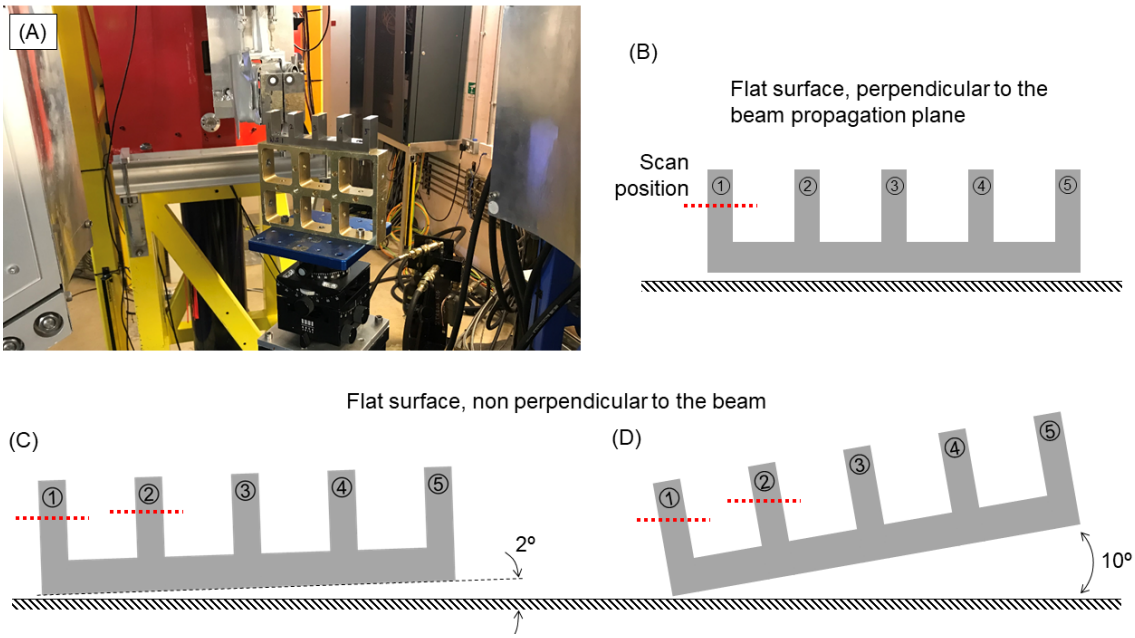


*Figure 12-1 Wall scans to determine the accuracy of the entry curve analysis software: (A) Examples of wall scans setup on ENGIN-X; (B) scans with surfaces perpendicular to the beam propagation plane; (B) scans with the sample tilted 2 ° from the horizontal plane; (C) scans with the sample tilted 10 ° from the horizontal plane.*

BrightnESS² is funded by the European Union Framework Programme for Research and Innovation Horizon 2020, under grant agreement 823867

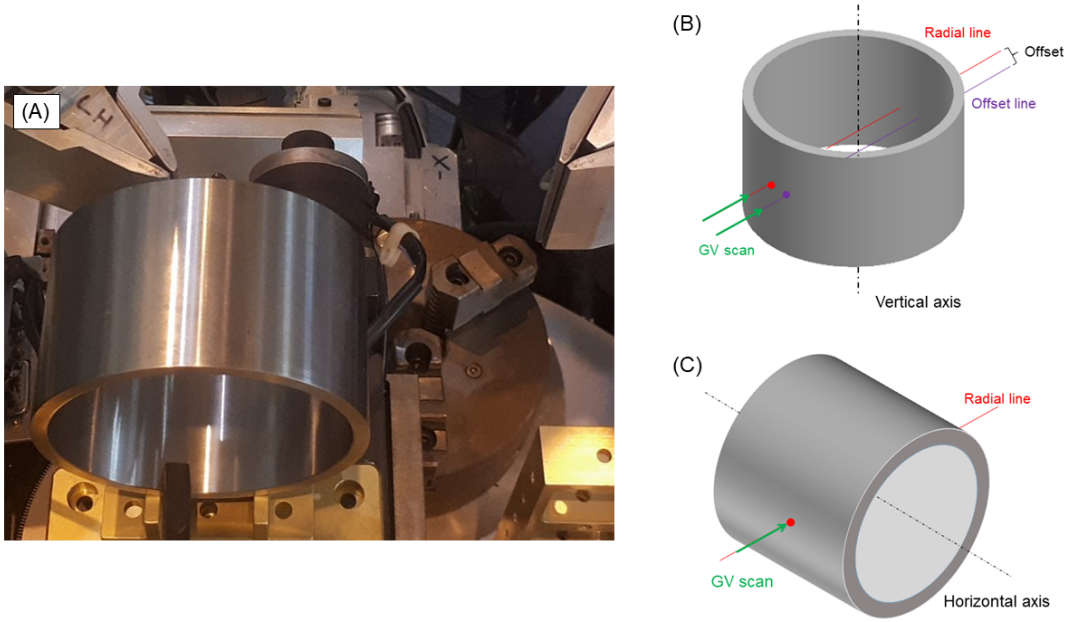


*Figure 12-2 Tube sample scans to determine the accuracy of the entry curve analysis software: (A) Example of setup on MPISI; (B) Scans with the curvature axis vertical, entry scans along radial line and at an offset from radial line; (C) Scans with the curvature axis horizontal, entry scans along radial line.*

For the Align software used on STRESS-SPEC, it can be observed that the average difference between wall scans and CMM measurements were ~50 µm, for the measurement of flat surface perpendicular to the beam propagation plane. There is no apparent disparity between the results from measurements using different detector positions and different beam incident wavelengths. The full details of the measurement results are presented in Annex A.2.4. The difference between the wall scan and CMM measurement for Wall1 measurements with 2° and 10° tilt were both below 50 µm. However, the differences were significantly higher for measurement of Wall2, which are 210 µm and 410 µm for 2° and 10° tilt, respectively. The measured intensity values, the fitted curves, and the neutron count monitor of the detector for Wall1 and Wall2 at both tilt angles are provided in Figure 12-4 for reference. For measurements on the Tube sample with the axis of the tube in the vertical direction, the difference between the wall scan and CMM measurements were ~170 µm for measurement along the radial line, and ~30 µm along the offset line at 5 mm from the radial line. For the measurement along the offset line at 30 mm from the radial line, the difference was over 500 µm. It is also indicated that, for most results, the differences were larger for measurements in reflection geometry, Table A.13. Results from the measurements with the axis of the tube in horizontal direction shows that the average difference between wall scan and the CMM measurement is ~100 µm.

For the Align software used on ENGIN-X, the result from measurement of flat surfaces perpendicular to the beam propagation plane showed the average difference between neutron and CMM results of 80 µm, for measurement using a 2 mm radial collimator. The value for a similar exercise using a 1 mm radial collimator was 50 µm. For the measurements of the Tube sample (axis vertical) along radial line, the average difference between the wall scans and CMM results were ~100 µm. For the measurement of the Tube sample along the offset line at 30 mm from the radial line, the average difference was higher than 500 µm. There are no significant disparities between the results from different collimators or measurements at different $\omega$-angles. Full details can be found in Annex A.4.2.

BrightnESS² is funded by the European Union Framework Programme for Research and Innovation Horizon 2020, under grant agreement 823867

*Table 12-2 Average differences between neutron measurements and CMM results, representing the accuracy of the entry curve analysis software*

| Instrument/ Software | Features | Details | Average differences (mm) |
|---|---|---|---|
| SALSA/ MathCad-based code | Flat surface, perpendicular to beam plane | | 0.04 |
| | Curved surface (axis vertical), Radial line | | 0.06 |
| STRESS-SPEC/ Align | Flat surface perpendicular to beam plane | | 0.05 |
| | Flat surface non-perpendicular to beam plane | Wall1 ($\chi$= 2° & 10°)<br>Wall2 ($\chi$= 2° & 10°) | 0.03<br>0.32 |
| | Curved surface (axis vertical), radial line | | 0.17 |
| | Curved surface (axis vertical), offset = 5 mm | | 0.03 |
| | Curved surface (axis vertical), offset = 30 mm | | 0.69 |
| | Curved surface (axis horizontal), radial line | | 0.10 |
| ENGIN-X/ Align | Flat surface perpendicular to beam plane | 2 mm Collimator<br>1 mm Collimator | 0.08<br>0.05 |
| | Curved surface (axis vertical), Radial line | 2 mm Collimator | 0.10 |
| | Curved surface (axis vertical), offset = 30 mm | 2 mm Collimator | 0.63 |
| MPISI/ Align& ScanManipulator | Flat surface perpendicular to beam plane | Align (1 mm Slit)<br>ScanManipulator ( 1 mm Slit)<br>Align (2 mm Col.)<br>ScanManipulator (2 mm Col.) | 0.06<br>0.07<br>0.15<br>0.15 |
| | Flat surface non-perpendicular to beam plane | Align (Tilt 2°)<br>ScanManipulator(Tilt 2°)<br>Align (Tilt 10°)<br>ScanManipulator (Tilt 10°) | 0.05<br>0.04<br>0.22<br>0.19 |
| | Curved surface (vertical axis), Radial line | Align<br>ScanManipulator | 0.11<br>0.14 |
| | Curved surface (vertical axis), offset = 5 mm | Align<br>ScanManipulator | 0.02<br>0.05 |
| | Curved surface (horizontal axis), Radial line | Align<br>ScanManipulator | 0.05<br>0.04 |

On MPISI, the wall scans were analysed using Align and ScanManipulator software. From Table 12-2, it can be observed that the average difference between wall scans (using a 1 mm secondary slit) and CMM results were ~70 µm. There was no apparent disparity between results from measurements using different detector angular position or measurement geometries, with the details given in Annex A.3.4, Table A-18 and A-19. The output of Align and ScanManipulator software shows very good agreement. Similar observation can be made for the results measured using a 2 mm secondary radial collimator configuration, however the average difference was notably higher, which is ~150 µm. For the measurement on flat surfaces not perpendicular to the beam propagation direction, the average difference was ~50 µm for measurement with tilt of 2°. For measurement with tilt of 10°, the average difference was ~200 µm. For the curved surface measurement with the curvature axis vertical direction, measurement along radial line yielded a difference between neutron scan and CMM results of above 100 µm, while the measurement along offset line showed the difference lower than 50 µm. With the curvature axis vertical direction, the measurement along radial line produced a difference of ~50 µm.

BrightnESS² is funded by the European Union Framework Programme for Research and Innovation Horizon 2020, under grant agreement 823867

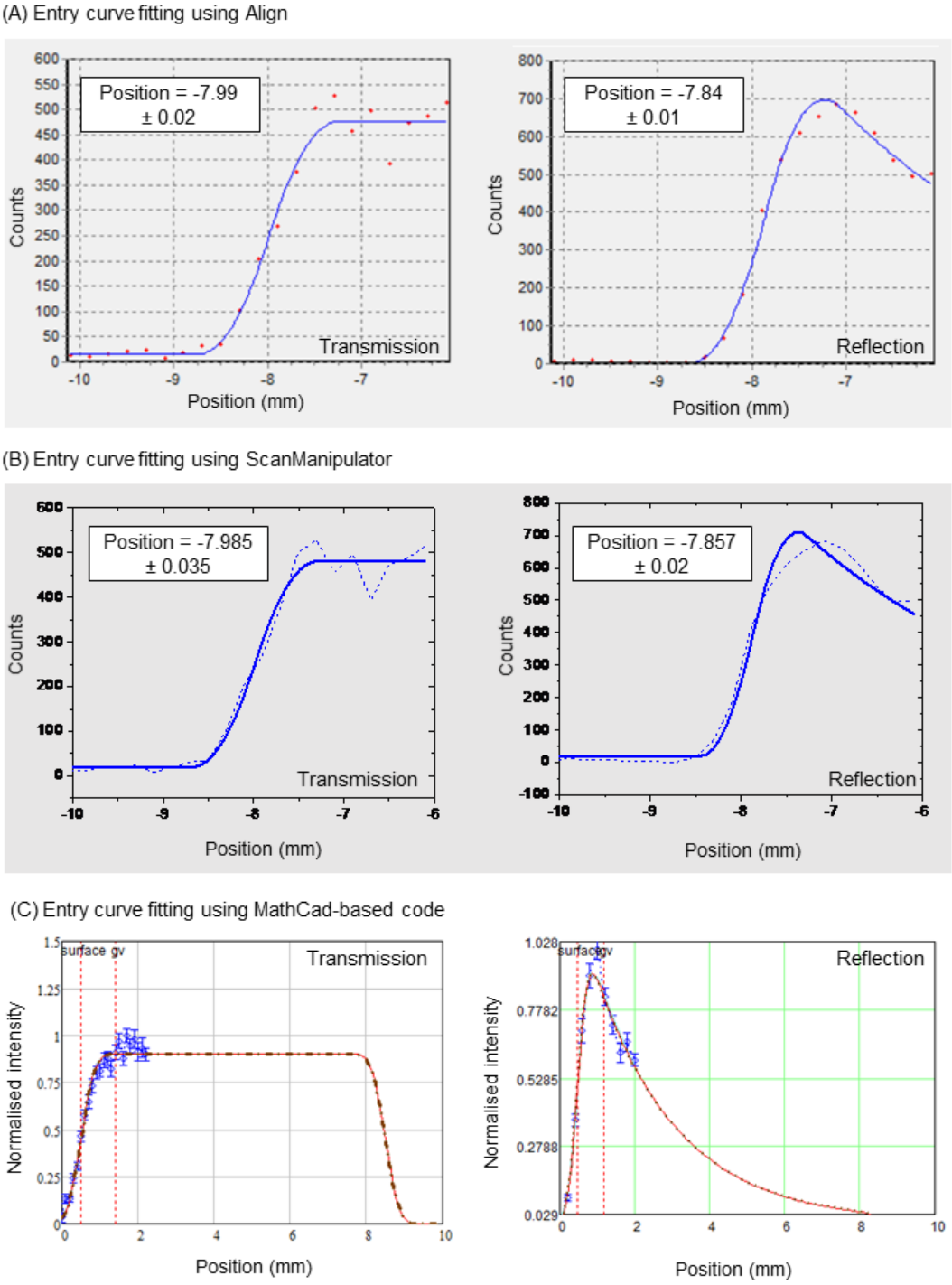


*Figure 12-3 Example of an entry scan intensity curve fitting using analysis tools: (A) Align, (B) ScanManipulator, and (C) MathCad-based code. The intensity curve is taken from an entry scan of Wall 1. Data for (A) and (B) is identical, taken from a MPISI measurement. Data for (C) is taken from a SALSA measurement.*

BrightnESS² is funded by the European Union Framework Programme for Research and Innovation Horizon 2020, under grant agreement 823867

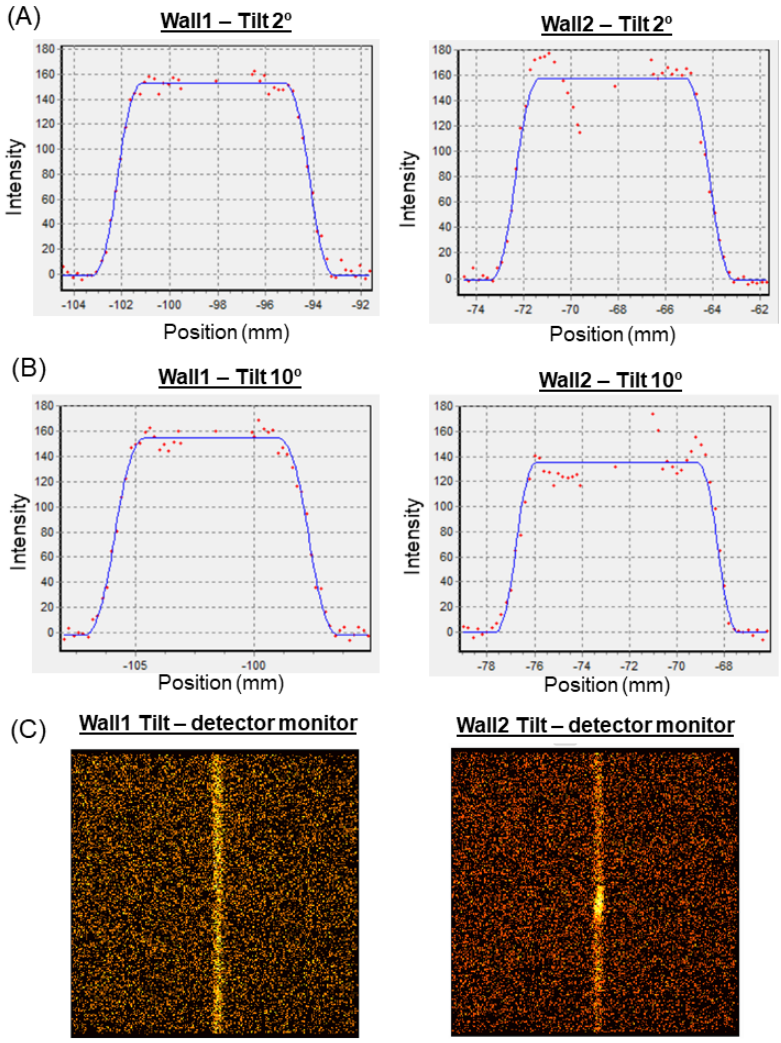


*Figure 12-4 Intensity curve and model fitting, of Wall1 and Wall2 with (A) 2 °and (B) 10 ° tilt; (C) Selected raw detector data frames of Wall1 and Wall2 with tilt. The intensity curve and the detector monitor of Wall2 measurement indicated possible large grain size or preferred orientation (evident from the non-uniform intensity along the Debye-Scherrer cone).*

## 12.3. Discussion

From the results above, a number of discussion points can be derived as follows:

1. The software packages implemented on each participating instrument were proven to be able to determine the position of flat surfaces that are perpendicular to the beam propagation plane with an accuracy of 100 µm or better. The accuracy was lower for measurement on MPISI using a 2 mm secondary radial collimator setup with GV 2 × 10 × 2 $mm^3$, with the average difference between wall scan and CMM of ~150 µm. This was due to less positional sensitivity at the larger beam width for this increased GV. However, this value is still below 10% of the 2 mm GV width, which is the objective.

2. For flat surfaces that are not perpendicular (i.e., tilted) to the beam propagation plane, the accuracy of the software is adversely affected by the height of the GV used for the measurement. Results from STRESS-SPEC on Wall1 (GV height of 2 mm), presented in Table A-12, showed that the software can determine the surface at 2° and 10° sample tilts to an accuracy better than 100

BrightnESS² is funded by the European Union Framework Programme for Research and Innovation Horizon 2020, under grant agreement 823867

µm. Results from the MPISI measurement, Table A-20, suggest that flat surface with 2° tilt can still be determined within the 100 µm accuracy using a GV height of 10 mm. However, at the larger tilt of 10° the accuracy is worse at ~200 µm.

3. The STRESS-SPEC results on Wall2 with 2° and 10° tilt, Table A-12, showed poorer accuracy (>200 µm), that is attributed to the large grain size effect within the Wall2 material revealed by the spotty Debye Scherrer ring observed on the detector monitor, Figure 12-4(C). This effect changes the shape of the intensity curve, Figure 12-4(B). Therefore, it can be inferred that a sample with large grain size and/or crystallographic texture can influence the accuracy of determination of the sample surface with entry scans. A possible solution is to accurately attach a calibration sample (fine grain, non-textured) that has the same material composition to the original test specimen, and perform the entry scan on the calibration sample instead. Another solution is to define the sample surface by other methods than diffraction, for instance using surface laser scans in conjunction with Strain Scanning Simulation Software (SScanSS) [31].

4. Analysis of the curved surface scans at radial line with the axis vertical using both Align and ScanManipulator indicated that the model used by the software produced inaccuracy of up to 300 µm, Table A-13 and A-21. The inaccuracy is even larger for measurement at offset line of 30 mm. This is expected since neither program considers sample curvature in the intensity curve model. MathCad-based code used on SALSA, which has the ability to input the radius of cylindrical samples in the fitting function, determine the position of curved surfaces with an accuracy better than 100 µm, Figure A-5. However, more experiments are needed to better represent the capability of the software in finding curved surfaces.

Scan results of curved surface with the axis horizontal direction (’axial’ direction) revealed that, using a simple function intended for modelling flat surfaces, the surface position could still be determined with an accuracy better than 100 µm. This applies to fitting the curved surface with radius of 50 mm using GV heights of 2 mm and 10 mm, Table A-13 and A-21.

BrightnESS² is funded by the European Union Framework Programme for Research and Innovation Horizon 2020, under grant agreement 823867

## 13. Summary

A summary of the results of the calibration measurements on the four participating neutron strain scanners is presented in Table 13-1. Results from the calibration campaign conclude that positioning uncertainties better than 100 µm can be attained by all the participating instruments. This result also confirms the positioning uncertainty analysis from the Round Robin exercise of VAMAS TWA20, where most of the participating instruments also demonstrated indirectly a positioning uncertainty around 100 µm.

Take-away points that can be inferred from this work are:

1. Instrument calibration with similar exercises and using common sets of specific geometric samples have been developed and demonstrated, and is to be followed for the achievement of the Neutron Quality Label (NQL).
2. The report has proven that the alignment procedures on each participating instrument can achieve uncertainties between reference point vs. centre of $\omega$-rotation better than 100 µm. It also proved that the sample alignment systems and procedures on each participating instrument have a precision of 100 µm or better. In addition, the effect of the change in detector angular position, with or without re-alignment, needs to be accounted for in the positioning uncertainty analysis.
3. For cases where a very accurate sample alignment is required, entry scans can be performed. Using the different entry scan analysis tools, the achievable accuracy for different sample geometries are listed in Table 13-1. For flat surfaces, the accuracy is 100 µm or better. However, entry scan of non-flat surfaces require an accurate geometric model to be implemented in the software tool.

This work has laid the groundwork for neutron strain scanner characterisation using a common protocol. From the lesson learned during the project, there are some scopes for future work which are:

- Evaluation of GV position as a function of re-adjusted detector positions.
- Evaluation of the influence on the GV height on the accuracy of entry scans for surface determination.
- Implementation of more geometric models for the entry curve analysis software used for sample alignment.

The next step of this project would be to implement the NQL, which calibration protocol and reporting template were constructed based on this work, to industrial measurements. This is to demonstrate the value of the NQL. This will be carried out within the BrightnESS$^2$ project and will be presented as deliverable D2.6.

BrightnESS$^2$ is funded by the European Union Framework Programme for Research and Innovation Horizon 2020, under grant agreement 823867

*Table 13-1 Summary of the calibration measurements on the four participating neutron strain scanners*

| | SALSA | STRESS-SPEC | MPISI | ENGIN-X |
|---|---|---|---|---|
| Precision of sample alignment system | ~50 µm | ~100 µm | ~100 µm | < 100 µm |
| Reference point vs. centre of $\omega$-rotation | 310 µm, due to defect of calibration sample. Investigation afterwards indicated accuracy around or better than 100 µm | 60 - 70 µm | 70-90 µm | < 100 µm |
| Accuracy of entry curve software | • MathCad-based code (SALSA)<br>– Flat surface, perpendicular = 50 µm<br>– Curved surface, axis vertical < 100 µm<br>• Align (STRESS-SPEC, MPISI, ENGIN-X)<br>– Flat surface, perpendicular < 100 µm<br>– Flat surface, not perpendicular = ~100 µm (using small GV height)<br>– Curved surface, axis vertical, radial & offset up to 5 mm < 200 µm<br>– Curved surface, axis vertical, offset = 30 mm > 500 µm<br>– Curved surface, axis horizontal = ~100 µm<br>• ScanManipulator (MPISI)<br>– Flat surface, perpendicular < 100 µm<br>– Flat surface, not perpendicular = ~100 µm (using small GV height)<br>– Curved surface, axis vertical, radial & offset up to 5 mm < 200 µm<br>– Curved surface, axis horizontal = ~100 µm | | | |
| Detector angular position vs. GV position | • Dependent on the scattered beam optics, changes in the detector angular position can lead to displacements in the GV position (up to 200 µm for 40 degree rotation)<br>• Detector/ secondary beam aperture alignment to be performed within the position of which the sample characterisation will be performed.<br>• Reproducibility of detector aperture alignment system is within 50 µm. | | | Not applicable |
| Reference point inaccuracy between detector banks | Not applicable | | | < 50 µm |

BrightnESS² is funded by the European Union Framework Programme for Research and Innovation Horizon 2020, under grant agreement 823867

## 14. Calibration Protocol and Reporting Template

Using the lesson learned from the calibration measurements reported in this text and taking into account the experiences and knowledge from the scientists of the four participating instruments, a common calibration protocol and reporting template is proposed. The two documents are prepared as the prerequisite for the Neutron Quality Label to be applied to a residual stress analysis using neutron diffraction. In the next deliverable (D2.6) the NQL will be applied to real industrial measurements.

The common calibration protocol serves as an accompanying document alongside the ISO 21432:2019(en) [13], and is proposed as a more detailed guideline for calibration procedures at different instruments and setups to achieve the required accuracy for stress measurements of engineering components. The protocol comprises specific suggestions to perform instrument alignment, quantification of the resulting positioning uncertainty, and neutron beam characterisation. The protocol is to be followed since the procedures comprise characterisation of parameters which are needed to be reported. It has been validated at multiple instruments, and it represents a solid and corroborated/ verified procedure to carry out instrument calibration. The protocol ensures that the stress analysis from the neutron diffraction measurement is based on the data that is scientifically sound. By following this protocol, one also should be able to identify any inconsistencies that present in terms of positioning accuracy. It is noteworthy that the protocol is not designed to identify and address the instrumentation issues in the beamline, although the issues might be implied during the exercises. The calibration protocol can be found in Annex B1.

The reporting template is proposed as a comprehensive list of information and parameters about the experiment and the instrumental setup, such as details on the monochromator, gauge volume dimension, beam alignment results, and pseudo-strain correction (if applicable). These details are necessary to allow the measurement to be interpreted and eventually reproduced at other times and/or on other instruments. The reporting template can be found in Annex B2.

Future suggestions and amendments may be considered in this calibration protocol and reporting template for NQL. Non-participating neutron sources are welcomed to join the NQL standard by submitting the same or a similar measurement exercise to the NQL partners who will study the case and discuss the acceptance.

BrightnESS² is funded by the European Union Framework Programme for Research and Innovation Horizon 2020, under grant agreement 823867

## Bibliography


[1] G.A. Webster, A.N. Ezeilo, Neutron scattering in engineering applications, Phys. B Condens. Matter. 234–236 (1997) 949–955. https://doi.org/https://doi.org/10.1016/S0921-4526(96)01221-5.

[2] S. Pierret, T. Etter, A. Evans, H. Van Swygenhoven, Origin of localized rafting in Ni-based single crystal turbine blades before service and its influence on the mechanical properties, Acta Mater. 61 (2013) 1478–1488. https://doi.org/https://doi.org/10.1016/j.actamat.2012.11.024.

[3] L. Edwards, M.E. Fitzpatrick, P.E. Irving, I. Sinclair, X. Zhang, D. Yapp, An integrated approach to the determination and consequences of residual stress on the fatigue performance of welded aircraft structures, J. ASTM Int. 3 (2006) 1–17. https://doi.org/10.1520/stp45330s.

[4] M. Preuss, P.J. Withers, G.J. Baxter, A comparison of inertia friction welds in three nickel base superalloys, Mater. Sci. Eng. A. 437 (2006) 38–45. https://doi.org/https://doi.org/10.1016/j.msea.2006.04.058.

[5] P.J. Bouchard, D. George, J.R. Santisteban, G. Bruno, M. Dutta, L. Edwards, E. Kingston, D.J. Smith, Measurement of the residual stresses in a stainless steel pipe girth weld containing long and short repairs, Int. J. Press. Vessel. Pip. 82 (2005) 299–310. https://doi.org/https://doi.org/10.1016/j.ijpvp.2004.08.008.

[6] A. Narayanan, M. Mostafavi, T. Pirling, S. Kabra, R. Lewis, M.J. Pavier, M.J. Peel, Residual stress in laser cladded rail, Tribol. Int. 140 (2019) 105844. https://doi.org/https://doi.org/10.1016/j.triboint.2019.105844.

[7] R. Pan, T. Pirling, J. Zheng, J. Lin, C.M. Davies, Quantification of thermal residual stresses relaxation in AA7xxx aluminium alloy through cold rolling, J. Mater. Process. Technol. 264 (2019) 454–468. https://doi.org/https://doi.org/10.1016/j.jmatprotec.2018.09.034.

[8] I.M. Ghitiu, C.M. Jalba, M.E. Florescu, A. Magureanu, The Use of Neutron Scattering in the Advancement of Additive Manufacturing, in: L. Monostori, V.D. Majstorovic, S.J. Hu, D. Djurdjanovic (Eds.), Proc. 4th Int. Conf. Ind. 4.0 Model Adv. Manuf., Springer International Publishing, Cham, 2019: pp. 192–201.

[9] F. Foadian, A. Carradó, H.G. Brokmeier, W.M. Gan, N. Schell, N. Al-Hamdany, H. Palkowski, Evolution of texture in precision seamless tubes investigated by synchrotron and neutron radiation measurement, Mater. Charact. 151 (2019) 582–589. https://doi.org/https://doi.org/10.1016/j.matchar.2019.03.041.

[10] SINE2020 portal, (n.d.). https://www.sine2020.eu/ (accessed April 3, 2020).

[11] C. Carlile, C. Petrillo, M. Carpineti, M. Donzelli, Neutron scattering facilities in {Europe} - Present status and future perspectives, Dipartimento di Fisica - Università degli Studi di Milano, Milan, 2016.

[12] Birghtness, (n.d.). https://brightness.esss.se/ (accessed April 3, 2020).

[13] Non-destructive testing—Standard test method for determining residual stresses by neutron diffraction., International Organization for Standardization, 2019.

[14] Standard test method for determining residual stresses by neutron diffraction, 2003.

[15] G.A. Webster, Neutron diffraction measurements of residual stress in a shrink-fit ring and plug, 2000.

[16] M.C. Smith, A.C. Smith, C. Ohms, R.C. Wimpory, International Journal of Pressure Vessels and Piping The NeT Task Group 4 residual stress measurement and analysis round robin on a three-pass slot-welded plate specimen, Int. J. Press. Vessel. Pip. 164 (2018) 3–21. https://doi.org/10.1016/j.ijpvp.2017.09.003.

[17] M.T. Hutchings, P.J. Withers, T.M. Holden, T. Lorentzen, Introduction to the Characterization of Residual Stress by Neutron Diffraction, CRC Press, Boca Raton, 2005.

[18] P.C. Brand, H.J. Prask, New methods for the alignment of instrumentation for residual-stress measurements by means of neutron diffraction, J. Appl. Crystallogr. 27 (1994) 164–176. https://doi.org/10.1107/S0021889893007605.

[19] T. Pirling, Precise analysis of near surface Neutron Strain Imaging measurements, Procedia Eng. 10 (2011) 2147–2152. https://doi.org/10.1016/j.proeng.2011.04.355.

[20] D. Marais, A.M. Venter, V. Luzin, Alignment and Calibration Procedures of the Necsa Neutron Strain Scanner, in: Mater. Res. Proc., Materials Research Forum LLC, Millersville, 2018: pp. 143–148.

[21] J. Šaroun, J.R. Kornmeier, M. Hofmann, P. Mikula, M. Vrána, Analytical model for neutron diffraction peak shifts due to the surface effect, J. Appl. Crystallogr. 46 (2013) 628–638. https://doi.org/10.1107/S0021889813008194.

[22] T. Pirling, G. Bruno, P.J. Withers, SALSA-A new instrument for strain imaging in engineering materials and components, Mater. Sci. Eng. A. 437 (2006) 139–144. https://doi.org/10.1016/j.msea.2006.04.083.


BrightnESS² is funded by the European Union Framework Programme for Research and Innovation Horizon 2020, under grant agreement 823867

[23] J.R. Santisteban, M.R. Daymond, J.A. James, L. Edwards, ENGIN-X: A third-generation neutron strain scanner, J. Appl. Crystallogr. 39 (2006) 812–825. https://doi.org/10.1107/S0021889806042245.

[24] J. Rebelo-Kornmeier, M. Hofmann, W.M. Gan, C. Randau, K. Braun, K. Zeitelhack, I. Defendi, J. Krueger, E. Faulhaber, H.G. Brokmeier, New Developments of the Materials Science Diffractometer {STRESS-SPEC}, in: Mech. Stress Eval. by Neutrons Synchrotron Radiat. VIII, Trans Tech Publications Ltd, 2017: pp. 151–156. https://doi.org/10.4028/www.scientific.net/MSF.905.151.

[25] C. Randau, U. Garbe, H. Brokmeier, StressTextureCalculator : a software tool to extract texture , strain and microstructure information from area-detector measurements, J. Appl. Crystallogr. (2011) 641–646. https://doi.org/10.1107/S0021889811012064.

[26] M. Hofmann, W. Gan, J. Rebelo-Kornmeier, STRESS-SPEC : Materials science diffractometer, J. Large-Scale Res. Facil. 1 (2015) 1–25.

[27] D. Marais, A.M. Venter, J. Markgraaff, Data processing at the South African Nuclear Energy Corporation SOC Ltd(Necsa) neutron diffraction facility, in: Proceeding of SAIP2015, 2016: pp. 143–148.

[28] A.M. Venter, P.R. van Heerden, D. Marais, J.C. Raaths, MPISI: The neutron strain scanner materials probe for internal strain investigations at the SAFARI-1 research reactor, Phys. B Condens. Matter. 551 (2018) 417–421. https://doi.org/10.1016/j.physb.2017.12.011.

[29] GeoGebra, (n.d.). https://www.geogebra.org/?lang=en (accessed May 18, 2020).

[30] T. Pirling, D.J. Hughes, J.S. Robinson, Precise Determination of Residual Stresses in Large Specimens by Neutron Diffraction, in: Mech. Stress Eval. by Neutrons Synchrotron Radiat., Trans Tech Publications Ltd, 2010: pp. 80–85. https://doi.org/10.4028/www.scientific.net/MSF.652.80.

[31] J.A. James, L. Edwards, Application of robot kinematics methods to the simulation and control of neutron beam line positioning systems, Nucl. Instruments Methods Phys. Res. Sect. A Accel. Spectrometers, Detect. Assoc. Equip. 571 (2007) 709–718. http://oro.open.ac.uk/7079/.

BrightnESS² is funded by the European Union Framework Programme for Research and Innovation Horizon 2020, under grant agreement 823867

# A. ANNEX: Measurement Results of the Beamtime Campaign

## A.1. Measurement results on SALSA

### A.1.1. Pin scan

*Table A-1 Measured GV position for different detector position $2\vartheta_{det}$, from pin scan exercises on SALSA ω = 0°; Fe(211) and (110); without re-alignment; GV 0.6 × 2 × 0.6 mm³*

| $2\vartheta_{det}$ | GV position in *y*-axis (unit in mm) | | |
|---|---|---|---|
| | Theoretical | Measured | Std. error |
| 93.5° | 0.00 | 0.02 | 0.01 |
| 49.5° | 0.00 | 0.10 | 0.01 |

### A.1.2. Foil scan

*Table A-2 Measured foil positions on SALSA*

Alignment position: Top foil *y* = 0.00; Bottom Foil *x* = 0.00; GV 0.6 × 2 × 0.6 mm³

| $2\vartheta_{det}$ | ω | Foil | Scan direction | Measured (mm) | Std. error (mm) | Offset (mm) |
|---|---|---|---|---|---|---|
| 93.5° | -133.3° | Top foil | *y*-axis | 0.13 | 0.01 | 0.13 |
| | | Bottom foil | *x*-axis | -0.40 | 0.01 | -0.40 |
| | -43.3° | Top foil | *y*-axis | -0.23 | 0.01 | -0.23 |
| | | Bottom foil | *x*-axis | -0.14 | 0.01 | -0.14 |
| | 46.7° | Top foil | *y*-axis | 0.03 | 0.01 | 0.03 |
| | | Bottom foil | *x*-axis | 0.22 | 0.01 | 0.22 |

BrightnESS² is funded by the European Union Framework Programme for Research and Innovation Horizon 2020, under grant agreement 823867

### A.1.3. Sample alignment system accuracy

*Table A-3 Measurement of 5-wall sample to determine the precision of sample alignment system on SALSA.*

GV 0.6 × 2 × 0.6 mm³

(i) $2\vartheta_{det}$= 83.6°; Fe(220); Transmission; Long counts (800 counts); unit in mm

| Surface | Alignment position | Accuracy | Measured position | Offset |
|---|---|---|---|---|
| Wall1A | -88.71 | 0.01 | -88.81 | -0.10 |
| Wall1B | -80.76 | 0.01 | -80.86 | -0.10 |
| Wall2A | -58.79 | 0.01 | -58.80 | -0.01 |
| Wall2B | -50.79 | 0.01 | -50.80 | -0.01 |
| | | | Std. Deviation | **0.05** |

(ii) $2\vartheta_{det}$= 83.6°; Fe(220); Transmission; Short counts (400 counts); unit in mm

| Surface | Alignment position | Accuracy | Measured position | Offset |
|---|---|---|---|---|
| Wall1A | -88.71 | 0.01 | -88.77 | -0.06 |
| Wall1B | -80.76 | 0.01 | -80.84 | -0.08 |
| Wall2A | -58.79 | 0.01 | -58.92 | -0.13 |
| Wall2B | -50.79 | 0.01 | -50.97 | -0.18 |
| Wall3A | -28.81 | 0.01 | -28.68 | 0.13 |
| Wall3B | -20.83 | 0.01 | -20.71 | 0.12 |
| Wall4A | 1.17 | 0.01 | 1.23 | 0.06 |
| Wall4B | 9.15 | 0.01 | 9.20 | 0.05 |
| Wall5A | 31.11 | 0.01 | 31.16 | 0.05 |
| Wall5B | 39.07 | 0.01 | 39.16 | 0.09 |
| | | | Std. Deviation | **0.11** |

(iii) $2\vartheta_{det}$= 83.6°; Fe(220); Reflection; Short counts (400 counts); unit in mm

| Surface | Alignment position | Accuracy | Measured position | Offset |
|---|---|---|---|---|
| Wall1A | -88.71 | 0.01 | -88.88 | -0.17 |
| Wall2A | -58.79 | 0.01 | -58.9 | -0.11 |
| Wall3A | -28.81 | 0.01 | -28.99 | -0.18 |
| Wall4A | 1.17 | 0.01 | 1.34 | 0.17 |
| Wall5A | 31.11 | 0.01 | 31.09 | -0.02 |
| | | | Std. Deviation | **0.14** |

BrightnESS² is funded by the European Union Framework Programme for Research and Innovation Horizon 2020, under grant agreement 823867

### A.1.4. Wall & Tube scan

*Table A-4 Comparison between wall thickness measured by CMM and by wall scan fitted by MathCad-based code on SALSA, for flat surface perpendicular to the beam propagation plane.*

GV 0.6 × 2 × 0.6 mm³

(i) $2\vartheta_{det}$= 83.6°; Fe(220); Transmission; Long counts (800 counts)

| Features | Wall thickness (mm) | | | Difference (mm) |
|---|---|---|---|---|
| | CMM | Accuracy | Wall scan | |
| Wall1 | 8.00 | 0.03 | 7.95 | 0.05 |
| Wall2 | 8.01 | 0.03 | 8.00 | 0.01 |

(ii) $2\vartheta_{det}$= 83.6°; Fe(220); Transmission; Short counts (400 counts)

| Features | Wall thickness (mm) | | | Difference (mm) |
|---|---|---|---|---|
| | CMM | Accuracy | Wall scan | |
| Wall1 | 8.00 | 0.03 | 7.94 | 0.07 |
| Wall2 | 8.01 | 0.03 | 7.96 | 0.05 |
| Wall3 | 8.02 | 0.03 | 7.97 | 0.05 |
| Wall4 | 8.02 | 0.03 | 7.97 | 0.05 |
| Wall5 | 8.00 | 0.03 | 8.00 | 0.00 |

(iii) $2\vartheta_{det}$= 83.6°; Fe(220); Reflection; Long count (800 counts)

| Features | Wall thickness (mm) | | | Difference (mm) |
|---|---|---|---|---|
| | CMM | Accuracy | Wall scan | |
| Wall1 | 8.00 | 0.03 | 8.00 | 0.00 |
| | | | Average (total) | 0.04 |

*Table A-5 Comparison between wall thickness measured by CMM and wall scan fitted by MathCad-based code on SALSA, for Tube sample (R = 50 mm) along radial line.*

Axis of the tube in vertical direction; Reflection; GV 0.6 × 2 × 0.6 mm³

| Features | Wall thickness (mm) | | | Difference (mm) |
|---|---|---|---|---|
| | CMM | Accuracy | Wall scan | |
| Rad-1 | 5.08 | 0.02 | 5.02 | 0.06 |

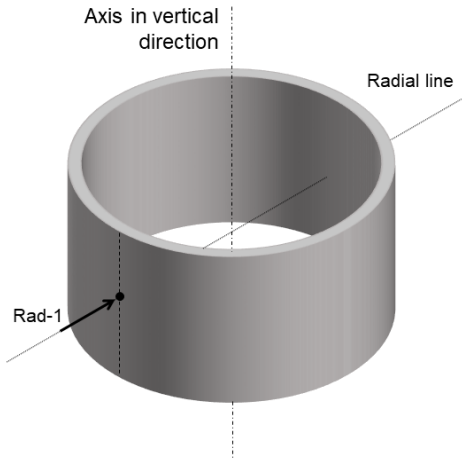


*Figure A-1 Scan position of the Tube sample on SALSA.*

BrightnESS² is funded by the European Union Framework Programme for Research and Innovation Horizon 2020, under grant agreement 823867

## A.2. Measurement results on STRESS-SPEC

### A.2.1. Pin scan

*Table A-6 Measured GV position for different detector position $2\vartheta_{det}$, from pin scan exercises on STRESS-SPEC*

GV 1 × 10 × 1 mm³

$\omega$ = −90°; Fe(211), Fe(200) and (110); secondary radial collimator, without re-alignment

| $2\vartheta_{det}$ | GV position in *y*-axis (unit in mm) | | |
|---|---|---|---|
| | Theoretical | Measured | Std. error |
| 92° | 0.00 | 0.03 | 0.00 |
| 72° | 0.00 | -0.18 | 0.01 |
| 49° | 0.00 | -0.24 | 0.01 |

$\omega$ = 0°; Fe(211), Fe(200) and (110); secondary slit, with re-alignment

| $2\vartheta_{det}$ | GV position in *y*-axis (unit in mm) | | |
|---|---|---|---|
| | Theoretical | Measured | Std. error |
| 92° | 0.00 | -0.29 | 0.00 |
| 72° | 0.00 | -0.24 | 0.01 |
| 49° | 0.00 | -0.25 | 0.01 |

### A.2.2. Foil scan

*Table A-7 Measured foil positions on STRESS-SPEC, using secondary radial collimator setup, without realignment*

Alignment position: Top foil *y* = 0.00; Bottom Foil *x* = 2.40; GV 1 × 10 × 1 mm³

| $2\vartheta_{det}$ | $\omega$ | Foil | Scan direction | Measured (mm) | Std. error (mm) | Offset (mm) |
|---|---|---|---|---|---|---|
| 92° | 136° | Top foil | *y*-axis | -0.09 | 0.00 | -0.09 |
| | | Bottom foil | *x*-axis | 2.47 | 0.00 | 0.07 |
| | 46° | Top foil | *y*-axis | -0.08 | 0.00 | -0.08 |
| | | Bottom foil | *x*-axis | 2.42 | 0.00 | 0.02 |
| | -44° | Top foil | *y*-axis | -0.16 | 0.00 | -0.16 |
| | | Bottom foil | *x*-axis | 2.43 | 0.00 | 0.03 |
| 72° | -54° | Top foil | *y*-axis | -0.34 | 0.01 | -0.34 |
| | | Bottom foil | *x*-axis | 2.31 | 0.01 | -0.09 |
| | 36° | Top foil | *y*-axis | 0.01 | 0.00 | 0.01 |
| | | Bottom foil | *x*-axis | 2.28 | 0.01 | -0.12 |
| | 126° | Top foil | *y*-axis | 0.05 | 0.01 | 0.05 |
| | | Bottom foil | *x*-axis | 2.55 | 0.01 | 0.15 |

BrightnESS² is funded by the European Union Framework Programme for Research and Innovation Horizon 2020, under grant agreement 823867

*Table A-8 Measured foil positions on STRESS-SPEC, using secondary slit, with re-alignment*

Alignment position: Top foil $y$ = 0.00; Bottom Foil $x$ = 2.40; GV 1 × 10 × 1 mm³

| $2\vartheta_{det}$ | $\omega$ | Foil | Scan direction | Measured (mm) | Std. error (mm) | Offset (mm) |
|---|---|---|---|---|---|---|
| 92° | 136° | Top foil | *y*-axis | -0.05 | 0.00 | -0.05 |
| | | Bottom foil | *x*-axis | 2.49 | 0.00 | 0.09 |
| | 46° | Top foil | *y*-axis | -0.12 | 0.00 | -0.12 |
| | | Bottom foil | *x*-axis | 2.39 | 0.00 | -0.01 |
| | -44° | Top foil | *y*-axis | -0.21 | 0.00 | -0.21 |
| | | Bottom foil | *x*-axis | 2.45 | 0.00 | 0.05 |
| 72° | -54° | Top foil | *y*-axis | -0.23 | 0.01 | -0.23 |
| | | Bottom foil | *x*-axis | 2.48 | 0.00 | 0.08 |
| | 36° | Top foil | *y*-axis | -0.13 | 0.00 | -0.13 |
| | | Bottom foil | *x*-axis | 2.44 | 0.01 | 0.04 |
| | 126° | Top foil | *y*-axis | -0.04 | 0.00 | -0.04 |
| | | Bottom foil | *x*-axis | 2.46 | 0.00 | 0.06 |

### A.2.3. Sample alignment system accuracy

*Table A-9 Measurement of 5-wall sample to determine the precision of sample alignment system on STRESS-SPEC using Si Monochromator, $2\theta_{det} = 83^\circ$*

GV 1 × 8 × 1 mm³

(i) $2\vartheta_{det}$= 83°; Fe(220); Transmission

| Surface | Position (mm) | | | | Offset (mm) |
|---|---|---|---|---|---|
| | Alignment | Accuracy | Measured | Std. error | |
| Wall1A | -101.00 | 0.10 | -101.12 | 0.04 | -0.12 |
| Wall1B | -93.00 | 0.10 | -93.18 | 0.04 | -0.18 |
| Wall2A | -71.00 | 0.10 | -71.25 | 0.03 | -0.25 |
| Wall2B | -63.00 | 0.10 | -63.21 | 0.04 | -0.21 |
| Wall3A | -41.00 | 0.10 | -41.23 | 0.04 | -0.23 |
| Wall3B | -33.00 | 0.10 | -33.16 | 0.04 | -0.16 |
| Wall4A | -11.00 | 0.10 | -11.09 | 0.04 | -0.09 |
| Wall4B | -3.00 | 0.10 | -3.21 | 0.04 | -0.21 |
| Wall5A | 19.00 | 0.10 | 18.60 | 0.04 | -0.40 |
| Wall5B | 27.00 | 0.10 | 26.65 | 0.04 | -0.35 |
| | | | | Std. Deviation | **0.10** |

(ii) $2\vartheta_{det}$= 83°; Fe(220); Reflection

| Surface | Position (mm) | | | | Offset (mm) |
|---|---|---|---|---|---|
| | Alignment | Accuracy | Measured | Std. error | |
| Wall1A | -101.00 | 0.10 | -101.17 | 0.02 | -0.17 |
| Wall1B | -93.00 | 0.10 | -93.20 | 0.03 | -0.20 |
| Wall2A | -71.00 | 0.10 | -71.19 | 0.02 | -0.19 |
| Wall2B | -63.00 | 0.10 | -63.11 | 0.02 | -0.11 |
| Wall4A | -11.00 | 0.10 | -11.27 | 0.02 | -0.27 |
| Wall4B | -3.00 | 0.10 | -3.32 | 0.03 | -0.32 |
| Wall5A | 19.00 | 0.10 | 18.57 | 0.02 | -0.43 |
| Wall5B | 27.00 | 0.10 | 26.56 | 0.02 | -0.44 |
| | | | | Std. Deviation | **0.12** |

BrightnESS² is funded by the European Union Framework Programme for Research and Innovation Horizon 2020, under grant agreement 823867

*Table A-10 Measurement of 5-wall sample to determine the precision of sample alignment system on STRESS-SPEC using Si monochromator at $2\vartheta_{det} = 102^\circ$ and Ge monochromator at $2\vartheta_{det} = 77.5^\circ$*

GV 1 × 8 × 1 mm³

(i) Si Monochromator; $2\vartheta_{det}$= 102°; Fe(311); Transmission

| Surface | Position (mm) | | | | Offset (mm) |
|---|---|---|---|---|---|
| | Alignment | Accuracy | Measured | Std. error | |
| Wall1A | -101.00 | 0.10 | -101.08 | 0.03 | -0.08 |
| Wall1B | -93.00 | 0.10 | -93.05 | 0.03 | -0.05 |
| Wall2A | -71.00 | 0.10 | -71.01 | 0.03 | -0.01 |
| Wall2B | -63.00 | 0.10 | -62.97 | 0.03 | 0.03 |
| | | | | Std. Deviation | **0.05** |

(ii) Si Monochromator; $2\vartheta_{det}$= 102°; Fe(311); Reflection

| Surface | Position (mm) | | | | Offset (mm) |
|---|---|---|---|---|---|
| | Alignment | Accuracy | Measured | Std. error | |
| Wall1A | -101.00 | 0.10 | -101.27 | 0.02 | -0.27 |
| Wall1B | -93.00 | 0.10 | -93.30 | 0.02 | -0.30 |
| Wall2A | -71.00 | 0.10 | -71.32 | 0.02 | -0.32 |
| Wall2B | -63.00 | 0.10 | -63.14 | 0.03 | -0.14 |
| | | | | Std. Deviation | **0.08** |

(iii) Ge Monochromator; $2\vartheta_{det}$= 77.5°; Fe(311); Transmission

| Surface | Position (mm) | | | | Offset (mm) |
|---|---|---|---|---|---|
| | Alignment | Accuracy | Measured | Std. error | |
| Wall1A | -101.00 | 0.10 | -100.96 | 0.03 | 0.04 |
| Wall1B | -93.00 | 0.10 | -92.93 | 0.03 | 0.07 |
| Wall2A | -71.00 | 0.10 | -70.90 | 0.04 | 0.10 |
| Wall2B | -63.00 | 0.10 | -62.90 | 0.03 | 0.10 |
| | | | | Std. Deviation | **0.03** |

BrightnESS² is funded by the European Union Framework Programme for Research and Innovation Horizon 2020, under grant agreement 823867

### A.2.4. Wall & Tube scan

*Table A-11 Comparison between CMM result and wall scan fitted by Align software on STRESS-SPEC, for flat surface perpendicular to the beam propagation plane.*

GV 1 × 8 × 1 $mm^3$

(i) Si monochromator; $2\vartheta_{det}$= 83°; Fe(220); Transmission

| Features | Wall thickness (mm) | | | | Difference (mm) |
|---|---|---|---|---|---|
| | CMM | Accuracy | Wall scan | Std. error | |
| Wall1 | 8.00 | 0.03 | 7.94 | 0.06 | 0.06 |
| Wall2 | 8.01 | 0.03 | 8.04 | 0.06 | 0.03 |
| Wall3 | 8.02 | 0.03 | 8.07 | 0.05 | 0.05 |
| Wall4 | 8.02 | 0.03 | 7.88 | 0.06 | 0.14 |
| Wall5 | 8.00 | 0.03 | 8.05 | 0.06 | 0.05 |

(ii) Si monochromator; $2\vartheta_{det}$= 83°; Fe(220); Reflection

| Features | Wall thickness (mm) | | | | Difference (mm) |
|---|---|---|---|---|---|
| | CMM | Accuracy | Wall scan | Std. error | |
| Wall1 | 8.00 | 0.03 | 7.97 | 0.04 | 0.03 |
| Wall2 | 8.01 | 0.03 | 8.08 | 0.03 | 0.07 |
| Wall4 | 8.02 | 0.03 | 7.95 | 0.04 | 0.07 |
| Wall5 | 8.00 | 0.03 | 7.99 | 0.03 | 0.01 |

(iii) Si monochromator; $2\vartheta_{det}$= 102°; Fe(311); Transmission

| Features | Wall thickness (mm) | | | | Difference (mm) |
|---|---|---|---|---|---|
| | CMM | Accuracy | Wall scan | Std. error | |
| Wall1 | 8.00 | 0.03 | 8.03 | 0.04 | 0.03 |
| Wall2 | 8.01 | 0.03 | 8.04 | 0.04 | 0.03 |

(vi) Si monochromator; $2\vartheta_{det}$= 102°; Fe(311); Reflection

| Features | Wall thickness (mm) | | | | Difference (mm) |
|---|---|---|---|---|---|
| | CMM | Accuracy | Wall scan | Std. error | |
| Wall1 | 8.00 | 0.03 | 7.97 | 0.03 | 0.03 |
| Wall2 | 8.01 | 0.03 | 8.18 | 0.04 | 0.17 |

(v) Ge monochromator; $2\vartheta_{det}$= 77.5°; Fe(311); Transmission

| Features | Wall thickness (mm) | | | | Difference (mm) |
|---|---|---|---|---|---|
| | CMM | Accuracy | Wall scan | Std. error | |
| Wall1 | 8.00 | 0.03 | 8.03 | 0.04 | 0.03 |
| Wall2 | 8.01 | 0.03 | 8.00 | 0.05 | 0.01 |
| | | | | Average (total) | **0.05** |

BrightnESS² is funded by the European Union Framework Programme for Research and Innovation Horizon 2020, under grant agreement 823867

*Table A-12 Comparison between CMM result and wall scan fitted by Align software on STRESS-SPEC, for flat surface not perpendicular to the beam propagation plane.*

Si monochromator; $2\vartheta_{det}$= 83°; Fe(220); Transmission; GV 1 × 2 × 1 mm³

| Tilt | Features | Wall thickness (mm) | | | | Difference (mm) |
|---|---|---|---|---|---|---|
| | | CMM | Accuracy | Wall scan | Std. error | |
| 2° | Wall1 | 8.00 | 0.03 | 8.02 | 0.06 | 0.02 |
| | Wall2 | 8.01 | 0.03 | 8.22 | 0.05 | 0.21 |
| 10° | Wall1 | 8.12 | 0.03 | 8.16 | 0.06 | 0.04 |
| | Wall2 | 8.13 | 0.03 | 8.54 | 0.05 | 0.41 |

*Table A-13 Comparison between CMM result and wall scan fitted by Align software on STRESS-SPEC, for Tube sample (R = 50 mm). Scan position indicated in Figure A-2.*

GV 1 × 8 × 1 mm³

(i) Axis of the tube in vertical direction; *Transmission; **Reflection

| Features | Wall thickness (mm) | | | | Difference (mm) |
|---|---|---|---|---|---|
| | CMM | Accuracy | Wall scan | Std. error | |
| Rad-1* | 5.08 | 0.02 | 4.98 | 0.06 | 0.10 |
| Rad-1** | 5.08 | 0.02 | 4.84 | 0.04 | 0.24 |
| Off-5* | 5.10 | 0.02 | 5.13 | 0.06 | 0.03 |
| Off-5** | 5.10 | 0.02 | 5.13 | 0.03 | 0.03 |
| Off-30* | 6.35 | 0.03 | 6.79 | 0.08 | 0.44 |
| Off-30** | 6.35 | 0.03 | 7.28 | 0.06 | 0.93 |

(ii) Axis of the tube in horizontal direction; *Transmission; **Reflection

| Features | Wall thickness (mm) | | | | Difference (mm) |
|---|---|---|---|---|---|
| | CMM | Accuracy | Wall scan | Std. error | |
| Rad-2* | 5.08 | 0.02 | 5.16 | 0.05 | 0.08 |
| Rad-2** | 5.08 | 0.02 | 4.86 | 0.04 | 0.22 |
| Rad-3* | 5.08 | 0.02 | 5.14 | 0.04 | 0.06 |
| Rad-3** | 5.08 | 0.02 | 5.11 | 0.03 | 0.03 |
| | | | | Average (ii) | **0.10** |

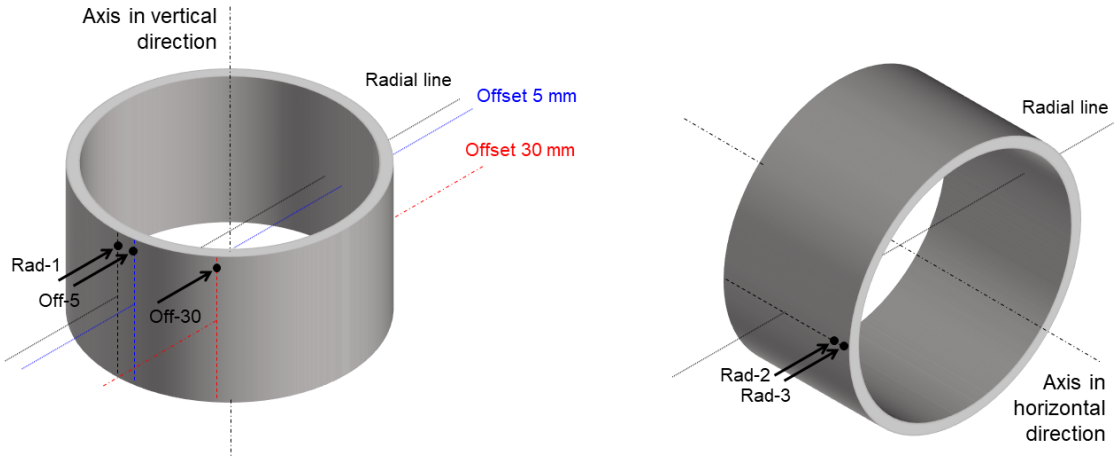


*Figure A-2 Scan position of the Tube sample on STRESS-SPEC.*

BrightnESS² is funded by the European Union Framework Programme for Research and Innovation Horizon 2020, under grant agreement 823867

## A.3. Measurement results on MPISI

### A.3.1. Pin scan

*Table A-14 Measured GV position for different detector position $2\vartheta_{det}$, from pin scan exercises on MPISI*

$\omega$ = 0°; Fe(211), Fe(110) and (220); secondary slit, with re-alignment; GV 1 × 10 × 1 mm³

| $2\vartheta_{det}$ | GV position in *y*-axis (unit in mm) | | |
|---|---|---|---|
| | Theoretical | Measured | Std. error |
| 90° | 0.00 | 0.03 | 0.01 |
| 50° | 0.00 | 0.09 | 0.01 |
| 105° | 0.00 | 0.05 | 0.02 |

### A.3.2. Foil scan

*Table A-15 Measured foil positions on MPISI, using primary and secondary slits, with re-alignment*

Alignment position: Top foil *y* = 5.20; Bottom Foil *x* = -26.92; GV 1 × 10 × 1 mm³

| $2\vartheta_{det}$ | $\omega$ | Foil | Scan direction | Measured (mm) | Std. error (mm) | Offset (mm) |
|---|---|---|---|---|---|---|
| 90° | 45° | Top foil | *y*-axis | 5.28 | 0.02 | 0.08 |
| | | Bottom foil | *x*-axis | -26.97 | 0.01 | -0.05 |
| | 135° | Top foil | *y*-axis | 5.36 | 0.01 | 0.16 |
| | | Bottom foil | *x*-axis | -26.85 | 0.01 | 0.07 |
| | -45° | Top foil | *y*-axis | 5.18 | 0.01 | -0.02 |
| | | Bottom foil | *x*-axis | -26.90 | 0.01 | 0.02 |
| | -135° | Top foil | *y*-axis | 5.22 | 0.01 | 0.02 |
| | | Bottom foil | *x*-axis | -26.76 | 0.01 | 0.16 |
| 50° | -54° | Top foil | *y*-axis | 5.26 | 0.02 | 0.06 |
| | | Bottom foil | *x*-axis | -26.98 | 0.01 | -0.06 |
| | 36° | Top foil | *y*-axis | 5.34 | 0.01 | 0.14 |
| | | Bottom foil | *x*-axis | -26.89 | 0.02 | 0.03 |
| | 126° | Top foil | *y*-axis | 5.28 | 0.02 | 0.08 |
| | | Bottom foil | *x*-axis | -26.77 | 0.01 | 0.15 |

BrightnESS² is funded by the European Union Framework Programme for Research and Innovation Horizon 2020, under grant agreement 823867

### A.3.3. Sample alignment system accuracy

*Table A-16 Measurement of 5-wall sample to determine the precision of sample alignment system on MPISI, transmission geometry. Data analysed using Align and ScanManipulator.*

GV 1 × 10 × 1 mm³

(i) $2\vartheta_{det}$ = 80°, Fe(220), Transmission

| Surface | Position (mm) | | | | | | | |
|---|---|---|---|---|---|---|---|---|
| | Alignment | Accuracy | Align | | | ScanManipulator | | |
| | | | Measured | Std. error | Offset | Measured | Std. error | Offset |
| Wall1A | 0.00 | 0.10 | -0.02 | 0.03 | -0.02 | -0.01 | 0.02 | -0.01 |
| Wall1B | -8.10 | 0.10 | -7.99 | 0.04 | 0.11 | -7.99 | 0.02 | 0.11 |
| Wall2A | -29.90 | 0.10 | -29.94 | 0.06 | -0.04 | -29.92 | 0.02 | -0.02 |
| Wall2B | -38.00 | 0.10 | -38.11 | 0.03 | -0.11 | -38.12 | 0.02 | -0.12 |
| Wall3A | -59.81 | 0.10 | -59.99 | 0.03 | -0.18 | -60.01 | 0.02 | -0.20 |
| Wall3B | -67.90 | 0.10 | -68.03 | 0.05 | -0.13 | -68.02 | 0.02 | -0.12 |
| Wall4A | -89.81 | 0.10 | -89.74 | 0.04 | 0.08 | -89.74 | 0.02 | 0.07 |
| Wall4B | -97.81 | 0.10 | -97.78 | 0.02 | 0.03 | -97.77 | 0.02 | 0.04 |
| Wall5A | -119.71 | 0.10 | -119.86 | 0.03 | -0.15 | -119.87 | 0.02 | -0.16 |
| Wal5B | -127.81 | 0.10 | -127.78 | 0.02 | 0.03 | -127.77 | 0.02 | 0.04 |
| | | | | Std. Dev | **0.10** | | Std. Dev | **0.11** |

(ii) $2\vartheta_{det}$ = 55°, Fe(200), Transmission

| Surface | Position (mm) | | | | | | | |
|---|---|---|---|---|---|---|---|---|
| | Alignment | Accuracy | Align | | | ScanManipulator | | |
| | | | Measured | Std. error | Offset | Measured | Std. error | Offset |
| Wall1A | 0.00 | 0.10 | -0.05 | 0.04 | -0.05 | -0.04 | 0.03 | -0.04 |
| Wall1B | -8.10 | 0.10 | -7.98 | 0.03 | 0.12 | -7.98 | 0.02 | 0.12 |
| Wall2A | -29.90 | 0.10 | -29.96 | 0.04 | -0.05 | -29.97 | 0.03 | -0.07 |
| Wall2B | -38.00 | 0.10 | -37.91 | 0.04 | 0.09 | -37.92 | 0.03 | 0.08 |
| | | | | Std. Dev | **0.09** | | Std. Dev | **0.09** |

BrightnESS² is funded by the European Union Framework Programme for Research and Innovation Horizon 2020, under grant agreement 823867

*Table A-17 Measurement of 5-wall sample to determine the precision of sample alignment system on MPISI, reflection geometry. Data analysed using Align and ScanManipulator.*

GV 1 × 10 × 1 mm³

(i) $2\vartheta_{det} = 80°$, Fe(220), Reflection, $\omega = -140°$

| Surface | Position (mm) | | | | | | | |
|---|---|---|---|---|---|---|---|---|
| | Alignment | Accuracy | Align | | | ScanManipulator | | |
| | | | Measured | Std. error | Offset | Measured | Std. error | Offset |
| Wall1A | 0.00 | 0.10 | 0.06 | 0.00 | 0.06 | 0.08 | 0.20 | 0.08 |
| Wall1B | -8.10 | 0.10 | -7.86 | 0.01 | 0.24 | -7.85 | 0.20 | 0.25 |
| Wall2A | -29.90 | 0.10 | -29.87 | 0.00 | 0.03 | -29.85 | 0.14 | 0.05 |
| Wall2B | -38.00 | 0.10 | -37.81 | 0.01 | 0.19 | -37.79 | 0.14 | 0.21 |
| Wall3A | -59.81 | 0.10 | -59.89 | 0.00 | -0.08 | -59.87 | 0.31 | -0.06 |
| Wall3B | -67.90 | 0.10 | -67.79 | 0.01 | 0.11 | -67.76 | 0.31 | 0.14 |
| Wall4A | -89.81 | 0.10 | -89.74 | 0.00 | 0.07 | -89.73 | 0.15 | 0.08 |
| Wall4B | -97.81 | 0.10 | -97.76 | 0.01 | 0.05 | -97.74 | 0.15 | 0.07 |
| Wall5A | -119.71 | 0.10 | -119.69 | 0.00 | 0.02 | -119.66 | 0.14 | 0.05 |
| Wall5B | -127.81 | 0.10 | -127.66 | 0.01 | 0.15 | -127.63 | 0.14 | 0.18 |
| | | | | Std. Dev | **0.09** | | Std. Dev | **0.09** |

(ii) $2\vartheta_{det} = 80°$, Fe(220), Reflection, $\omega = 40°$

| Surface | Position (mm) | | | | | | | |
|---|---|---|---|---|---|---|---|---|
| | Alignment | Accuracy | Align | | | ScanManipulator | | |
| | | | Measured | Std. error | Offset | Measured | Std. error | Offset |
| Wall1A | 0.00 | 0.10 | 0.12 | 0.01 | 0.12 | 0.10 | 0.13 | 0.10 |
| Wall1B | -8.10 | 0.10 | -7.83 | 0.00 | 0.27 | -7.82 | 0.13 | 0.28 |
| Wall2A | -29.90 | 0.10 | -29.86 | 0.01 | 0.04 | -29.90 | 0.12 | 0.00 |
| Wall2B | -38.00 | 0.10 | -37.76 | 0.00 | 0.24 | -37.80 | 0.12 | 0.20 |
| Wall3A | -59.81 | 0.10 | -59.74 | 0.01 | 0.07 | -59.81 | 0.47 | 0.00 |
| Wall3B | -67.90 | 0.10 | -67.81 | 0.02 | 0.09 | -67.72 | 0.47 | 0.18 |
| Wall4A | -89.81 | 0.10 | -89.73 | 0.01 | 0.08 | -89.69 | 0.31 | 0.12 |
| Wall4B | -97.81 | 0.10 | -97.65 | 0.00 | 0.16 | -97.91 | 0.31 | -0.10 |
| Wall5A | -119.71 | 0.10 | -119.60 | 0.01 | 0.11 | -119.62 | 0.19 | 0.09 |
| Wal5B | -127.81 | 0.10 | -127.62 | 0.00 | 0.19 | -127.78 | 0.19 | 0.03 |
| | | | | Std. Dev | **0.08** | | Std. Dev | **0.11** |

BrightnESS² is funded by the European Union Framework Programme for Research and Innovation Horizon 2020, under grant agreement 823867

### A.3.4. Wall & Tube scan

*Table A-18 Comparison between CMM result and wall scan fitted by Align and ScanManipulator software on MPISI, for flat surface perpendicular to the beam propagation direction, transmission geometry.*

(i) $2\vartheta_{det} = 80°$; Fe(220); Transmission; Primary Slit - Secondary Slit; GV 1 × 10 × 1 mm³

| Features | Wall thickness (mm) | | | | | | | |
|---|---|---|---|---|---|---|---|---|
| | CMM | Accuracy | Align | | | ScanManipulator | | |
| | | | Wall scan | Std. error | Difference | Wall scan | Std. error | Difference |
| Wall1 | 8.00 | 0.03 | 7.98 | 0.03 | 0.02 | 7.96 | 0.05 | 0.04 |
| Wall2 | 8.00 | 0.03 | 8.20 | 0.03 | 0.20 | 8.18 | 0.07 | 0.17 |
| Wall3 | 8.00 | 0.03 | 8.01 | 0.03 | 0.01 | 8.05 | 0.06 | 0.04 |
| Wall4 | 8.00 | 0.03 | 8.03 | 0.03 | 0.03 | 8.05 | 0.04 | 0.04 |
| Wall5 | 8.00 | 0.03 | 7.90 | 0.03 | 0.10 | 7.92 | 0.04 | 0.09 |
| | | | | Average | **0.07** | | Average | **0.08** |

(ii) $2\vartheta_{det} = 55°$; Fe(200); Transmission; Primary Slit - Secondary Slit; GV 1 × 10 × 1 mm³

| Features | Wall thickness (mm) | | | | | | | |
|---|---|---|---|---|---|---|---|---|
| | CMM | Accuracy | Align | | | ScanManipulator | | |
| | | | Wall scan | Std. error | Difference | Wall scan | Std. error | Difference |
| Wall1 | 8.00 | 0.03 | 7.94 | 0.04 | 0.06 | 7.93 | 0.06 | 0.08 |
| Wall2 | 8.00 | 0.03 | 7.95 | 0.04 | 0.05 | 7.96 | 0.06 | 0.04 |
| | | | | Average | **0.06** | | Average | **0.06** |

(iii) $2\vartheta_{det} = 80°$; Fe(220); Transmission; Primary Slit - Secondary Collimator; GV 2 × 10 × 2 mm³

| Features | Wall thickness (mm) | | | | | | | |
|---|---|---|---|---|---|---|---|---|
| | CMM | Accuracy | Align | | | ScanManipulator | | |
| | | | Wall scan | Std. error | Difference | Wall scan | Std. error | Difference |
| Wall1 | 8.00 | 0.03 | 7.98 | 0.03 | 0.02 | 7.84 | 0.09 | 0.16 |
| Wall2 | 8.00 | 0.03 | 8.20 | 0.03 | 0.20 | 8.21 | 0.11 | 0.21 |
| Wall3 | 8.00 | 0.03 | 8.01 | 0.03 | 0.01 | 8.12 | 0.14 | 0.12 |
| Wall4 | 8.00 | 0.03 | 8.03 | 0.03 | 0.03 | 7.95 | 0.12 | 0.05 |
| Wall5 | 8.00 | 0.03 | 7.90 | 0.03 | 0.10 | 7.93 | 0.12 | 0.07 |
| | | | | Average | **0.07** | | Average | **0.12** |

(vi) $2\vartheta_{det} = 55°$; Fe(200); Transmission; Primary Slit - Secondary Collimator; GV 2 × 10 × 2 mm³

| Features | Wall thickness (mm) | | | | | | | |
|---|---|---|---|---|---|---|---|---|
| | CMM | Accuracy | Align | | | ScanManipulator | | |
| | | | Wall scan | Std. error | Difference | Wall scan | Std. error | Difference |
| Wall1 | 8.00 | 0.03 | 7.66 | 0.11 | 0.34 | 7.68 | 0.14 | 0.32 |
| Wall2 | 8.00 | 0.03 | 7.95 | 0.10 | 0.05 | 7.97 | 0.10 | 0.04 |
| | | | | Average | **0.19** | | Average | **0.18** |

BrightnESS² is funded by the European Union Framework Programme for Research and Innovation Horizon 2020, under grant agreement 823867

*Table A-19 Comparison between CMM result and wall scan fitted by Align and ScanManipulator on MPISI, for flat surface perpendicular to the beam propagation direction, reflection geometry.*

(i) $2\vartheta_{det} = 80°$; Fe(220); Reflection; Primary Slit - Secondary Slit; GV 1 × 10 × 1 mm³

| Features | CMM | Accuracy | Wall thickness (mm) | | | | | |
|---|---|---|---|---|---|---|---|---|
| | | | Align | | | ScanManipulator | | |
| | | | Wall scan | Std. error | Difference | Wall scan | Std. error | Difference |
| $\omega$ = -140° | | | | | | | | |
| Wall1 | 8.00 | 0.03 | 7.92 | 0.00 | 0.08 | 7.93 | 0.28 | 0.07 |
| Wall2 | 8.00 | 0.03 | 7.94 | 0.00 | 0.06 | 7.94 | 0.20 | 0.06 |
| Wall3 | 8.00 | 0.03 | 7.90 | 0.00 | 0.10 | 7.89 | 0.44 | 0.11 |
| Wall4 | 8.00 | 0.03 | 8.02 | 0.00 | 0.02 | 8.01 | 0.22 | 0.01 |
| Wall5 | 8.00 | 0.03 | 7.97 | 0.00 | 0.03 | 7.97 | 0.20 | 0.04 |
| $\omega$ = 40° | | | | | | | | |
| Wall1 | 8.00 | 0.03 | 7.95 | 0.00 | 0.05 | 7.91 | 0.19 | 0.09 |
| Wall2 | 8.00 | 0.03 | 7.90 | 0.00 | 0.10 | 7.90 | 0.17 | 0.10 |
| Wall3 | 8.00 | 0.03 | 8.07 | 0.00 | 0.07 | 7.91 | 0.67 | 0.09 |
| Wall4 | 8.00 | 0.03 | 7.92 | 0.00 | 0.08 | 8.21 | 0.44 | 0.21 |
| Wall5 | 8.00 | 0.03 | 8.02 | 0.00 | 0.02 | 8.16 | 0.26 | 0.16 |
| | | | | Average | **0.06** | | Average | **0.09** |

(ii) $2\vartheta_{det} = 80°$; Fe(220); Reflection; Primary Slit - Secondary Collimator; GV 2 × 10 × 2 mm³

| Features | CMM | Accuracy | Wall thickness (mm) | | | | | |
|---|---|---|---|---|---|---|---|---|
| | | | Align | | | ScanManipulator | | |
| | | | Wall scan | Std. error | Difference | Wall scan | Std. error | Difference |
| $\omega$ = -140° | | | | | | | | |
| Wall1 | 8.00 | 0.03 | 8.19 | 0.00 | 0.19 | 8.12 | 0.55 | 0.12 |
| Wall2 | 8.00 | 0.03 | 7.88 | 0.01 | 0.12 | 7.77 | 0.67 | 0.24 |
| Wall3 | 8.00 | 0.03 | 7.78 | 0.00 | 0.22 | 7.67 | 0.70 | 0.33 |
| Wall4 | 8.00 | 0.03 | 7.82 | 0.01 | 0.18 | 7.85 | 0.46 | 0.15 |
| Wall5 | 8.00 | 0.03 | 8.11 | 0.01 | 0.11 | 8.19 | 0.71 | 0.19 |
| $\omega$ = 40° | | | | | | | | |
| Wall1 | 8.00 | 0.03 | 8.35 | 0.00 | 0.35 | 8.13 | 1.03 | 0.13 |
| Wall2 | 8.00 | 0.03 | 8.20 | 0.00 | 0.20 | 8.11 | 0.60 | 0.11 |
| Wall3 | 8.00 | 0.03 | 7.83 | 0.00 | 0.17 | 7.56 | 0.87 | 0.44 |
| Wall4 | 8.00 | 0.03 | 8.20 | 0.00 | 0.20 | 8.08 | 0.67 | 0.08 |
| Wall5 | 8.00 | 0.03 | 8.18 | 0.00 | 0.18 | 8.10 | 0.54 | 0.10 |
| | | | | Average | **0.19** | | Average | **0.19** |

BrightnESS² is funded by the European Union Framework Programme for Research and Innovation Horizon 2020, under grant agreement 823867

*Table A-20 Comparison between CMM result and wall scan fitted by Align and ScanManipulator software on MPISI, for flat surface not perpendicular to the beam propagation direction (tilt = 2° and 10°).*

$2\vartheta_{det}$ = 80°; Fe(220); Transmission; Primary Slit - Secondary Slit; GV 1 × 10 × 1 mm³

| Features | Wall thickness (mm) | | | | | | | |
|---|---|---|---|---|---|---|---|---|
| | CMM | Accuracy | Align | | | ScanManipulator | | |
| | | | Wall scan | Std. error | Difference | Wall scan | Std. error | Difference |
| Tilt = 2° | | | | | | | | |
| Wall1 | 8.00 | 0.01 | 7.98 | 0.03 | 0.02 | 7.97 | 0.04 | 0.03 |
| Wall2 | 8.00 | 0.01 | 7.92 | 0.03 | 0.08 | 7.95 | 0.05 | 0.05 |
| | | | | Average | **0.05** | | Average | **0.04** |
| Tilt = 10° | | | | | | | | |
| Wall1 | 8.12 | 0.01 | 8.03 | 0.05 | 0.09 | 8.08 | 0.08 | 0.04 |
| Wall2 | 8.12 | 0.01 | 8.46 | 0.04 | 0.34 | 8.45 | 0.11 | 0.33 |
| | | | | Average | **0.22** | | Average | **0.19** |

*Table A-21 Comparison between CMM result and wall scan fitted by Align and ScanManipulator software on MPISI, for Tube sample (R = 50 mm). Scan position indicated in Figure A-3. Axis of the tube in vertical and horizontal direction.*

$2\vartheta_{det}$ = 80°; Fe(220); *)Transmission, **)Reflection; Primary-Secondary Slit; GV 1 × 10 × 1 mm³

| Features | Wall thickness (mm) | | | | | | | |
|---|---|---|---|---|---|---|---|---|
| | CMM | Accuracy | Align | | | ScanManipulator | | |
| | | | Wall scan | Std. error | Difference | Wall scan | Std. error | Difference |
| *axis vertical* | | | | | | | | |
| Rad-1* | 5.10 | 0.01 | 4.97 | 0.04 | 0.13 | 4.98 | 0.05 | 0.12 |
| Rad-2* | 5.10 | 0.01 | 5.29 | 0.03 | 0.19 | 5.31 | 0.06 | 0.21 |
| Rad-1** | 5.10 | 0.01 | 5.11 | 0.01 | 0.01 | 5.01 | 0.03 | 0.09 |
| | | | | Average | **0.11** | | Average | **0.14** |
| Off-5* | 5.10 | 0.01 | 5.10 | 0.04 | 0.00 | 5.12 | 0.07 | 0.02 |
| Off-5** | 5.10 | 0.01 | 5.07 | 0.01 | 0.03 | 5.02 | 0.03 | 0.08 |
| | | | | Average | **0.02** | | Average | **0.05** |
| *axis horizontal* | | | | | | | | |
| Rad-3* | 5.10 | 0.01 | 5.15 | 0.03 | 0.05 | 5.10 | 0.09 | 0.00 |
| Rad-4* | 5.10 | 0.01 | 5.06 | 0.01 | 0.04 | 5.03 | 0.03 | 0.07 |
| | | | | Average | **0.05** | | Average | **0.04** |

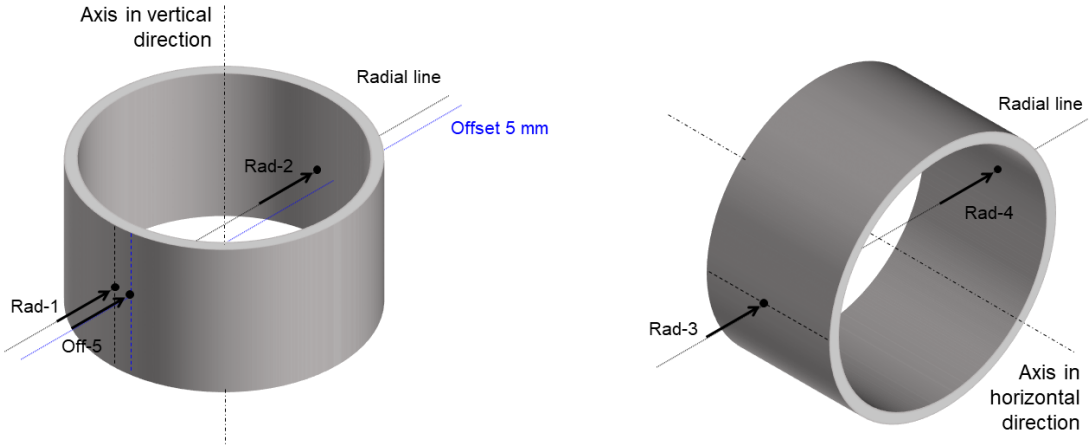


*Figure A-3 Scan position of the Tube sample on MPISI.*

BrightnESS² is funded by the European Union Framework Programme for Research and Innovation Horizon 2020, under grant agreement 823867

## A.4. Measurement results on ENGIN-X

### A.4.1. Sample alignment system accuracy

*Table A-22 Measurement of 5-wall sample to determine the precision of sample alignment system on ENGINX at ω of −135° and −45°.*

(i) $\omega$= −135°; North Bank = Reflection; South Bank = Transmission; GV 2 × 10 × 2 mm³

| Surface | Position (mm) | | | | | | | |
|---|---|---|---|---|---|---|---|---|
| | Alignment | Accuracy | North Bank | | | South Bank | | |
| | | | Measured | Std. error | Offset | Measured | Std. error | Offset |
| Wall1A | -84.15 | 0.10 | -84.09 | 0.03 | 0.05 | -84.13 | 0.08 | 0.02 |
| Wall1B | -76.15 | 0.10 | -76.07 | 0.03 | 0.07 | -76.18 | 0.11 | -0.03 |
| Wall2A | -54.15 | 0.10 | -54.06 | 0.03 | 0.08 | -54.15 | 0.08 | -0.01 |
| Wall2B | -46.15 | 0.10 | -46.06 | 0.03 | 0.08 | -46.14 | 0.11 | 0.00 |
| Wall3A | -24.15 | 0.10 | -24.10 | 0.03 | 0.04 | -24.10 | 0.10 | 0.04 |
| Wall3B | -16.15 | 0.10 | -16.13 | 0.03 | 0.01 | -16.21 | 0.14 | -0.07 |
| Wall4A | 5.86 | 0.10 | 5.87 | 0.03 | 0.01 | 5.84 | 0.09 | -0.02 |
| Wall4B | 13.86 | 0.10 | 13.80 | 0.03 | -0.06 | 13.78 | 0.13 | -0.08 |
| Wall5A | 35.86 | 0.10 | 35.88 | 0.03 | 0.02 | 35.85 | 0.08 | -0.01 |
| Wall5B | 43.86 | 0.10 | 43.80 | 0.03 | -0.05 | 43.80 | 0.12 | -0.05 |
| | | | | Std. Dev | **0.05** | | Std. Dev | **0.04** |
| | | | | Average | **0.03** | | Average | **-0.02** |

(ii) $\omega$= −45°; North Bank = Transmission; South Bank = Reflection; GV 2 × 10 × 2 mm³

| Surface | Position (mm) | | | | | | | |
|---|---|---|---|---|---|---|---|---|
| | Alignment | Accuracy | North Bank | | | South Bank | | |
| | | | Measured | Std. error | Offset | Measured | Std. error | Offset |
| Wall1A | -84.15 | 0.10 | -84.17 | 0.13 | -0.03 | -84.21 | 0.06 | -0.06 |
| Wall1B | -76.15 | 0.10 | -76.26 | 0.10 | -0.12 | -76.27 | 0.04 | -0.13 |
| Wall2A | -54.15 | 0.10 | -54.14 | 0.13 | 0.00 | -54.24 | 0.08 | -0.10 |
| Wall2B | -46.15 | 0.10 | -46.23 | 0.10 | -0.09 | -46.29 | 0.05 | -0.15 |
| Wall3A | -24.15 | 0.10 | -24.15 | 0.13 | -0.01 | -24.24 | 0.08 | -0.10 |
| Wall3B | -16.15 | 0.10 | -16.30 | 0.09 | -0.16 | -16.30 | 0.05 | -0.16 |
| Wall4A | 5.86 | 0.10 | 5.76 | 0.12 | -0.10 | 5.73 | 0.07 | -0.13 |
| Wall4B | 13.86 | 0.10 | 13.69 | 0.10 | -0.17 | 13.68 | 0.04 | -0.18 |
| Wall5A | 35.86 | 0.10 | 35.91 | 0.18 | 0.05 | 35.76 | 0.06 | -0.10 |
| Wall5B | 43.86 | 0.10 | 43.63 | 0.12 | -0.23 | 43.68 | 0.04 | -0.18 |
| | | | | Std. Dev | **0.09** | | Std. Dev | **0.04** |
| | | | | Average | **-0.08** | | Average | **-0.13** |

BrightnESS² is funded by the European Union Framework Programme for Research and Innovation Horizon 2020, under grant agreement 823867

*Table A-23 Measurement of 5-wall sample to determine the precision of sample alignment system on ENGINX at ω of 45° and 135°.*

(i) $\omega$= 45°; North Bank = Reflection; South Bank = Transmission; GV 2 × 10 × 2 mm³

| Surface | Position (mm) | | | | | | | |
|---|---|---|---|---|---|---|---|---|
| | Alignment | Accuracy | North Bank | | | South Bank | | |
| | | | Measured | Std. error | Offset | Measured | Std. error | Offset |
| Wall1A | -84.15 | 0.10 | -84.00 | 0.06 | 0.14 | -84.10 | 0.14 | 0.04 |
| Wall1B | -76.15 | 0.10 | -76.18 | 0.04 | -0.04 | -76.15 | 0.08 | -0.01 |
| Wall2A | -54.15 | 0.10 | -54.13 | 0.08 | 0.01 | -54.07 | 0.15 | 0.07 |
| Wall2B | -46.15 | 0.10 | -46.13 | 0.05 | 0.01 | -46.14 | 0.09 | 0.00 |
| Wall3A | -24.15 | 0.10 | -24.15 | 0.08 | -0.01 | -24.11 | 0.11 | 0.03 |
| Wall3B | -16.15 | 0.10 | -16.16 | 0.05 | -0.02 | -16.14 | 0.08 | 0.00 |
| Wall4A | 5.86 | 0.10 | 5.91 | 0.06 | 0.05 | 5.92 | 0.11 | 0.06 |
| Wall4B | 13.86 | 0.10 | 13.82 | 0.04 | -0.04 | 13.83 | 0.08 | -0.03 |
| Wall5A | 35.86 | 0.10 | 35.89 | 0.06 | 0.03 | 35.90 | 0.11 | 0.05 |
| Wal5B | 43.86 | 0.10 | 43.84 | 0.04 | -0.02 | 43.84 | 0.09 | -0.02 |
| | | | | Std. Dev | **0.05** | | Std. Dev | **0.03** |
| | | | | Average | **0.02** | | Average | **0.02** |

(ii) ω= 135°; North Bank = Transmission; South Bank = Reflection; GV 2 × 10 × 2 mm³

| Surface | Position (mm) | | | | | | | |
|---|---|---|---|---|---|---|---|---|
| | Alignment | Accuracy | North Bank | | | South Bank | | |
| | | | Measured | Std. error | Offset | Measured | Std. error | Offset |
| Wall1A | -84.15 | 0.10 | -83.98 | 0.10 | 0.16 | -83.98 | 0.03 | 0.16 |
| Wall1B | -76.15 | 0.10 | -76.10 | 0.12 | 0.04 | -75.98 | 0.03 | 0.16 |
| Wall2A | -54.15 | 0.10 | -53.99 | 0.10 | 0.15 | -53.95 | 0.04 | 0.19 |
| Wall2B | -46.15 | 0.10 | -46.09 | 0.12 | 0.05 | -45.92 | 0.04 | 0.22 |
| Wall3A | -24.15 | 0.10 | -23.98 | 0.10 | 0.16 | -23.99 | 0.03 | 0.15 |
| Wall3B | -16.15 | 0.10 | -16.11 | 0.12 | 0.03 | -15.99 | 0.03 | 0.15 |
| Wall4A | 5.86 | 0.10 | 6.00 | 0.10 | 0.14 | 5.96 | 0.03 | 0.10 |
| Wall4B | 13.86 | 0.10 | 13.85 | 0.12 | -0.01 | 13.96 | 0.03 | 0.10 |
| Wall5A | 35.86 | 0.10 | 35.99 | 0.10 | 0.13 | 35.99 | 0.03 | 0.13 |
| Wal5B | 43.86 | 0.10 | 43.85 | 0.12 | -0.01 | 44.09 | 0.03 | 0.23 |
| | | | | Std. Dev | **0.07** | | Std. Dev | **0.04** |
| | | | | Average | **0.09** | | Average | **0.16** |

BrightnESS² is funded by the European Union Framework Programme for Research and Innovation Horizon 2020, under grant agreement 823867

*Table A-24 Measurement of 5-wall sample to determine the precision of sample alignment system on ENGINX at ω of −135 °, −45 °, and 45 °.*

North bank; GV 1 × 15 × 1 mm³

(i) $\omega$ = -135°; Transmission

| Surface | Position (mm) | | | | |
|---|---|---|---|---|---|
| | Alignment | Accuracy | Measured | Std. error | Offset |
| Wall1A | -30.44 | 0.10 | -30.48 | 0.08 | -0.04 |
| Wall1B | -22.52 | 0.10 | -22.52 | 0.12 | 0.00 |
| Wall2A | -0.49 | 0.10 | -0.55 | 0.08 | -0.06 |
| Wall2B | 7.46 | 0.10 | 7.48 | 0.11 | 0.02 |
| Wall3A | 29.39 | 0.10 | 29.38 | 0.08 | -0.01 |
| Wall3B | 37.43 | 0.10 | 37.42 | 0.11 | -0.01 |
| | | | | Std. Dev | **0.03** |

(ii) $\omega$ = -45°; Reflection

| Surface | Position (mm) | | | | |
|---|---|---|---|---|---|
| | Alignment | Accuracy | Measured | Std. error | Offset |
| Wall1A | -30.44 | 0.10 | -30.59 | 0.03 | -0.15 |
| Wall1B | -22.52 | 0.10 | -22.55 | 0.03 | -0.03 |
| Wall2A | -0.49 | 0.10 | -0.64 | 0.03 | -0.15 |
| Wall2B | 7.46 | 0.10 | 7.43 | 0.03 | -0.03 |
| Wall3A | 29.39 | 0.10 | 29.30 | 0.03 | -0.09 |
| Wall3B | 37.43 | 0.10 | 37.15 | 0.03 | -0.28 |
| | | | | Std. Dev | **0.09** |

(iii) $\omega$ = 45°; Transmission

| Surface | Position (mm) | | | | |
|---|---|---|---|---|---|
| | Alignment | Accuracy | Measured | Std. error | Offset |
| Wall1A | -30.44 | 0.10 | -30.79 | 0.12 | -0.35 |
| Wall1B | -22.52 | 0.10 | -22.75 | 0.08 | -0.23 |
| Wall2A | -0.49 | 0.10 | -0.76 | 0.11 | -0.27 |
| Wall2B | 7.46 | 0.10 | 7.25 | 0.08 | -0.21 |
| | | | | Std. Dev | **0.06** |

BrightnESS² is funded by the European Union Framework Programme for Research and Innovation Horizon 2020, under grant agreement 823867

### A.4.2. Wall & Tube scan

*Table A-25 Comparison between CMM result and wall scan fitted by Align software on ENGIN-X, for flat surface perpendicular to the beam propagation direction. Measured using 2 mm radial Collimator.*

GV 2 × 10 × 2 mm³

| Features | Wall thickness (mm) | | | | | | | |
|---|---|---|---|---|---|---|---|---|
| | CMM | Accuracy | North Bank | | | South Bank | | |
| | | | Wall scan | Std. error | Difference | Wall scan | Std. error | Difference |
| $\omega$ = −135°; North Bank = Reflection; South Bank = Transmission | | | | | | | | |
| Wall1 | 8.01 | 0.00 | 8.02 | 0.00 | 0.01 | 7.95 | 0.07 | 0.06 |
| Wall2 | 8.01 | 0.01 | 8.00 | 0.00 | 0.01 | 8.01 | 0.07 | 0.00 |
| Wall3 | 8.01 | 0.01 | 7.97 | 0.00 | 0.04 | 7.89 | 0.10 | 0.12 |
| Wall4 | 8.01 | 0.01 | 7.93 | 0.00 | 0.08 | 7.94 | 0.09 | 0.07 |
| Wall5 | 8.00 | 0.01 | 7.92 | 0.00 | 0.08 | 7.95 | 0.09 | 0.05 |
| | | | | Average | **0.04** | | Average | **0.06** |
| $\omega$ = −45°; North Bank = Transmission; South Bank = Reflection | | | | | | | | |
| Wall1 | 8.01 | 0.00 | 7.91 | 0.09 | 0.10 | 7.94 | 0.05 | 0.05 |
| Wall2 | 8.01 | 0.01 | 7.91 | 0.09 | 0.10 | 7.95 | 0.06 | 0.06 |
| Wall3 | 8.01 | 0.01 | 7.85 | 0.09 | 0.16 | 7.94 | 0.06 | 0.05 |
| Wall4 | 8.01 | 0.01 | 7.93 | 0.07 | 0.08 | 7.95 | 0.06 | 0.06 |
| Wall5 | 8.00 | 0.01 | 7.72 | 0.13 | 0.28 | 7.92 | 0.05 | 0.06 |
| | | | | Average | **0.14** | | Average | **0.07** |
| $\omega$ = 45°; North Bank = Reflection; South Bank = Transmission | | | | | | | | |
| Wall1 | 8.01 | 0.00 | 7.82 | 0.05 | 0.19 | 7.95 | 0.11 | 0.11 |
| Wall2 | 8.01 | 0.01 | 8.00 | 0.06 | 0.01 | 7.93 | 0.12 | 0.06 |
| Wall3 | 8.01 | 0.01 | 7.99 | 0.06 | 0.02 | 7.97 | 0.07 | 0.05 |
| Wall4 | 8.01 | 0.01 | 7.91 | 0.05 | 0.10 | 7.91 | 0.07 | 0.06 |
| Wall5 | 8.00 | 0.01 | 7.95 | 0.05 | 0.05 | 7.94 | 0.07 | 0.06 |
| | | | | Average | **0.07** | | Average | **0.07** |
| $\omega$ = 135°; North Bank = Transmission; South Bank = Reflection | | | | | | | | |
| Wall1 | 8.01 | 0.00 | 7.88 | 0.06 | 0.13 | 8.00 | 0.00 | 0.00 |
| Wall2 | 8.01 | 0.01 | 7.90 | 0.07 | 0.11 | 8.03 | 0.00 | 0.06 |
| Wall3 | 8.01 | 0.01 | 7.87 | 0.07 | 0.14 | 8.00 | 0.00 | 0.05 |
| Wall4 | 8.01 | 0.01 | 7.85 | 0.07 | 0.16 | 8.00 | 0.00 | 0.06 |
| Wall5 | 8.00 | 0.01 | 7.86 | 0.07 | 0.14 | 8.10 | 0.00 | 0.06 |
| | | | | Average | **0.14** | | Average | **0.03** |
| | | | | | | Total Average | | **0.08** |

BrightnESS² is funded by the European Union Framework Programme for Research and Innovation Horizon 2020, under grant agreement 823867

*Table A-26 Comparison between CMM result and wall scan fitted by Align software on ENGIN-X, for flat surface perpendicular to the beam propagation direction. Measured using 1 mm radial Collimator.*

North Bank; GV 1 × 15 × 1 mm³

| Features | Wall thickness (mm) | | | | |
|---|---|---|---|---|---|
| | CMM | Accuracy | Wall scan | Std. error | Difference |
| $\omega$ = −135°; Transmission | | | | | |
| Wall1 | 8.01 | 0.01 | 7.96 | 0.09 | 0.05 |
| Wall2 | 8.01 | 0.01 | 8.03 | 0.08 | 0.02 |
| Wall3 | 8.01 | 0.01 | 8.04 | 0.08 | 0.03 |
| $\omega$ = −45°; Reflection | | | | | |
| Wall1 | 8.01 | 0.01 | 8.04 | 0.00 | 0.03 |
| Wall2 | 8.01 | 0.01 | 8.07 | 0.00 | 0.06 |
| Wall3 | 8.01 | 0.01 | 7.85 | 0.00 | 0.16 |
| $\omega$ = 45°; Transmission | | | | | |
| Wall1 | 8.01 | 0.01 | 8.04 | 0.09 | 0.03 |
| Wall2 | 8.01 | 0.01 | 8.01 | 0.08 | 0.00 |
| | | | | Average | 0.05 |

*Table A-27 Comparison between CMM result and wall scan fitted by Align software on ENGIN-X, for the tube sample (R = 50 mm) along radial line. Scan position is indicated in Figure A-4.*

GV 2 × 10 × 2 mm³

| Features | Wall thickness (mm) | | | | | | | |
|---|---|---|---|---|---|---|---|---|
| | CMM | Accuracy | North Bank | | | South Bank | | |
| | | | Wall scan | Std. error | Difference | Wall scan | Std. error | Difference |
| $\omega$ = −135°; North Bank = Transmission; South Bank = Reflection | | | | | | | | |
| Rad-1 | 5.11 | 0.01 | 5.26 | 0.12 | 0.15 | 5.31 | 0.00 | 0.20 |
| Rad-2 | 5.10 | 0.01 | 4.94 | 0.11 | -0.16 | 5.05 | 0.00 | -0.05 |
| $\omega$ = −45°; North Bank = Reflection; South Bank = Transmission | | | | | | | | |
| Rad-1 | 5.11 | 0.01 | 5.18 | 0.00 | 0.07 | 5.08 | 0.14 | -0.03 |
| Rad-2 | 5.10 | 0.01 | 5.19 | 0.00 | 0.09 | 4.95 | 0.12 | -0.15 |
| $\omega$ = 45°; North Bank = Transmission; South Bank = Reflection | | | | | | | | |
| Rad-1 | 5.11 | 0.01 | 5.15 | 0.11 | 0.04 | 5.00 | 0.06 | -0.11 |
| Rad-2 | 5.10 | 0.01 | 4.91 | 0.12 | -0.19 | 5.05 | 0.02 | -0.05 |
| $\omega$ = 135°; North Bank = Reflection; South Bank = Transmission | | | | | | | | |
| Rad-1 | 5.11 | 0.01 | 4.99 | 0.06 | -0.12 | 5.11 | 0.12 | 0.00 |
| Rad-2 | 5.10 | 0.01 | 5.04 | 0.02 | -0.06 | 5.05 | 0.13 | -0.05 |
| | | | | | | | Total average | **0.10** |

*Table A-28 Comparison between CMM result and wall scan fitted by Align software on ENGIN-X, for the tube sample (R = 50 mm) along offset line. Scan position is indicated in Figure A-4.*

GV 2 × 10 × 2 mm³

| Features | Wall thickness (mm) | | | | | | | |
|---|---|---|---|---|---|---|---|---|
| | CMM | Accuracy | North Bank | | | South Bank | | |
| | | | Wall scan | Std. error | Difference | Wall scan | Std. error | Difference |
| $\omega$ = −135°; North Bank = Transmission; South Bank = Reflection | | | | | | | | |
| Off-30-1 | 6.40 | 0.01 | 6.85 | 0.19 | 0.45 | 6.96 | 0.00 | 0.56 |
| Off-30-2 | 6.40 | 0.01 | 7.07 | 0.17 | 0.67 | 7.09 | 0.22 | 0.69 |

BrightnESS² is funded by the European Union Framework Programme for Research and Innovation Horizon 2020, under grant agreement 823867

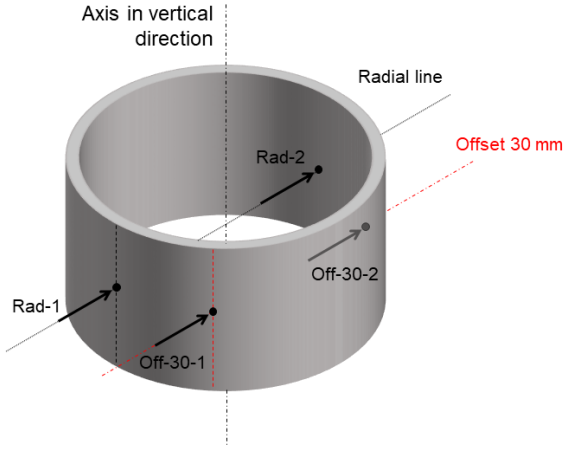


*Figure A-4 Scan position of the Tube sample on ENGIN-X.*

## A.5. CMM results

**Set 1**

5-wall

| Features | Wall thickness (mm) | Accuracy (mm) |
|---|---|---|
| Wall1 | 8.00 | 0.01 |
| Wall2 | 8.01 | 0.01 |
| Wall3 | 8.02 | 0.01 |
| Wall4 | 8.02 | 0.01 |
| Wall5 | 8.00 | 0.01 |

Tube

| Features | Wall thickness (mm) | Accuracy (mm) |
|---|---|---|
| Rad-1 | 5.08 | 0.01 |
| Rad-2 | 5.15 | 0.01 |

**Set 2**

5-wall

| Features | Wall thickness (mm) | Accuracy (mm) |
|---|---|---|
| Wall1 | 8.01 | 0.01 |
| Wall2 | 8.01 | 0.01 |
| Wall3 | 8.01 | 0.01 |
| Wall4 | 8.01 | 0.01 |
| Wall5 | 8.00 | 0.01 |

Tube

| Features | Wall thickness (mm) | Accuracy (mm) |
|---|---|---|
| Rad-1 | 5.11 | 0.01 |
| Rad-2 | 5.10 | 0.01 |

BrightnESS² is funded by the European Union Framework Programme for Research and Innovation Horizon 2020, under grant agreement 823867

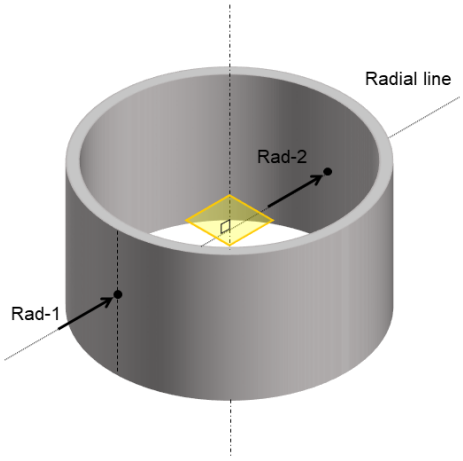


*Figure A-5 CMM measurement position of the Tube sample.*

BrightnESS² is funded by the European Union Framework Programme for Research and Innovation Horizon 2020, under grant agreement 823867

# B. ANNEX: Calibration Protocol and Reporting

## B.1. Calibration protocol

All the procedures in this protocol apply to both monochromatic and TOF neutron strain scanners, unless stated otherwise.

### B.1.1. Determination of the centre of *ω*-rotation

The general procedure to determine the centre of *ω*-rotation axis is proposed as follows.

(a) Securely mount a calibration pin on the sample stage, near the approximate position of the centre of *ω*-rotation.

(b) Determine the position of the pin. This can be measured mechanically using a dial gauge or optically using telecentric camera.

(c) Determine the offset between the pin position and the centre of *ω*-rotation. This is performed by measuring the pin position at multiple *ω*-angles [18, 20]. Using a telecentric camera system with image recognition software, the trace of the pin position at different *ω*-angles can be recorded and fitted to directly determine the centre of *ω*-rotation.

(d) Move the pin to the centre of *ω*-rotation, and record the position in the sample stage coordinate system.

Adjust the optical axis of the sample alignment system (e.g., camera, theodolite) to the centre of the *ω*-rotation.

### B.1.2. Alignment of the beam apertures

The general procedure to align the beam apertures is as follows.

(a) Set the detector on the angular position at which the main sample characterisation will be performed. For TOF instruments equipped with two detector banks, this position is normally fixed at ±90°.

(b) Securely mount a calibration pin on the centre of *ω*-rotation. The diameter of the pin is preferably be smaller than the width of the gauge volume. In the case when larger diameter pin is used, ensure that the full diameter of the pin is measured.

(c) Align the secondary/diffracted beam aperture by either: (i) scanning the secondary beam aperture while keeping the calibration pin fixed at the centre of *ω*-rotation, or; (ii) scanning the pin along the centre line of the primary/incident beam. Illustration is provided in Figure 8-4. For TOF instruments with two detector banks, the alignment of the two beam apertures can be performed simultaneously with a single pin scan.

(d) Fit the peak-shaped intensity curve from the scan, e.g., using a Gaussian function, to determine the position of the maximum intensity of the beam. Using method (i), this is the position of the pin at the centre of *ω*-rotation. For method (ii), this is the current position of the optical axis of the secondary beam aperture.

(e) Position the optical axis on the centre of *ω*-rotation by adjusting the secondary beam aperture.

BrightnESS² is funded by the European Union Framework Programme for Research and Innovation Horizon 2020, under grant agreement 823867

(f) Repeat steps (c)-(e) for the primary beam aperture. Note that now the pin scan should be made along the centre line of the secondary/diffracted beam, if method (ii) is used. For TOF instruments with two detector banks the intensity curve can be taken from both detector banks and the result can be averaged.

(g) After adjusting the beam apertures, repeat the pin scan and note the final offset position between the optical axes and the centre of $\omega$-rotation. The accuracy should be better than 10% of the gauge volume width.

Note 1: On monochromatic instruments, some cases require measurement to be performed using different detector angular positions. Without realignment of beam apertures at different detector angular positions, the position of the reference position may be critically displaced depending on the requirements of the measurement and positioning resolution (i.e. RS gradient) (see example in Subsection5.3.1). If the measurements are to be performed without realignment, the displacement would need to be reported in uncertainty analysis.

Note 2: On monochromatic instruments, if measurements are to be performed with realignment, $d_0$ stress-free reference samples would need to be measured on each detector angular position to compensate the peak shift in the strain calculation due to the change of beam aperture configuration.

**B.1.3. Measurement of reference point vs. centre of $\omega$-rotation**

Quantification of the reference point position (i.e., the centre of the IGV) with respect to the centre of $\omega$rotation represents the final misalignment of a given setup after the instrument alignment procedures. This can be carried out by performing foil scans as described in Section 5.1. The following steps applies:

(a) Position the detector at the angular position at which the main sample characterisation will be performed. For TOF instruments, this position is normally fixed at ±90°.

(b) Securely mount the calibration Foils & pin sample, Figure 9-5, or similar, on the sample stage.

(c) Using the sample alignment system (e.g., camera or theodolite), position each of the mutually perpendicular foils to the centre of $\omega$-rotation. Note the absolute positions. These are referred to as the alignment positions.

(d) Rotate the sample table to the first $\omega$-angle so that the first foil is parallel with the bisector between the primary and the secondary beam (i.e., the scattering vector). With this setup, the second foil should be normal to the bisector.

(e) Scan both foils around each of their alignment position, as illustrated in Figure 10-2. Each foil should be scanned along one of the *xy*-axis of the sample stage.

(f) Repeat step (e) for a minimum of three $\omega$-angles, 90° apart, Figure 10-2. Measurements at more $\omega$-angles can be carried out subject to available beamtime.

(g) Fit the peak-shaped intensity curve from each foil scan, e.g., using Gaussian, to determine the measured foil position.

(h) Determine the offset between the measured and alignment position, Eq. B.1.

BrightnESS² is funded by the European Union Framework Programme for Research and Innovation Horizon 2020, under grant agreement 823867

(i) Using the offset, determine the *XY* coordinate of the sample at each $\omega$ angle, by transforming the sample stage coordinate system to the instrument coordinate system with rotation by angle $\omega$, Eq. B.2. The *XY*position of the reference point is (0, 0).

(j) Determine the position of the centre of $\omega$-rotation relative to the reference point, from the *XY* sample coordinates at different $\omega$-angles. For measurement at three $\omega$-angles, the centre can be found by solving the equation of a circle passing through 3 points, Eq. B.3. For measurements at more $\omega$-angles, the centre can be determined through a least-square best fit circle based on the coordinates.

Note 1: The table below is given as an example of reference point vs. centre of $\omega$ rotation determination, with detector angular position at $2\vartheta_1$ and the calibration foils measured at three $\omega$-angles: $\omega_{ij}$, $\omega_{kl}$ and $\omega_{mn}$. The two mutually perpendicular calibration foils are Foil 1 and Foil 2, which is scanned along *x*- and *y*-axis, respectively.

Note 2: A graphical analysis as described in Section 5.2, can also be performed to determine the position of the reference point vs. the centre of $\omega$-rotation.

| $2\vartheta_{det}$ | $\omega$ | Foil | Scan axis | Alignment position | Measured position | Offset (*x*, *y*) | Sample coordinate (*X*, *Y*) |
|---|---|---|---|---|---|---|---|
| $2\vartheta_1$ | $\omega_{ij} = 2\,\vartheta_1/2$ | 1 | *x* | $a_i$ | $b_i$ | $x_i = b_i - a_i$ (B.1) | $X_{ij} = x_i \cos\omega_{ij} + y_j \sin\omega_{ij}$ (B.2) |
| | | 2 | *y* | $a_j$ | $b_j$ | $y_i = b_j - a_j$ | $Y_{ij} = -x_i \sin\omega_{ij} + y_j \cos\omega_{ij}$ |
| | $\omega_{kl} = \omega_{ij} + 90°$ | 1 | *x* | $a_k$ | $b_k$ | $x_k$, $y_l$ | $X_{kl}$, $Y_{kl}$ |
| | | 2 | *y* | $a_l$ | $b_l$ | | |
| | $\omega_{mn} = \omega_{ij} - 90°$ | 1 | *x* | $a_m$ | $b_m$ | $x_m$, $y_n$ | $X_{mn}$, $Y_{mn}$ |
| | | 2 | *y* | $a_n$ | $b_n$ | | |

Equation of circle:

$$X^2 + Y^2 + DX + EY + F = 0 \qquad \text{(B.3)}$$

solving *D*, *E*, *F* for:

$$X_{ij}^2 + Y_{ij}^2 + DX_{ij} + EY_{ij} + F = 0$$
$$X_{kl}^2 + Y_{kl}^2 + DX_{kl} + EY_{kl} + F = 0$$
$$X_{mn}^2 + Y_{mn}^2 + DX_{mn} + EY_{mn} + F = 0$$

**B.1.4. Measurement of GV size**

Determination of the GV size can be described as follows:

1. Securely mount a calibration pin or foil, with pin diameter or foil thickness smaller than the opening of the corresponding beam apertures.
2. Position the calibration pin or foil to the centre of $\omega$-rotation.
3. Scan the pin or foil across/perpendicular to the beam of interest (incident or diffracted).

Fit the resulting intensity curve to determine the size of the GV, using appropriate model depending on the type of beam apertures. For radial collimators, the GV size can be determined from the FWHM of the Gaussian fit of the intensity curve. For slits the GV size can be determined by using error function (erf) to describe the edges of the intensity curve, (for example as applied on ENGIN-X [23]).

BrightnESS² is funded by the European Union Framework Programme for Research and Innovation Horizon 2020, under grant agreement 823867

### B.1.5. Determination of sample alignment system precision

Determination of the precision of the sample alignment system is carried out by performing systematic surface scans as described in Section 6.1. The following steps applies:

(a) Position the detector to measure the desired reflection, e.g., Fe(220) or Fe(311) for the 5-Wall sample.

(b) Securely mount the 5-Wall sample on the sample stage.

(c) Align the vertical wall surfaces using the sample alignment system and record the alignment position, Figure 11-1(B).

(d) Scan all the vertical wall surfaces, as illustrated in Figure 11-1(A).

(e) Fit the resulting intensity curve using an entry scan analysis tool to determine the measured position of each wall.

Determine the precision of the sample alignment system from the standard deviation of the offsets between the alignment position and the measured position of all the wall surfaces.

## B.2. Reporting template

The reporting of Neutron Quality Label can be found on the following page.

BrightnESS² is funded by the European Union Framework Programme for Research and Innovation Horizon 2020, under grant agreement 823867

NEUTRONS FOR SOCIETY

necsa We're in your world South African Nuclear Energy Corporation Ltd

FRM II Forschungs-Neutronenquelle Heinz Maier-Leibnitz

Science & Technology Facilities Council ISIS Neutron and Muon Source

# NEUTRON STRAIN CHARACTERIZATION REPORT

NQL Neutron Quality Label 01/06/2020

## COMPANY :

## TITLE :



**ABSTRACT:**

**INSTITUTE:**
**INSTRUMENT:**
**Address:**
**Date :**
**Ref. N :**
**Contact :**

**COMPANY:**
**Address:**
**Contact:**

Document Distribution

Mail distribution

| DOCUMENT REVIEWS | | | |
|---|---|---|---|
| **NAME** | **FUNCTION** | **DATE** | **SIGNATURE** |
| | | | |
| | | | |
| | | | |

| INDEX | DATE | MODIFICATION | PAGE(S) |
|---|---|---|---|
| 0 | | Creation | |
| | | | |
| | | | |
| | | | |
| | | | |
| | | | |
| | | | |

## SUMMARY

# 1. INTRODUCTION

## 1.1. Aim of the measurement and material

Functionality of the industrial component and/or fabrication routes.
Definition of critical regions for RS mapping/ in-situ experiment conditions.

## 1.2. Preliminary and/or complementary information

Fabrication history, geometry, composition, phases, microstructure, texture, homogeneity.
Previous measurements of RS gradients (laboratory, synchrotron, neutrons) and/or simulations in the context for the neutron characterization.

## 2. CALIBRATION REPORT

### 2.1. General Instrument set up

| Monochromator | | | nominal values | units |
|---|---|---|---|---|
| | Type: | | | |
| | cut | | | |
| | hkl used | | | |
| | omega angle | | | Deg |
| | take-off angle | | | Deg |
| | wavelength | | | Å |
| | curvture | | | m |
| | distance to ref. point | | | m |
| | Other: | | | |
| **Time of Flight - ToF** | | | **nominal values** | **units** |
| | total flight path | | | m |
| | wavelength range | | | A |
| | channel width | | | S |
| | inc. beam divergence | | | Deg |
| | Other | | | |
| **Primary optics** | | | **nominal values** | **units** |
| ☐ slit | Primary slit width - PSW | | | mm |
| | Primary slit height - PSH | | | mm |
| | Primary slit distance - PSD | | | mm |
| ☐ collimator | horizontal | focal distance | | mm |
| | | focal width | | FWHM |
| | vertical | focal distance | | mm |
| | | focal width | | FWHM |
| **Secondary optics** | | | **nominal values** | **units** |
| ☐ slit | Secondary slit width - SSW | | | 1 / mm |
| | Secondary slit height - SSH | | | 1 / mm |
| | Secondary slit distance - SSD | | | 1 / mm |
| ☐ collimator | horizontal | focal distance | | 1 / mm |
| | | focal width | | FWHM / mm |

| Detector | | | nominal values | Units |
|---|---|---|---|---|
| Distance to reference point | | | | m |
| Beam | ☐ Monochromated | Position Sensitive PSD | | |
| | | Ref. Det. Distance | | mm |
| | | Area | | $cm^2$ |
| | | Pixel size hor./vert. | | Deg |
| | | angular range hor./vert | | Deg |
| | | Other: | | |
| | ☐ TOF | angular acceptance horiz | | Deg |
| | | Angular acceptance vert | | Deg |
| | | Other: | | |

| Sample Stage | nominal values | Units |
|---|---|---|
| **Type Hexapod / XYZ table**<br>positioning accuracy<br>repeatability<br>Other : | | |
| **Type omega rotation**<br>positioning accuracy<br>repeatability<br>Other : excentricity vs 2Thetha | | |
| **Type cradle ±45°**<br>positioning accuracy<br>repeatability<br>Other : sphere o. conf. | | |
| **Type Rotation stage 360**<br>positioning accuracy<br>repeatability<br>excentricity | | |
| **Type Temperature**<br>Room temperature test<br>Furnace<br>accuracy<br>repeatability<br>Other : | | |
| **Type Loading rig**<br>Load range<br>accuracy<br>repeatability<br>Other : | | |



## 2.2. Particular Instrument Calibration for the measurement

| Detector calibration | | Measured values | uncertainty | units |
|---|---|---|---|---|
| channel width | | | | Deg |
| Ref. Detector distance | | | | mm |
| Other: | | | | |
| **Beam alignment** | | | | |
| Pin diameter | | | | mm |
| Primary beam | horizontal | | | fwhm / mm |
| | Vertical | | | mm |
| Secondary beam | horizontal | | | fwhm / mm |
| error on beam position | | | | µm |
| Other: | | | | |
| **Wavelength spread, shape of gauge volume** | | | | |
| Fe-sheet (diagonal scan) | | | | mm |
| delta lamba | | | | A |
| Other: | | | | |

### 2.3. Comments and related graphs

| Reference point determination | Description |
|---|---|
| | |
| **Beam characterization** | **Description** |
| | |
| **Powder Reference measurement** | **Description** |
| | |
| **Incident intensity distribution** | **Description** |
| | |
| **Pseudo-strain characterization** | **Description** |
| | |

# 3. MEASUREMENTS REPORT

## 3.1. Component set up for strain and regions measured

- Schematic figure of the component placed at the instrument sample stage and q vector (strain component), detector positioning and reflexion traced
- Detailed information about regions mapped within the component (reference points, sample coordinate system, etc)
- Measured directions (strain components), number of measured points / lines etc and step size including GV dimensions
- Other

## 3.2. Peak position

- Peak fit description: full profile analysis method, single peak profile, number of neutrons counted in peak, background function, smoothing functions, interpolation, distorted peak profiles, etc
- times of flight $t_{hkl}$ ± uncertainty, 2Thetha ±uncertainty, FWHM ± uncertainty, Peak height ± uncertainty, Peak height/Background Ratio
- Other:

## 3.3. Strain

- Unstrained reference ($d_0$)
- Strain plots
- Other

## 3.4. Stress

- Diffraction elastic constants and Poisson's ratio (provide the source of those)
- Stress plots
- Other

## 3.5. Reliability of results

Regarding the calculations, uncertainties were determined in accordance with ISO/IEC Guide 98-3 [1]. Additional guidelines taken into account are found in [2].



[1] ISO/IEC Guide 98-3, *Uncertainty of measurement — Part 3: Guide to the expression of uncertainty in measurement (GUM: 1995)*
[2] Taylor B .N., K uyatt C.E., "Guidelines for Evaluating and Expressing the Uncertainty of NIST Measurement Results", NIST Technical Note 1297 1994; see also http:// physics .nist .gov/ cuu/Uncertainty/ index .html

## 4. CONCLUSIONS AND/OR RECOMMENDATIONS

Final remarks, possible problems found during the measurements and implementations, complementary studies / measurements in the laboratory facilities and/or neutron facilities, etc.

**ANEX I**

**ANEX II**